UNIVERSITÀ DEGLI STUDI DI MILANO
SCUOLA DI DOTTORATO
TERRA, AMBIENTE E BIODIVERSITÀ

Dottorato di Ricerca in Scienze della Terra
Ciclo XXIV

Sedimentological and magnetic anisotropy analyses on paleocurrent directions in turbidites from the northern Apennines (Italy)

Ph.D. Thesis

Eleonora Dall'Olio
Matricola R08030

Tutori
Dott. Fabrizio Felletti
Prof. Giovanni Muttoni

Anno Accademico
2010-2011

Coordinatore
Prof.ssa Elisabetta Erba

Index

Abstract

This PhD thesis focuses on the validation of an objective method to define paleocurrent directions in turbiditic systems: the anisotropy of magnetic susceptibility (AMS). The final purpose of this study is to calibrate paleocurrent directions estimated with this geophysical method to directions estimated from classic sedimentological indicators, and therefore verify the applicability of this method to cases where sedimentological paleocurrent indicators are absent such as in drill cores.

Two selected turbiditic units outcropping in the northern Apennines, the Marnoso Arenacea Formation (Miocene, northern Apennines) and on the Castagnola Formation (Oligo-Miocene, Tertiary Piedmont Basin), were investigated. These basins have different depositional settings: the Marnoso Arenacea Formation filled a foredeep basin nearly 200 km long and 60 km wide, whereas the Castagnola Formation filled an episutural basin 6 km long and 4 km wide. AMS analyses were successfully applied to both formations on a total of 853 samples taken in a wide range of depositional intervals selected by means of detailed sedimentological analyses, and were successively cross-validated by direct estimates of flow directions from sedimentological indicators (*ripple marks*, *flute marks*, etc.).

In the Marnoso Arenacea Formation, a robust correlation between magnetic fabric and paleocurrent directions obtained from sedimentological indicators was found in massive, parallel-laminated, and cross-laminated sandstones. These depositional intervals show well-clustered AMS data with an overall flow-aligned fabric. Instead, highly dispersed AMS fabrics are apparently common in convoluted and undulated sandstones as well as in debrites, suggesting depositional processes that partially prevented grains' orientation (e.g., en masse freezing) or post-depositional processes that disrupted the original current-induced fabric (e.g., post-depositional dewatering). AMS fabrics typical of deposition in standing water was observed in the hemipelagites of the Castagnola Formation. Instead, in the fine-grained sediments of the

Marnoso Arenacea Formation (White Marlstone beds), an AMS fabric interpreted as current-induced was observed and interpreted as due to muddy contourites.

The study on the Castagnola Formation was carried out primarily to evaluate the effects of basin confinement on turbidity flow dynamics. In this small, confined turbidite system, we observed a strong correlation between magnetic fabric and bed-thickness distribution whereby beds thicker than ~1.20 m show high magnetic fabric variability and maximum susceptibility axes dispersion, whereas beds thinner than ~1.20 m show better developed magnetic fabrics with maximum susceptibility axes oriented consistently parallel to the mean paleoflow direction from flute casts. We believe that ~1.20 m represents a thickness threshold separating large flows that covered the entire basin floor interacting in a complex fashion with the basin's margins from small volume flows that did not interact with the basin's margins and produced better-defined flow-aligned AMS fabrics.

Potential future developments of this thesis are:

(1) deepening of our understanding on the relationships between grains' orientations and magnetic minerals that contribute to the AMS signal by means of textural analyses, neutron diffraction and x-ray tomography. Preliminary results indicate that paramagnetic muscovite principally controls the observed current induced AMS fabric;

(2) testing the AMS method on drill core samples, where *flow marks* (i.e., *flute casts*) are either absent or non-observable.

Key worlds

anisotropy of magnetic susceptibility; turbidites; Marnoso Arenacea Formation; Castagnola Formation; paleocurrent directions; white marlstone beds; confined turbidite system

Chapter 1

Introduction

Sedimentary geology deals with ancient depositional environments. As Lyell and his theory of Uniformitarianism said, the Earth is altered by processes uniform throughout time. The changes that in the past produced the features of the Earth's surface are the same that happen today. The study of rocks (ancient environments) and the observation of actual processes (modern environments) are useful to explain the story that lived and lives the Earth.

This PhD project focuses on the validation of a method to define paelocurrent directions in turbiditic systems applying an objective tool: the anisotropy of magnetic susceptibility (AMS). The final purpose of this study is to calibrate this method in order to be able to apply it on subsurface cores and in case studies where sedimentological paleocurrent indicators are absent.

1.1 The deep-sea environments and the magnetic susceptibility

Reliable means of determining the environment in which a sedimentary rock was deposited would be extremely useful in correlation, in forecasting probable facies changes, in deciphering paleogeography, and in judging expectable variations in organic content and in porosity patterns that might be significant in the search for oil and gas. In most instances the best clues to the nature of the environment of deposition are to be sought in the physical and faunal characteristics of the rocks themselves. [...] the physical characteristics of the rocks can be made to tell the environmental story.

Rich, 1950

...and finding a connection with this citation by Rich, I can say that the physical characteristic I will focus on is the magnetic susceptibility and that I will apply it in order to investigate ancient deep sea environments.

But why are ancient deep sea environments important? What is a turbiditic system? And what is magnetic susceptibility and its anisotropy?

Deep-water turbiditic systems are volumetrically the most important accumulations of sand in deep-sea and they represent one of the frontier areas for hydrocarbon exploration and exploitation (Viana, 2008). Recent advances in field-based facies analysis have shown that turbiditic systems are characterized by a great variability in terms of size, geometry, facies, and stacking patterns. This variability is the result of the interplay between several factors, such as sea-level change, local and regional tectonic settings, basin size and shape, sediment type and frequency of depositional events, and volume of gravity flows (Mutti, 1992; Pickering et al., 1995; Mulder and Alexander, 2001; Nilsen et al., 2008; Mutti et al., 2009).

The evaluation of paleocurrent directions within turbiditic systems, integrated with the aforementioned variability, is essential to construct depositional models at the basin scale. Much work has been done to model facies heterogeneities that could be expected in deep-sea deposits, but relatively few methods are available to estimate paleocurrent directions. Traditionally, sedimentological current indicators (*ripple marks*, *flute marks*, etc.) are used to obtain paleocurrent directions, but these are not always present in outcrop sections and are virtually absent in drill cores. This limitation requires the identification of an alternative, objective method to define paleocurrent directions in turbiditic successions. Some authors (Rees, 1965; Galehouse, 1968; Hamilton & Rees, 1970; Argenton et al., 1975; Schieber & Ellwood, 1993; Liu et al., 2005; Pares et al., 2007; Veloso et al., 2007) suggested that the AMS is a useful tool to study paleocurrents in sedimentary rocks (e.g., turbiditic, fluvial, tide-dominated deltaic and estuarine environments). The method has the advantage to be time-saving and to allow analyze large datasets objectively, whereas methods based on sedimentological indicators and grain fabric orientation are usually time-consuming and not always reliable.

The magnetic susceptibility is a dimensionless physic property of rocks that indicate the degree of magnetisation in response to an external magnetic field. The magnetic susceptibility *H* is the constant of proportionality that put into connection the strength of the induced magnetisation *M* to the strength of the applied field *H*: $\boldsymbol{M = K * H}$ (Tarling & Hrouda, 1993). Its anistotropy, the AMS, is defined by an ellipsoid with three perpendicular axes of maximum (k_1), medium (k_2) and minimum (k_3) susceptibility, and it is considered to reflect the preferred

alignment of ferromagnetic and/or paramagnetic particles during transport and deposition. The AMS is considered to be a proxy for the preferred alignment of natural magnetic particles attained in the final stages of sediment transport, with the maximum susceptibility axis, k_{max}, and the minimum susceptibility axis, k_{min}, approximating the preferred orientation of the longest and shortest magnetic grain axes, respectively (e.g., Hamilton and Rees, 1970; Taira and Scholle, 1979; Tarling and Hrouda, 1993; Borradaile et al., 1999). This method is based on the fact that a current is able to orient paramagnetic grains (e.g., phyllosilicates, olivines, pyroxenes, anphiboles), diamagnetic grains (e.g., quartz, calcite, feldspars), and ferromagnetic (sensu lato) grains (e.g., magnetite, goethite, hematite), and that the resulting AMS ellipsoid (Fig. 1.1) reflects the orientation imparted by the current to such grains (e.g., Ellwood, 1980; Lowrie and Hirt, 1987; Taira, 1989; Sagnotti and Meloni, 1993; Parés et al., 2007). For example, during deposition of phyllosilicates, which are very common in siliciclastic turbidites, the grain's short shape axis falls perpendicular to the bedding plane. As a result, an oblate fabric develops (well-developed foliation). The AMS fabric mimics this because in phyllosilicates the short shape axis corresponds to the crystallographic c-axis as well as to the minimum susceptibility direction, and therefore a magnetic foliation (defined by the plane containing k_{max} and k_{int}), develops parallel to the depositional surface. When currents are present (Fig. 1.1), hydraulic forces control grains alignment (current-induced fabric; Shor et al., 1984). The long shape axis of elongated paramagnetic grains, as well as of large ferromagnetic grains, lines up either parallel or perpendicular to the current direction in case of moderate or high hydrodynamic regimes, respectively. The AMS fabric reflects this because in such elongated grains, the maximum susceptibility axis commonly lies broadly along the particle length. Consequently, a magnetic lineation can develop as revealed by a clustering of the k_{max} axes either parallel or perpendicular to the current direction depending on the hydrodynamic boundary conditions.

Conversely, settling in still water produces an horizontal fabric (Fig. 1.1) with minimum susceptibility axes clustered around the pole to the depositional plane within which maximum and intermediate susceptibility axes are uniformly dispersed, defining a planar, near-horizontal, gravity-induced settling fabric (Ellwood, 1980; Tarling and Hrouda, 1993; Pares et al., 2007).
After deposition, the fabric may be affected by compaction, bioturbation, and disruption by migration of trapped fluids and/or gas, or by tectonic deformation. Thus, studies of the AMS fabric can also provide information on post-depositional processes.

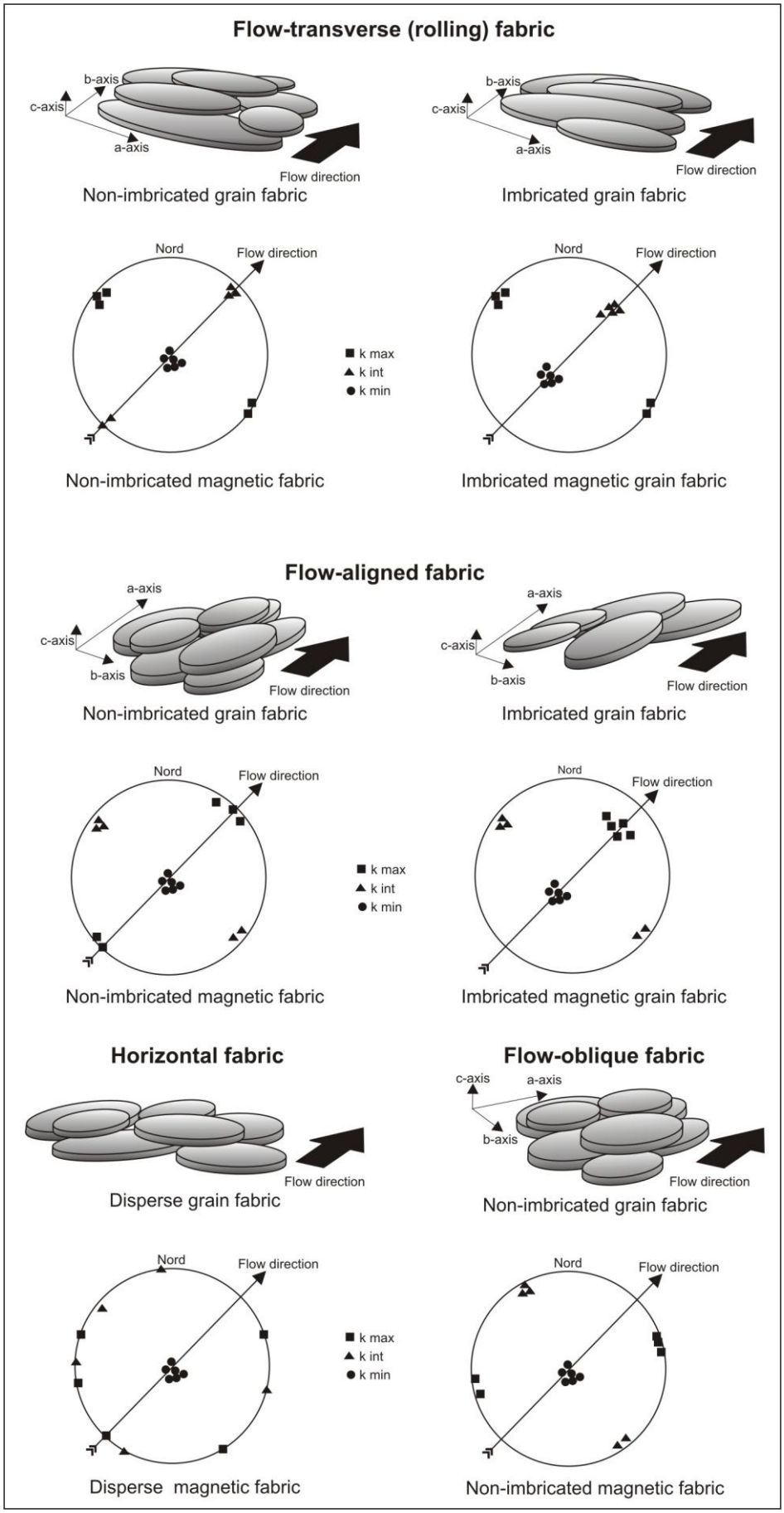

Fig. 1.1 - Main types of anisotropic grain shape fabrics, presented by schematic drawings of the orientation of elongated grains and by the orientation of the three principal orthogonal axes in upper hemisphere stereograms. For the types of fabric shown, non-imbricated and imbricated subtypes are shown on the left- and right-hand side, respectively. Horizontal fabric is non-imbricated by definition. a=long grain axis; b=grain axis of intermediate length; c=short grain axis.

Table 1 - Comparison of the two studied basin.

	Marnoso Arenacea Formation	**Castagnola Formation**
Basin size (present time)	Max length ~ 180 km NW-SE Max width ~ 40 km SW-NE	Max length ~ 6 km SW-NE Max width ~ 4 km NW-SE
Max thickness of the system	~ 3000 m (Ricci Lucchi, 1975; Boccaletti et al., 1990; Vai, 2001; Costa et al., 1998)	900 m (Baruffini et al., 1994)
Average palaeocurrent trends	From NE to SW (siliciclastic turbidites) From SW to NE (hybrid and carbonatic turbidites)	From SW to NE (dispersion up to 180°)
Volume sediment entrapped	Individual flow deposits commonly contain ~ 3–15 km^3 of sediment. The largest Contessa mega-bed contains over 35 km^3 of sediment (Amy & Talling, 2006)	5 x 10^9 m^3 (total), 1.3 x 10^9 m^3 (sand) (Baruffini et al., 1994)
Depositional style	Flat and aggradational	Flat and aggradational
Shape of sandstones bodies	Tabular	Almost tabular
Geometry of beds	Tabular. Sandstone beds fine upward into mudstones.	Tabular. Sandstone beds fine upward into mudstones. Rare erosional surfaces
Max. lateral extension of individual beds	More than 200 km	6 km, corresponding to the width of the basin
Stacking patterns	Small-scale cycles of bed thick	Small-scale cycles of bed thick
Terminations	Gradual pinch-outs onto the lateral basin marging	Rapid pinch-outs (average angle of onlap: 10°, generally flows impinged the palaeoslope at high angle); Gradual pinch-outs (average angle of onlap: 5°, generally flows impinged the palaeoslope at low angle).
Facies association	Classical Tc-e/Td-e Bouma sequences (dilute turbulent flows); Classical Ta-e, Tb-e e Bouma sequences (concentrated to dilute turbulent flows); Massive and graded sandstone beds (concentrated flows with aggradational depositional features); Debrites.	Classical Tc-e/Td-e Bouma sequences (dilute turbulent flows); Massive and graded sandstone beds, frequent delayed grading (concentrated flows with aggradational depositional features); Sandstone beds and sandstone/mudstone couplets, formed by repetitions of massive, plane-parallel laminated and cross-laminated sandstone depositional divisions (mildly concentrated flows with complex internal organization).

1.2 The case studies: the Marnoso Arenacea and the Castagnola turbidite systems

In order to contribute to understand the relationships between sedimentological characteristics and AMS fabric, two selected turbiditic units outcropping in the Northern Apennines have been studied. Sampling has been focused on the Marnoso Arenacea Formation (Miocene, Northern Apennines) (Fig. 1.2) and on the Castagnola Formation (Oligo-Miocene, Tertiary Piedmont Basin) (Fig. 1.3).

The Marnoso Arenacea (Ricci Lucchi and Ori, 1985) is a foredeep basin nearly 200 km long and 60 km wide (Fig. 1.2), whereas the Castagnola Formation (Stocchi et al., 1992) is an episutural basin 6 km long and 4 km wide (Fig. 1.3). These two basin have been chosen because of different factors: (i) they are well-known in the literature, (ii) they are provided with good outcrops, (iii) paleocurrent directions are measurable from sedimentological indicators at the base of most turbidite beds (i.e., *flute marks*), (iv) they are characterized by different sedimentological settings that allow apply the method in different depositional contests (Tab. 1), (v) they are provided with numerous key marker beds that allow high-resolution stratigraphic correlations at the basin scale.

The Marnoso Arenacea Formation

The MA Fm. is a non-channelized, mainly siliciclastic turbidite system (Ricci Lucchi and Valmori, 1980; Amy and Talling, 2006; Muzzi Megalhaes and Tinterri, 2010). It is partly buried under tectonic or sedimentary units both to the W and to the NE of its present outcrop area. The MA is a composite, wedge-shaped turbidite succession representing the final filling of a Miocene migrating Apennine foredeep complex, which accumulated between the Langhian and the Tortonian (Ricci Lucchi and Valmori, 1980; Fig. 1.2). The sediment thickness is up to 3 km (Ricci Lucchi, 1975; Boccaletti et al., 1990; Vai, 2001; Costa et al., 1998). To the southeast, the thickness decreases rapidly, suggesting the presence of a structural high within the southeastern (Umbrian) part of the basin (Argnani and Ricci Lucchi, 2001). Paleocurrent directions measured at the base of turbidite beds indicate axial flows from the NW to the SE (in present-day coordinates; Fig. 1.2). In addition, minor volumes of carbonate and hybrid turbidites, derived from shallow-water carbonate platforms located along the southern and southeastern margins of the basin, in the Gubbio area of Umbria, are also present (Gandolfi et al., 1983).

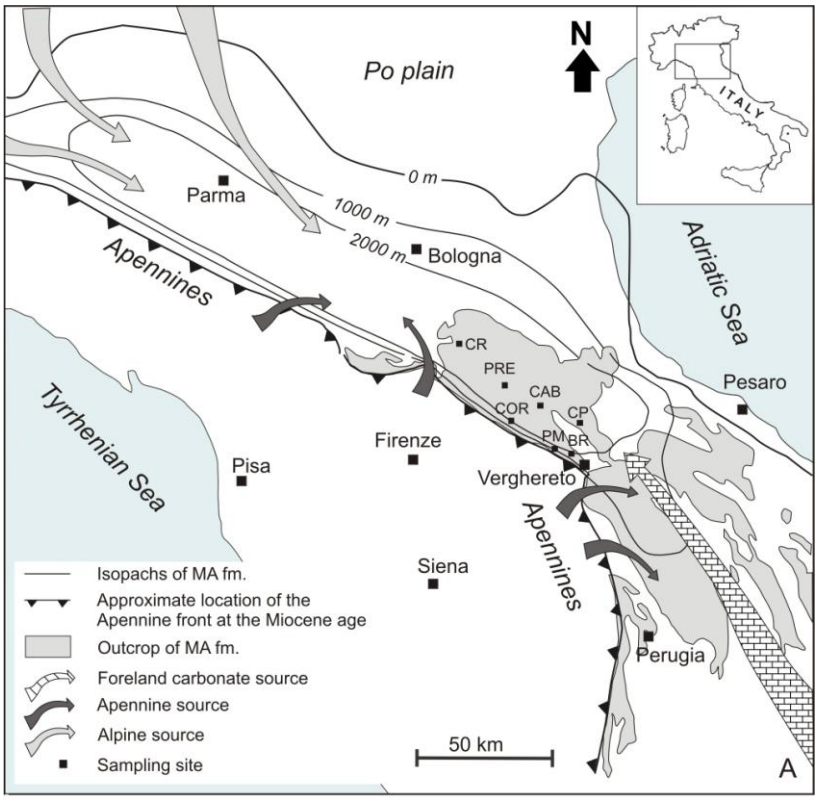

Fig. 1.2 - Map showing the outcrop area and thickness of the Marnoso Arenacea Formation (after Argnani and Ricchi Lucchi, 2001; isopachs in the Po plain subsurface from Dondi et al., 1992) and location of the sampling sites (dots). Sediment sources were located mainly in the Alps but also the Apennines including foreland carbonate ramps in the south.

The Castagnola Formation turbidite system

The Castagnola Formation turbidite system (Oligo-miocene) was deposited in a structural depression by large volume gravity flows charged with fine-grained sediment that evolved from high-density to low-density turbidity currents during their run-out. The axis of the basin is oriented ENE–WSW (Fig. 1.3) and the thickness of the deepwater sediments is of at least 800 m. Flute casts at the base of the Castagnola turbidite system indicate paleocurrents coming mainly from the NE.

As we are interested to calibrate the method and to determine which sediment composition and texture (grain size and sedimentary structures) work best for the application of the AMS methodology, numerous turbiditic sandstone beds have been sampled throughout different depositional intervals (e.g, fine- to medium-grained massive sands, fine- to medium-grained parallel-laminated sands, fine-grained cross-laminated sands and hemipelagites). The obtained AMS results have been compared to paleoflow directions measured throughout sedimentological indicator (i.e., *flute marks*) present at the base of the beds. In order to

understand minerals carrying on the paleomagnetic signal, textural analyses have been carried out.

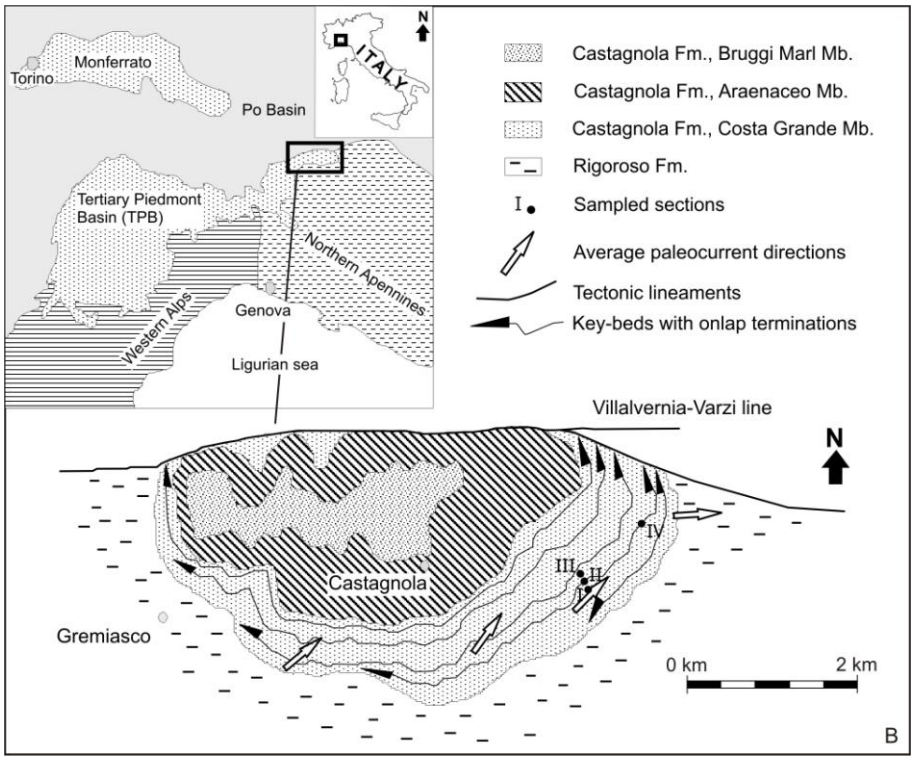

Fig. 1.3 - Location of the Tertiary Piedmont Basin (Italy), geological sketch map of the Castagnola basin (redrawn and modified after Stocchi et al., 2002) and sampling sections (dots).

1.3 Methods: paleomagnetic and textural analyses

Samples for paleomagnetic analyses, performed in different depositional intervals (e.g. massive, parallel-laminated, cross-laminated intervals), were collected in situ with a water-cooled rock drill and oriented with a magnetic compass. Cylindrical samples have been reduced in the laboratory to standard dimension (2,5 cm in diameter, 2,22 cm in height for a total volume of ~10 cm3).

Paleomagnetic analyses carried out are:

- ***AMS (Anisotropy of Magnetic Susceptibility)***. AMS analyses, described in detail above, have been carried out on a total of 853 cylindrical oriented samples (551 coming from the Marnoso Arenacea Fm. and 302 from the Castagnola Fm.). The susceptibility of each specimen was measured in 15 directions with a KLY-3 Kappabridge adopting the standard measurement scheme of the Agico KLY-3 User's Guide (1998). A susceptibility

tensor was then fit to the data by means of least square analysis, and the errors of the fit were calculated using multivariate statistics (Agico KLY-3 User's Guide, 1998). Susceptibility tensors were subsequently rotated into tilt-corrected coordinates using site-mean bedding attitudes, and then plotted on stereographic projections.

- ***AIRM (Anisotropy of Isothermal Remanent Magnetization)***. The most common method used to determine the magnetic remanence tensor in a rock sample, and therefore estimate the contribution to magnetic anisotropy due to ferromagnetic particles, involves magnetizing a sample repeatedly in different directions and measuring the intensity of the component of magnetic remanence that is acquired parallel to the applied field (Tarling & Hrouda, 1993). AIRM is obtained by applying a direct field along a sample's axis and measuring the induced remanence, which is subsequently AF demagnetized using a tumbler device allowing to repeat the procedure for the other two orthogonal axes (Tarling & Hrouda, 1993). A total of 43 cylindrical samples (coming from the Marnoso Arenacea Fm.) have been magnetized using an Agico Pulse Magnetizer PUM-1 in a direct field of 20 mT, and demagnetized with a Molspin Demagnetizer in a field of 50 mT. The data have been rotated into tilt-corrected coordinates using site-mean bedding attitudes, and then plotted on stereographic projections, and compared with the AMS plots.
- ***IRM (Isothermal Remanent Magnetization)***. This analysis involves the short-term exposure of a sample to increasing magnetizing fields at constant temperature (Butler, 2004), and is used to define the ferromagnetic minerals content of a rock. Experiments have been carried out on a total of 39 cylindrical samples (23 coming from the Marnoso Arenacea Fm. and 16 from the Castagnola Fm.) by imparting, at room temperature, a magnetizing field progressively increasing from 10 mT to 2.470 mT generated by an ASC Scientific Pulse Magnetizer IM 10-30, and measuring the induced remanence after each magnetizing step with a 755 2G Enterprises cryogenic magnetometer.
- ***ThIRM (Thermal demagnetization of a three-component IRM).*** The thermal demagnetization of a three-component IRM provides information on the ferromagnetic content of a rock (Lowrie, 1990). The sample is magnetized along three orthogonal axes (x, y and z) by applying fields 0.1 T, 0.4 T and 2.5 T, respectively, which are then subjected to stepwise thermal demagnetization (Lowrie, 1990). The analysis has been carried out on 33 samples (23 coming from the Marnoso Arenacea Fm. and 10 from the

Castagnola Fm.). The IRM intensity of each orthogonal IRM component has been plotted as a function of temperature.

- ***NRM (Natural Remanent Magnetization)***. The NRM analysis is useful to reconstruct the paleogeography of the basin. A total of 198 samples (157 coming from the Marnoso Arenacea Fm. and 41 from the Castagnola Fm.) have been thermally demagnetized in increasing steps from room temperature up to 450 °C, and the NRM was measured after each heating with a 2G 755 cryogenic magnetometer. Magnetic components of the NRM were calculated using standard least-square analysis on linear portions of the demagnetization paths and plotted on equal-area projections and on vector end-point demagnetization diagrams.

Paleomagnetic analyses have been integrated with the following textural analyses.

- ***Image analysis***: it is a bi-dimensional analysis carried out on thin section. By cutting sections along two defined planes (parallel to the paleocurrent direction and perpendicular to it), it is possible to have a three-dimensional reconstruction. This analysis, conducted using the ImageJ software (Rasband, 2008), permits to observe the different orientation of grains in the sediment. Diamagnetic, paramagnetic and ferromagnetic minerals can be detected and the data can be compared to paleocurrents measured in situ and to AMS analyses.
- ***Neutron diffraction***: the internal structure of samples, with a volume of nearly 1 cm^3, is investigated throughout this analysis (Zucali et al., 2002). Neutron diffraction is an experimental technique for quantitative texture analysis. With this analysis (carried out at the Institut Laue-Langevin of Grenoble - France), three-dimensional crystallographic information can be collected and crystal preferential orientations can be visualized through polar figures.
- ***X-ray tomographic analysis***: this analysis is based on the use of x-ray beams that cross the sample and reach the detector. The investigated area has a volume that is nearly 0,4 cm^3. Tomography is an analysis that permits the reconstruction of an object into a 3D image starting from a series of closely spaced slices. The slices are obtained by many separate projections around the object itself (Jerram and Higgins, 2007). The analyses have been carried out at the Elettra Synchrotron in Trieste (Italy) using a X-ray source. Minerals and pores are distinguished in X-ray tomography on the basis of their linear attenuation coefficient, μ. This parameter depends on the electron density of the mineral,

the effective atomic number of the mineral, and the energy of the incoming X-ray beam (Jerram and Higgins, 2007).

1.4 Organization of the thesis and presentation of data and results

The data collected during this PhD have been interpreted and presented in three distinct papers; two of these papers were submitted to international ISI journals, whereas the third one is going to be submitted. These papers constitute chapters 2, 3, and 4 of this thesis. In particular:

Chapter 2 - PAPER #1: *The anisotropy of magnetic susceptibility as a tool to detect paleoflow directions in the Miocene Marnoso Arenacea turbidites (northern Apennines, Italy)* – E. Dall'Olio, F. Felletti and G. Muttoni – submitted to *Sedimentology.*

Chapter 3 - PAPER #2: C*onstraints on mechanisms of deep-water mudstone deposition in the Marnoso Arenacea Formation (Miocene, Italy) through magnetic fabric analysis* - E. Dall'Olio, F. Felletti and G. Muttoni – submitted to *Journal of Sedimentary Research.*

Chapter 4 - PAPER #3: T*he anisotropy of magnetic susceptibility (AMS) as a tool to discriminate flow dynamics in a confined turbidite system (Castagnola Formation, Tertiary Piedmont Basin, NW Italy)* - E. Dall'Olio, F. Felletti and G. Muttoni.

Chapter 5 – In this chapter the first results obtained throughout textural analyses are shown. These analyses were carried out in order to investigate the relationship between grains' orientation and minerals that bring the AMS signal.

Chapter 6 - This last chapter will provide a summary of the results while attempting to give an answer to the main question of this PhD: is the AMS a useful tool to define paleocurrent directions in turbiditic systems?

References

Agico KLY-3 User's Guide (Ver. 2.2 Nov. 1998) Modular system for measuring magnetic susceptibility, anysotropy of magnetic susceptibility, and temperature variation of magnetic susceptibility. AGICO Advanced Geoscience Instruments CO. Brno, Czech Republic.

Amy, L.A. and Talling, P.J (2006). Anatomy of turbidites and linked debrites based on long distance (120 x 30 km) bed correlation, Marnoso Arenacea Formation, Northern Apennines, Italy. *Sedimentology*, **53**, 161-212.

Argenton, H., Bobier, C. and Polveche, J. (1975). La mésure de l'anisotropie de susceptibilité magnetique dans les flysches; application à la recherche des directions des paleocourants. *Sedimentary Geology*, **14**, 2, 149-167.

Argnani, A. and Ricci Lucchi, F. (2001) Tertiary siliciclastic turbidite systems of the Northern Apennines. In: Apennines and Adjacent Mediterranean Basins (Vai, G.B. and Martini, P. Eds.), Kluwer Academic Publishers, 327-350.

Boccaletti, M., Calamita, F., Deiana, G., Gelati, R., Massari, F., Moratti, G. and Ricci Lucchi, F. (1990) Migrating foredeep-thrust belt system in the northern Apennines and southern Alps. *Palaeogeography Palaeoclimatology Palaeoecology*, **77**, 1, 3-14.

Borradaile, G.J., Fralick, P.W. and Lagroix, F. (1999) Acquisition of anhysteretic remanence and tensor subtraction from AMS isolates true palaeocurrent grain alignments. In: Palaeomagnetism and Diagenesis in Sediments (Tarling, D.H. and Turner, P. Eds), Geological Society, London, Special Publications, **151**, 139-145.

Butler, R.F. (2004). Paleomagnetism: Magnetic Domains to Geologic Terranes. *Electronic Edition. Departement of Chemistry and Physics, University of Portland – Portland, Oregon.*

Costa, E., Pialli, G. and Plesi, G. (1998) Foreland basins of the Northern Apennines; relationships with passive subduction of the Adriatic lithosphere. *Memorie della Societa Geologica Italiana*, **52**, 595-606.

Ellwood, B.B. (1980) Induced and remanent magnetic properties of marine sediments as indicators of depositional processes. *Marine Geology*, **38**, 233-244.

Galehouse, J.S. (1968) Anisotropy of magnetic susceptibility as a paleocurrent indicator; a test of method. *Geological Society of America Bulletin*, **79**, 3, 387-390.

Gandolfi, G., Paganelli, L. and Zuffa, G.G. (1983) Petrology and dispersal directions in the Marnoso Arenacea Formation (Miocene, northern Apennines). *Journal of Sedimentary Petrology*, **53**, 493–507.

Hamilton, N. and Rees, A.I. (1970) The use of magnetic fabric in paleocurrent estimation. In: Paleogeophysics (Runcorn, S.K. Ed.). London, Academic Press, 445-464.

Jerram, D.A., and Higgins, M.D. (2007). 3D Analysis of Rock Textures: Quantifying Igneous Microstructures. *Elements*, **3**, 4, pp. 239-245.

Liu, B., Saito, Y., Yamazaki, T., Abdeldayem, A., Oda, H., Hori, K. and Zhao, Q. (2005) Anisotropy of magnetic susceptibility (AMS) characteristics of tide-influenced sediments in the Late Pleistocene-Holocene Changjiang incised valley fill, China. *Journal of Coastal Research*, **21**, 5, 1031–1041.

Lowrie, W. (1990) Identification of ferromagnetic minerals in a rock by coercivity and unblocking temperature properties. *Geophysical Research Letters*, **17**, 2, 159-162

Lowrie, W. and Hirt, A.M. (1987) Anisotropy of magnetic susceptibility in the Scaglia Rossa pelagic limestone. *Earth and Planetary Science Letters*, **82**, 349-356.

Mulder, T. and Alexander, J. (2001) The physical character of subaqueous sedimentary density currents and their deposits. *Sedimentology*, **48**, 269–299.

Mutti, E. (1992) Turbidite Sandstones. Ente Nazionale Idrocarburi (ENI) – Università di Parma, 275 pp.

Mutti, E., Bernoulli, D., Lucchi, F. R. and Tinterri, R. (2009) Turbidites and turbidity currents from Alpine 'flysch' to the exploration of continental margins. *Sedimentology*, **56,** 267–318.

Muzzi Magalhaes, P. and Tinterri, R. (2010) Stratigraphy and depositional setting of slurry and contained (reflected) beds in the Marnoso Arenacea Formation (Langhian-Serravallian) Northern Apennines, Italy. *Sedimentology*, **57**, 7, 1685-1720.

Nilsen, T.H., Shew, R.D., Steffens, G.S. and Studlick, J.R.J. (2008) Atlas of Deep-water Outcrops. *AAPG Studies in Geology*, **56**, 504 pp.

Parés, J.M., Hassold, N.J.C., Rea, D.K. and van der Pluijm, B.A. (2007) Paleocurrent directions from paleomagnetic reorientation of magnetic fabrics in deep-sea sediments at the Antarctic Peninsula Pacific margin (ODP Sites 1095, 1101). *Marine Geology*, **242,** 261–269.

Pickering, K.T., Hiscott, R.N., Kenyon, N.H., Ricci Lucchi, F. and Smith, R.D.A. (1995) Atlas of Deep Water Environments: Architectural Style in Turbidite Systems. (Chapman & Hall, New York), 303–306.

Rees, A.J. (1965) The use of anisotropy of magnetic susceptibility in the estimation of sedimentary fabric. *Sedimentology*, **4**, 257-283.

Rasband, W. S. (2008) ImageJ. US National Institutes of Health, Bethesda, Maryland, USA. http://rsb.info.nih.gov/ij/index.html

Ricci Lucchi, F. (1975) Depositional cycles in two turbidite formations of northern Apennines (Italy). *Journal of Sedimentary Petrology*, **45**, 1, 3-43.

Ricci Lucchi, F., and Ori, G.G. (1985). Field excursion D: syn-orogenic deposits of a migrating basin system in the NW Adriatic foreland.

Ricci Lucchi, F. and Valmori, E. (1980) Basin-wide turbidites in a Miocene, over-supplied deep-sea plain: a geometrical analysis. *Sedimentology*, **27**, 241–270.

Rich, J.L. (1950) Flow markings, grooving, and intra-stratal crumpling as a criteria for recognition of slope deposits, with illustrations from Silurian rocks of Wales. *Bulletin of the American Association of Petroleum Geologists*, **34**, 4,. 717-741.

Sagnotti, L. and Meloni, A. (1993) Pleistocene rotations and strain in southern Italy: the example of the Sant'Arcangelo Basin. *Annali di Geofisica*, **XXXVI**, 2, 83-95.

Schieber, J. and Ellwood, B.B. (1993) Determination of basinwide paleocurrent patterns in a shale succesion from anisotropy of magnetic susceptibility (AMS): a case of study of the Mid-Proterozoic Newland Formation, Montana. *Journal of Sedimetary Petrology*, **63**, 878-880.

Shor, A.N., Kent, D.V. and Flood, R.D. (1984) Contourite or turbidite? Magnetic fabric of fine-grained Quaternary sediments, Nova Scotia continental rise. In: Fine-Grained

Sediments; Deep- Water Processes and Facies (Stow, D.A.V. and Piper, D.J.W. Eds.). *Geological Society of London, Special Publication*, **15**, 257-273.

Stocchi, S., Cavalli, C., and Baruffini, L. (1992). I depositi torbiditici di Guaso (Pirenei centro meridionali), Gremiasco e Castagnola (settore orientale del BTP): geometria e correlazioni di dettaglio. *Atti Ticinensi di Scienze della Terra*, **35**, pp. 154-177.

Taira, A. (1989) Magnetic fabric and depositional processes. In: Sedimentary facies in the Active Plate Margin (Taira, A. and Masuda, F. Eds). Tokyo, Terra Scientific Publishing, 44-77.

Taira, A. and Scholle, P.A. (1979) Deposition of resedimented sandstone beds in the Pico Formation, Ventura Basin, California, as interpreted from magnetic fabric measurements. *Bulletin Geological Society of America*, **90**, 952-962.

Tarling, D.H. and Hrouda, F. (1993) The Magnetic Anisotropy of Rocks. Chapman & Hall, London.

Vai, G.B. (2001) GSSP, IUGS and IGC; an endless story toward a common language in the earth sciences. *Episodes*, **24**, 1, 29-31.

Veloso, E.E., Anma, R., Ota, T., Komiya, T., Kagashima, S. and Yamazaki, T. (2007) Paleocurrent patterns of the sedimentary sequence of the Taitao ophiolite constrained by anisotropy of magnetic susceptibility and paleomagnetic analyses. *Sedimentary Geology*, **201**, 446–460.

Viana, A.R. (2008) Economic relevance of Conturites. In: Rebesco M, Camerlenghi A (eds) Contourites. *Developments in Sedimentology*, **60**, pp. 493-510.

Zucali, M., Chateigner, D., Dugnani, M., Lutterotti, L., and Ouladdiaf, B. (2002). Quantitative texture analysis of glaucophanite deformed under eclogite facies conditions (Sesia-Lanzo Zone, Western Alps); comparison between X-ray and neutron diffraction analysis. *Geological Society, London, Special Publications*, **200**, pp 239-253.

Chapter 2

Paper #1

The anisotropy of magnetic susceptibility as a tool to detect paleoflow directions in the Miocene Marnoso Arenacea turbidites (northern Apennines, Italy)

Eleonora Dall'Olio[1*], Fabrizio Felletti[1] and Giovanni Muttoni[1]

1 Dipartimento di Scienze della Terra "Ardito Desio". Università degli Studi di Milano. Via Mangiagalli 34, 20133 Milano, Italy.

Paper submitted to *Sedimentology*.

Abstract

Turbiditic systems are characterized by a great variability in size, geometry, facies, and stacking patterns. The development of depositional models at the basin scale is essential to understand this variability. Models require an accurate knowledge of the paleocurrent directions within the turbiditic systems. Traditionally, sedimentological current indicators (flute marks, ripple marks, etc.) are used to obtain paleocurrent directions, but these are not always present in outcrop sections and are virtually absent from drill cores. This limitation raises the need to identify an alternative, objective method to define paleocurrent directions in turbiditic successions. The anisotropy of magnetic susceptibility (AMS) is a useful tool to estimate paleocurrents in sedimentary rocks (e.g. turbiditic, fluvial, tide-dominated deltaic and estuarine environments). This method is based on the fact that a current is able to orient para- and ferromagnetic grains and minerals. The AMS ellipsoid often reflects the orientation imparted by the current to such grains. The Marnoso Arenacea Formation is a well-known foredeep basin of Miocene age that comprises well-exposed stratigraphic sections. Different depositional facies have been sampled for AMS and additional rock-magnetic analyses; AMS fabrics have been compared to sedimentological indicators of paleocurrent direction at the base of turbidite beds; a good agreement between paleocurrents from flute casts and AMS measurements has been observed, even if a relatively small but consistent offset of ~15–20° seems to be present. Nonetheless, these data confirm the substantial validity of the AMS method as a tool to estimate flow directions in absence of sedimentological indicator. Finally, paleomagnetic analyses from the literature were used to reconstruct the paleogeography of the Marnoso Arenacea basin and make inferences about the origin and direction of transport of the sediments.

Key words

turbidites, Marnoso Arenacea Formation, Miocene, anisotropy of magnetic susceptibility, paleocurrent directions

Introduction

Deep-water turbiditic systems are by volume amongst the largest sand units of the deep sea and represent one of the frontier areas for hydrocarbon exploration and exploitation (Viana, 2008). Recent advances in field-based facies analysis have shown that turbiditic systems are characterized by a great variability in terms of size, geometry, facies, and stacking patterns. This variability is the result of the interplay between several factors, such as sea-level change, local and regional tectonic settings, basin size and shape, sediment type and frequency of depositional events, and volume of gravity flows (Mutti, 1992; Pickering et al., 1995; Mulder and Alexander, 2001; Nilsen et al., 2008; Mutti et al., 2009). The evaluation of paleocurrent directions in gravity flows is a basic requirement to interpret the depositional architecture of turbiditic successions as well as the structure and texture of the constituent beds.

Paleocurrent directions are traditionally estimated through sedimentological indicators (i.e., ripple marks, flute marks) or by means of optical analyses on thin sections aimed at determining the orientation of elongated grains within the sediment. However, sedimentological indicators are not always present in outcrop sections and they are virtually absent from drill cores. This limitation raises the need to identify an alternative, objective method to define paleocurrent directions in turbiditic successions. The analysis of the anisotropy of magnetic susceptibility (AMS) of rocks represents one such alternative method. The AMS is a relatively inexpensive and highly effective technique that investigates the magnetic fabric directly correlated to gravity flows. In standing water deposition, the minimum susceptibility axes are clustered around the pole to the depositional plane within which maximum and intermediate susceptibility axes are uniformly dispersed, defining a planar, near-horizontal, gravity-induced settling fabric, whereas the magnetic fabric of sediments deposited from flowing water is typified by a current-oriented magnetic foliation plane (e.g., Ellwood, 1980; Lowrie and Hirt, 1987; Taira, 1989; Sagnotti and Meloni, 1993; Pares et al., 2007).

In this study, we applied the AMS in conjunction with other paleomagnetic techniques to define flow directions in different depositional intervals of the Marnoso Arenacea turbiditic system of Miocene age outcropping in the northern Apennines of Italy. The well-exposed stratigraphic sections selected for this study are characterized by the presence of evident sedimentological indicators of paleocurrent direction (i.e., flute casts and ripple marks) at the base of the beds, which have been used to validate the AMS measurements. As we are also interested in determining which sediment composition and texture (grain size and sedimentary structures) work best for the application of the AMS method, distinct sandstone beds pertaining to different

depositional intervals (e.g, massive, laminated, and convoluted sandstones, debrites, as well as white marlstone beds separating turbiditic layers), have been selected for sampling by means of detailed sedimentological analyses.

Geological setting

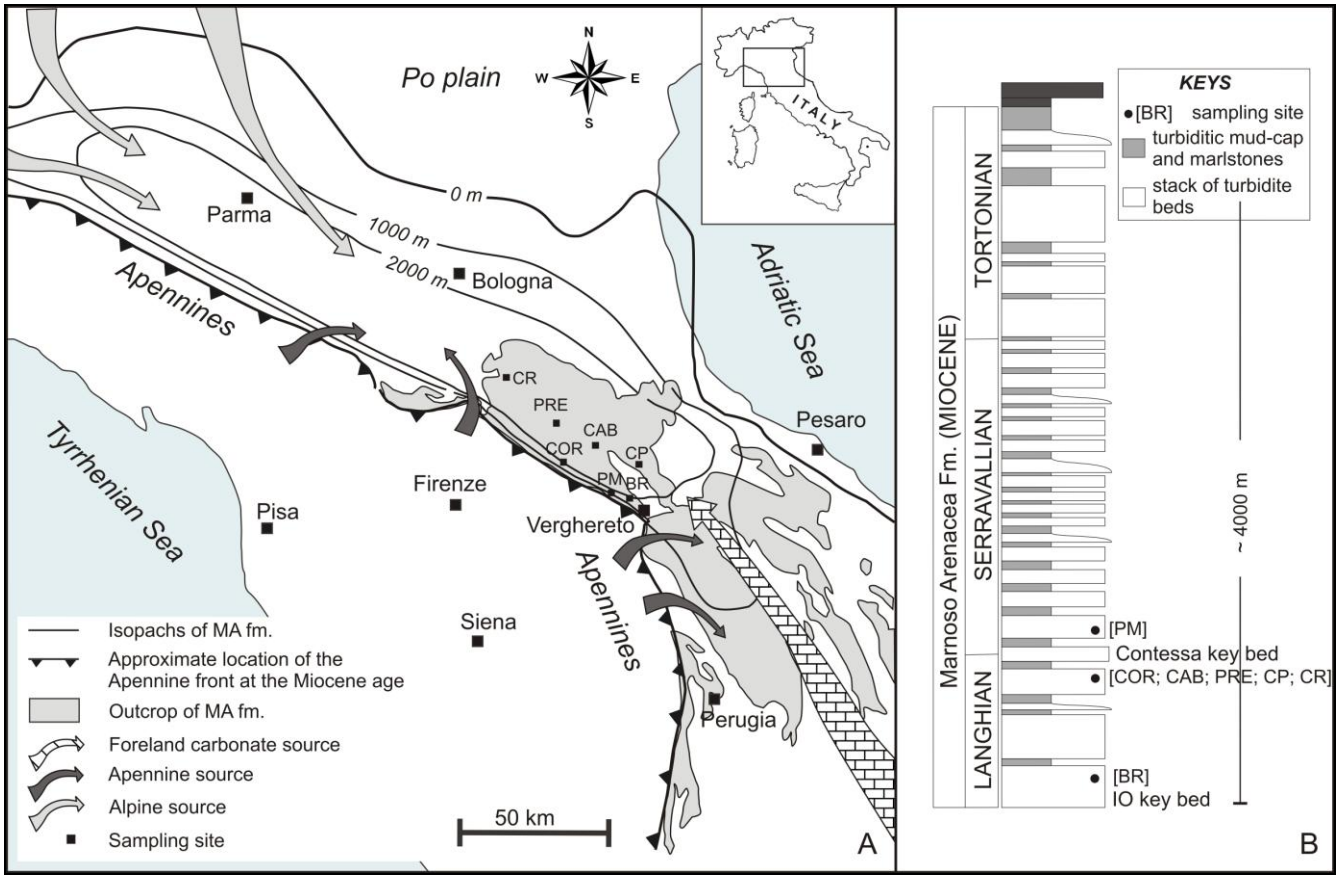

Fig 2.1 – A) Map showing the outcrop area and thickness of the Marnoso Arenacea Formation (after Argnani and Ricchi Lucchi, 2001; isopachs in the Po plain subsurface from Dondi et al., 1992) and location of the sampling sites (dots). Sediment sources were located mainly in the Alps but also the Apennines including foreland carbonate ramps in the south. B) Schematic stratigraphical log of the Marnoso Arenacea Formation.

The Marnoso Arenacea Formation (hereafter MA) is a non-channelized, mainly siliciclastic turbidite system (Ricci Lucchi and Valmori, 1980; Amy and Talling, 2006; Muzzi Megalhaes and Tinterri, 2010) that crops out extensively over an area 180 km long and 40 km wide in the northern Apennines from Emilia to Umbria (Fig. 2.1A), and it is partly buried under tectonic or sedimentary units both to the W and to the NE of its present outcrop area. The MA is a

composite, wedge-shaped turbidite succession representing the final filling of a Miocene migrating Apennine foredeep complex, which accumulated between the Langhian and the Tortonian (Ricci Lucchi and Valmori, 1980; Fig. 2.1B). Palinspastic restorations indicate an original width of the MA basin of about 140–90 km and a sediment thickness of up to 3 km (Ricci Lucchi, 1975; Boccaletti et al., 1990; Vai, 2001; Costa et al., 1998). The 1 km-ishopach (Dondi et al., 1982; Argnani and Ricci Lucchi, 2001) defines an elongate basin extending for at least 400 km along the Apennine front (Fig. 2.1A). To the southeast, the thickness of the MA decreases rapidly, suggesting the presence of a structural high within the southeastern (Umbrian) part of the basin (Argnani and Ricci Lucchi, 2001). Paleogeographic reconstructions as well as petrographic and paleocurrent analyses revealed longitudinal transport patterns within the elongated MA basin, fed mainly by Alpine (crystalline) sources through multiple entry points located to the N and W in present-day coordinates. Most paleocurrent directions measured at the base of turbidite beds indicate axial flows from the NW to the SE (in present-day coordinates; Fig. 2.1A). In addition, minor volumes of carbonate and hybrid turbidites, derived from shallow-water carbonate platforms located along the southern and southeastern margins of the basin, in the Gubbio area of Umbria (Fig. 2.1A), are also present (Gandolfi et al., 1983). These carbonate and hybrid turbidites flowed from the SE to the NW (in present-day coordinates), in the opposite direction of the aforementioned siliciclastic turbidites, and comprise key marker beds that allow high-resolution stratigraphic correlations. Furthermore, slumps and turbidite flows have been reported coming also from active thrust fronts located to the west of the basin (Ricci Lucchi, 1975). Scarcity of *in situ* benthic fossils prevents definite conclusions about paleobathymetry (most macrofossils and macroforaminifera quoted in literature appear reworked). Rare agglutinated foraminifera (Vai, 2001) and abundant bioturbations (McBridge and Picard, 1991; Monaco and Checconi, 2008; Monaco 2008) suggest a bathyal depth on the order of ~1000 m.

Siliciclastic turbidites make up about 90% of the fan lobe and basin-plain deposits, and are characterized by mudstone caps (Bouma's T_e division) representing 1/3 to 1/2 of each turbidite bed. Carbonate-rich marlstones contribute for the reminder 10% of the total sediment volume. Turbidites belong to two distinct classes (Ricci Lucchi and Valmori, 1980): (i) thin turbidites arranged in multilayered stacks, which tend to wedge-out and shale-out gradually down-current, and (ii) single turbidite beds of large volume and spatial extent referred to as basin-wide turbidites (or megaturbidites), which tend to maintain a virtually constant thickness (and sand/mud ratio) over distances of km to tens of km. These megaturbidites are multi-sourced and

constitute laterally traceable marker beds, such as the carbonate-rich *Contessa* megabed or the *Colombine* megaturbidites comprised of hybrid arenites, skeletal calcarenites, and marlstones.

Facies description

A ~60 m-thick stratigraphical interval comprised between the Contessa and the Fiumicello marker beds (Carta Geologica dell'Appennino Emiliano-Romagnolo 1:10.000) (Fig. 2.1B) have been selected for investigation. Seven stratigraphic sections (Fig. 2.1A), measured bed-by bed (Malgesini et al., 2009), have been sampled in different depositional intervals (*sensu* Harms, 1975; Walker, 1984), described hereafter.

Massive sandstones (Bouma's T_a interval). These intervals lack stratification and are characterized by a gradual normal grading (Amy and Talling, 2006). They are commonly interpreted as the product of deposition at rates of suspended load fallout high enough to suppress tractional transport (Arnott and Hand, 1989 Allen, 1991). Under these circumstances, quick dumping of sediment may occur in highly depletive flows (*sensu* Kneller and Branney, 1995) or rapidly waning flows. *En masse* freezing of a debris flow (Shanmugam, 1996) is not considered as an alternative mechanism to explain the absence of laminations in these graded sandstones. Although the massive beds used in the present study were selected carefully, it cannot be ruled out that some samples were collected from depositional intervals that appear massive by eye, but were formed in upper plane-bed or current ripple flow regimes.

Parallel-laminated sandstones (Bouma's T_b interval). These sandstones comprise alternations of laminae of different grain size, usually present at the top of stratified planar beds or massive beds with normal grading. Laminae formation is related to traction coupled with fall-out in upper flow regimes (Lowe, 1982; Ghibaudo, 1992).

Cross-laminated sandstones (Bouma's T_c interval). These sandstones are characterized by ripple-cross laminations related to traction coupled with fall-out under lower flow regimes conductive to ripples formation. They represent the final flow stages, in which flow density and velocity are sufficiently low for bedform development (Lowe, 1982; Ghibaudo, 1992).

Undulated sandstones. These medium-grained sandstones consist of a series of broad, symmetrical undulations, between 20 and 50 cm in wavelength and 2 to 4 cm in amplitude. The undulations are ~10 cm-thick, and generally occur above a graded basal division. They grade upward with decreasing amplitude into parallel laminae. The crests of the undulations are

roughly parallel to the sole mark directions. They are interpreted as longitudinal features and generated by upper flow regimes (Walker, 1967).

Convoluted sandstones. These medium- to fine-grained sandstones are characterized by the presence of convolute laminae with load structures. In some cases, a thick basal sandstone division with undulated and convoluted laminae passes directly into an upper mudstone unit through a medium-thick liquefied unit with contorted pseudonodules. There is usually a discrepancy between paleocurrent directions determined by flute casts at the base of the beds, and those determined by the vergence of convoluted folds. Convoluted laminae are often associated with ripples that indicate paleocurrents moving in the opposite direction of those indicated by the flute casts. Magalhaes and Tinterri (2010) interpreted this facies of the MA as being associated with cyclic wave loading related to shear stress caused by trains of moving internal waves.

Debrites. Debrites are non-graded, matrix-supported sandstones (Talling et al., 2004; Amy & Talling, 2006) showing chaotically distributed clasts in a swirly matrix fabric containing a percentage of mud variable from very low (less than 10%) to high (20 to 50%). The base of the debrites typically lack well-developed flutes and are often relatively flat or they display shallow linear grooves. Correlation of distant sections in the MA basin and elsewhere show that both mud-poor (sandy) debrites and mud-rich (muddy) debrites can extend laterally for up to 60 x 30 km and pinch-out abruptly in down-flow and cross-flow directions, in a fashion consistent with *en masse* deposition (Talling et al., 2004; Amy & Talling, 2006; Malgesini et al., 2009). Amy & Talling (2006) interpret debrites as cohesive flows with sufficiently high sediment concentration (either sand or mud) to inhibit segregation of particles of differential size. They use the term debris flow to denote flows from which such *en masse* deposition occurs.

White Marlstone (WM) beds. These beds sharply overlie Bouma's T_e intervals of turbiditic origin from which they can be distinguished by their texture, lighter color, greater carbonate content (25–45%; chiefly from planktonic foraminifera and coccoliths, and rare benthic foraminifera), and lesser total organic content (~1 % T.O.C versus ~2 % T.O.C of the Bouma's T_e divisions). Their thickness is on the order of < 20 cm, rarely exceeding 50 cm, and the grain size is comprised between mud and silt. They are characterized by a massive, speckled, and generally featureless aspect with rare primary laminations (partially destroyed by bioturbation), and centimetre- to decimetre-scale color banding reflecting subtle compositional variations. The WM beds appear widespread in the basin plain and are commonly interpreted as hemipelagites

(Mutti and Ricci Lucchi, 1972, 1975; Rupke, 1976; Mutti, 1977, 1979; Mutti and Johns, 1979; Talling et al., 2007).

The anisotropy of magnetic susceptibility

After the pioneering work of Rees (1965), several authors applied the AMS to study paleocurrents in sedimentary rocks, obtaining useful results especially in sediments of appropriate grain size, usually clay and fine sand (Galehouse, 1968; Hamilton and Rees, 1970; Argenton et al., 1975; Taira and Scholle, 1979; Hiscott & Middleton, 1980; Ledbetter and Ellwood, 1980; Knode et al., 1990; Schieber and Ellwood, 1993; Tarling and Hrouda, 1993; Hiscott et al., 1997; Liu et al., 2001; Liu et al., 2005; Pares et al., 2007; Veloso et al., 2007; Baas et al., 2007). The AMS is considered to be a proxy for the preferred alignment of natural magnetic particles attained in the final stages of sediment transport, with the maximum susceptibility axis, k_{max}, and the minimum susceptibility axis, k_{min}, approximating the preferred orientation of the longest and shortest magnetic grain axes, respectively (e.g., Hamilton and Rees, 1970; Taira and Scholle, 1979; Tarling and Hrouda, 1993; Borradaile et al., 1999). This method is based on the fact that a current is able to orient paramagnetic grains (e.g., phyllosilicates, olivines, pyroxenes, anphiboles), diamagnetic grains (e.g., quartz, calcite, feldspars), and ferromagnetic (*sensu lato*) grains (e.g., magnetite, goethite, hematite), and that the resulting AMS ellipsoid (Fig. 2.2) reflects the orientation imparted by the current to such grains (e.g., Ellwood, 1980; Lowrie and Hirt, 1987; Taira, 1989; Sagnotti and Meloni, 1993; Parés et al., 2007).

For example, during deposition of phyllosilicates, which are very common in siliciclastic turbidites, the grain's short shape axis falls perpendicular to the bedding plane. As a result, an oblate fabric develops (well-developed foliation). The AMS fabric mimics this because in phyllosilicates the short shape axis corresponds to the crystallographic c-axis as well as to the minimum susceptibility direction, and therefore a magnetic foliation (defined by the plane containing k_{max} and k_{int}), develops parallel to the depositional surface. When currents are present (Fig. 2.2), hydraulic forces control grains alignment (current-induced fabric; Shor et al., 1984). The long shape axis of elongated paramagnetic grains, as well as of large ferromagnetic grains, lines up either parallel or perpendicular to the current direction in case of moderate or high hydrodynamic regimes, respectively. The AMS fabric reflects this because in such elongated

grains, the maximum susceptibility axis commonly lies broadly along the particle length. Consequently, a magnetic lineation can develop as revealed by a clustering of the k_{max} axes either parallel or perpendicular to the current direction depending on the hydrodynamic boundary conditions.

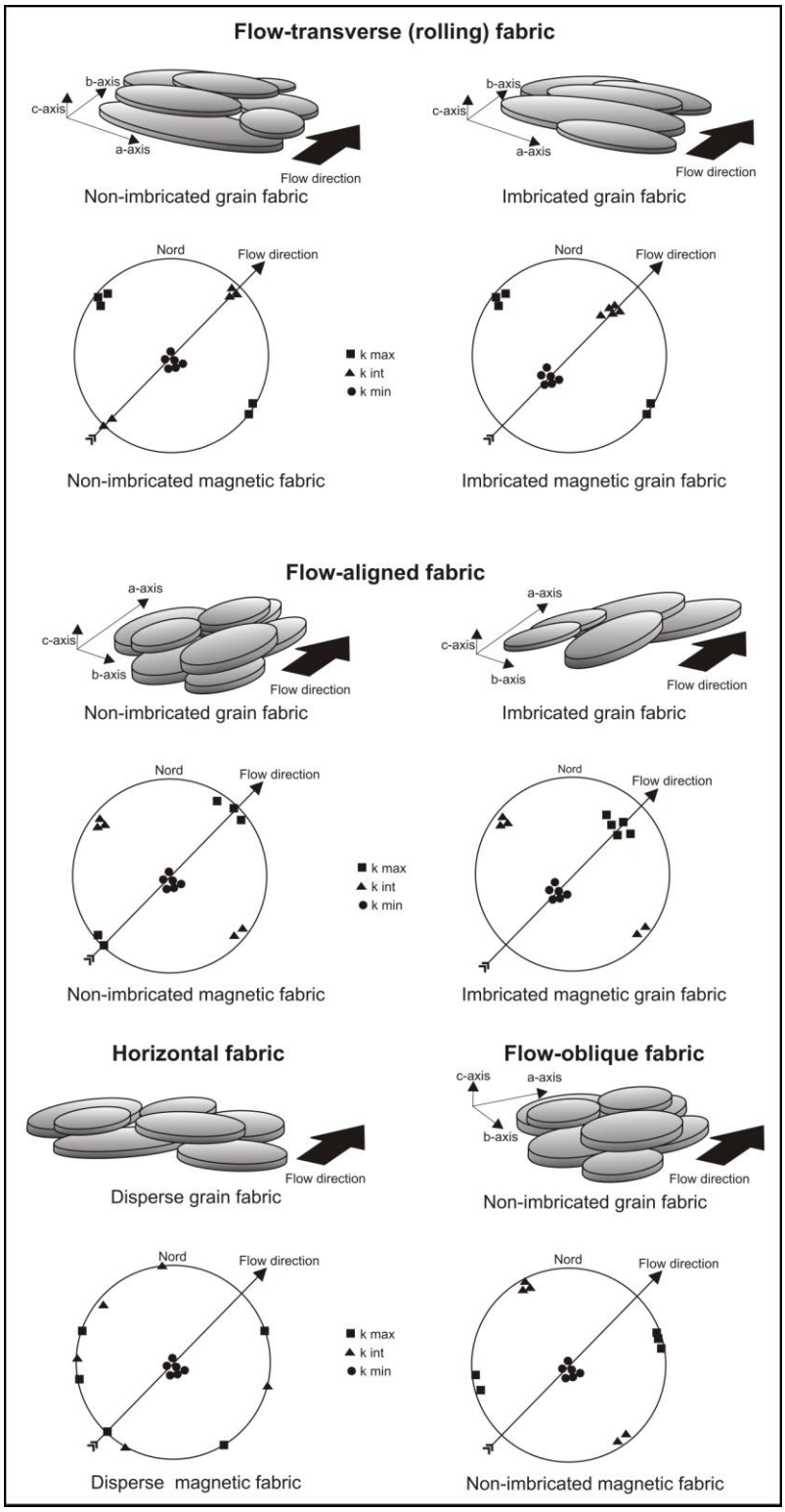

Fig 2.2 - Main types of anisotropic grain shape fabrics, presented by schematic drawings of the orientation of elongated grains and by the orientation of the three principal orthogonal axes in upper hemisphere stereograms. For the types of fabric shown, non-imbricated and imbricated subtypes are shown on the left- and right-hand side, respectively. Horizontal fabric is non-imbricated by definition. a=long grain axis; b=grain axis of intermediate length; c=short grain axis.

Conversely, settling in still water produces an horizontal fabric (Fig. 2.2) with minimum susceptibility axes clustered around the pole to the depositional plane within which maximum and intermediate susceptibility axes are uniformly dispersed, defining a planar, near-horizontal, gravity-induced settling fabric (Ellwood, 1980; Tarling and Hrouda, 1993; Pares et al., 2007).
After deposition, the fabric may be affected by compaction, bioturbation, and disruption by migration of trapped fluids and/or gas, or by tectonic deformation. Thus, studies of the AMS fabric can also provide information on post-depositional processes.

Sampling and methods

Data have been acquired according to the following procedure.
1) In order to obtain a direct estimate of flow directions, we measured with a magnetic compass the orientation of flute casts at the base of turbidite beds (Fig. 2.3A and B). Flute marks can be represented by protuberances in the actual sandstone bed or hollows in the underlying mud layer (Rich, 1950), and are produced by a current in its initial (high energy) stages when erosion can take place. Their long axis is oriented parallel to the average current direction (Kuenen, 1957) and their shape is asymmetric, allowing to distinguish between up- and down-current direction.
2) Samples for AMS and other paleomagnetic analyses have been collected with a water-cooled rock drill and oriented with a magnetic compass in different depositional facies within 7 distinct stratigraphic sections (Fig. 2.1). Selected marker beds were sampled in multiple sections to study grains' orientation up- and down-current within the same flow unit. Cylindrical samples have been reduced in the laboratory to standard ~10 cm^3 dimension.
3) AMS analyses have been carried out on 551 samples with a KLY-3 Kappabridge adopting the standard measurement scheme illustrated in Agico KLY-3 User's Guide (1998). A susceptibility tensor was then fit to the data by means of least square analysis, and the errors of the fit were calculated using multivariate statistics (Agico KLY-3 User's Guide, 1998). Susceptibility tensors were subsequently rotated into tilt-corrected coordinates using site-mean bedding attitudes, and then plotted on stereographic projections.
4) In order to estimate the contribution of ferromagnetic (s.l.) particles to the AMS, the anisotropy of isothermal remanent magnetization (AIRM) (Tarling & Hrouda, 1993) was measured on 43 cylindrical samples. Each sample was AF-demagnetized in a field of 50 mT with a Molspin tumbler demagnetizer, then magnetized along a given direction in a direct field of 20

mT with a PUM-1 Agico Pulse Magnetizer, and, finally, the induced magnetic remanence was measured on a Agico JR6 spinner magnetometer; this procedure was applied for each sample along 12 different directions. The AIRM data have then been rotated into tilt-corrected coordinates using site-mean bedding attitudes, and then plotted on stereographic projections for comparison with the AMS plots.

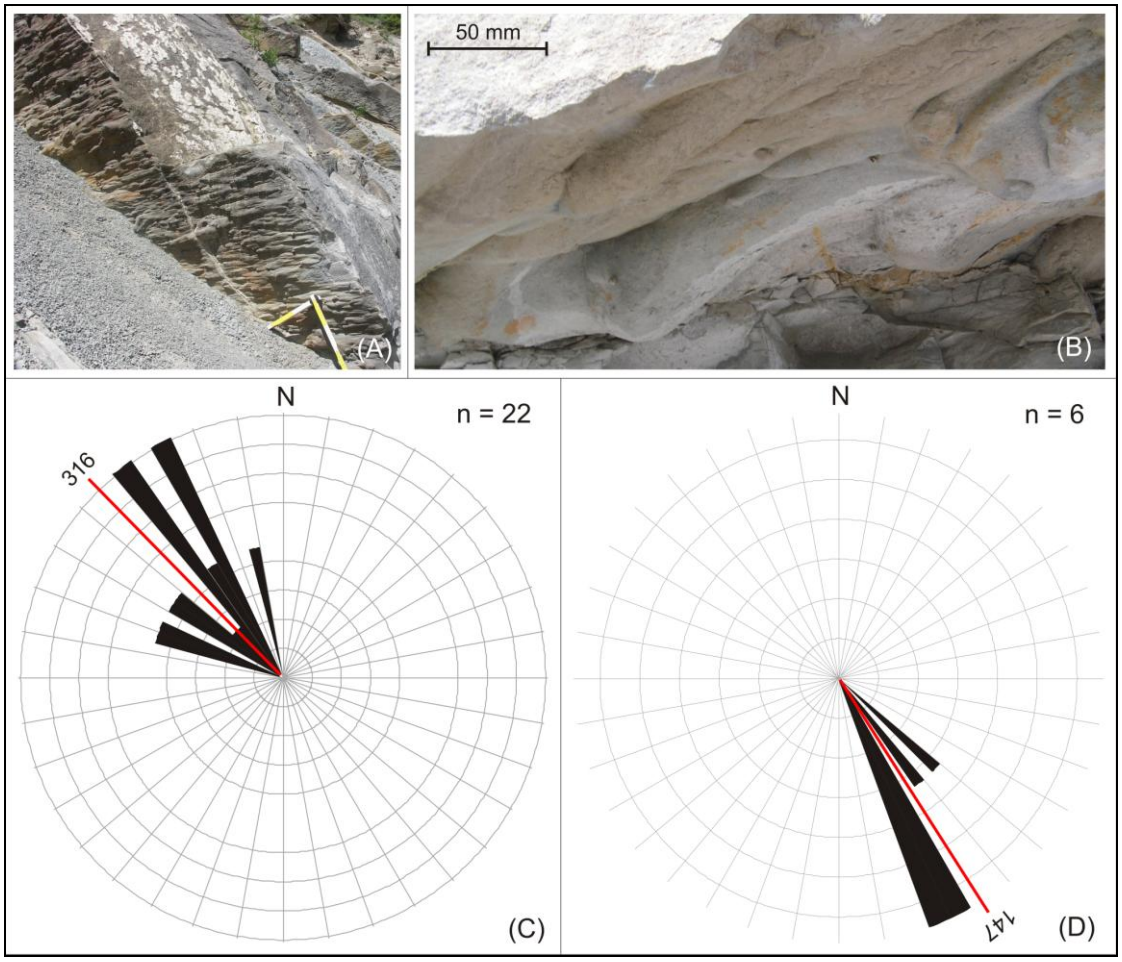

Fig. 2.3 – In situ measurements of flute marks present at the base of turbiditic beds (panels A and B) allowed reconstructing average paleocurrent directions from the NW (316°E) in siliciclastic turbidites (panel C) and from the SE (147°E) in carbonatic and hybrid turbidites (panel D); N = geographic north, n = number of measurements. See text for discussion.

5) The nature of the ferromagnetic (s.l.) has been determined by means of isothermal remanent magnetization (IRM) acquisition curves and thermal demagnetization of a 3-component IRM (Lowrie, 1990). IRM curves have been obtained for 23 samples by imparting a magnetizing field progressively increasing from 10 mT to 2.5 T with a ASC Scientific Pulse Magnetizer IM 10-30, and measuring the induced remanence after each magnetizing step with a 2G Enterprises 755

DC-SQUID cryogenic magnetometer. The same samples, magnetized in three orthogonal directions in fields of 2.5 T, 0.4 T and 0.1 T, have then been subjected to thermal demagnetization up to 670 °C with the magnetic remanence measured after each magnetizing step with a 2G Enterprises 755 DC-SQUID cryogenic magnetometer.

6) Thin sections have been cut parallel and perpendicular to the flow direction (determined by flute casts) for optical scrutiny and image analysis using ImageJ software (Rasband, 2008).

7) To define amount and sense of vertical-axis tectonic rotations of Apennine thrust sheets, and restore AMS and AIRM data to a pre-rotation paleogeography, the natural remanent magnetization (NRM) of the sediments has been studied by thermally demagnetizing a total of 157 fresh samples in increasing steps from room temperature up to 450 °C, and measuring the NRM after each heating step with a 2G Enterprises 755 DC-SQUID cryogenic magnetometer. Magnetic components of the NRM were calculated using standard least-square analysis on linear portions of the demagnetization diagrams and plotted on equal-area projections in *in situ* and tilt-corrected coordinates. All paleomagnetic analyses were carried out at the Alpine Laboratory of Paleomagnetism of Peveragno, Italy.

Data and interpretation

Measurements of flute-casts (Fig. 2.3A and B) at the base of the sampled beds indicate that siliciclastic turbidites flowed from the NW (316°E) to the SE (136°E) (average of 22 measurements; Fig. 2.3C), whereas carbonatic and hybrid turbidites flowed from the SE (147°E) to the NW (327°E) (average of 6 measurements; Fig. 2.3D), i.e., opposite to the siliciclastic turbidites. Tilt-corrected AMS axes of siliciclastic turbidite sites have been rotated into a common reference flow direction of 316-136°E, whereas tilt-corrected AMS axes of carbonatic and hybrid turbidite sites have been rotated into a common reference direction of 147-327°E to ease data comparison at the basin scale. For example (Fig. 2.4), siliciclastic turbidite sites CP2 and COR4a are characterized by actual flow directions from flute-casts of 328°E and 293°E, respectively, and well-grouped magnetic susceptibility axes (k_{max}, k_{int}, k_{min}) that we rotated by 12° counter-clockwise and 23° clockwise, respectively, into the reference mean flow direction of 316°E.

AMS data for the different sampled facies are summarized in Table 2.1 and described in detail hereafter.

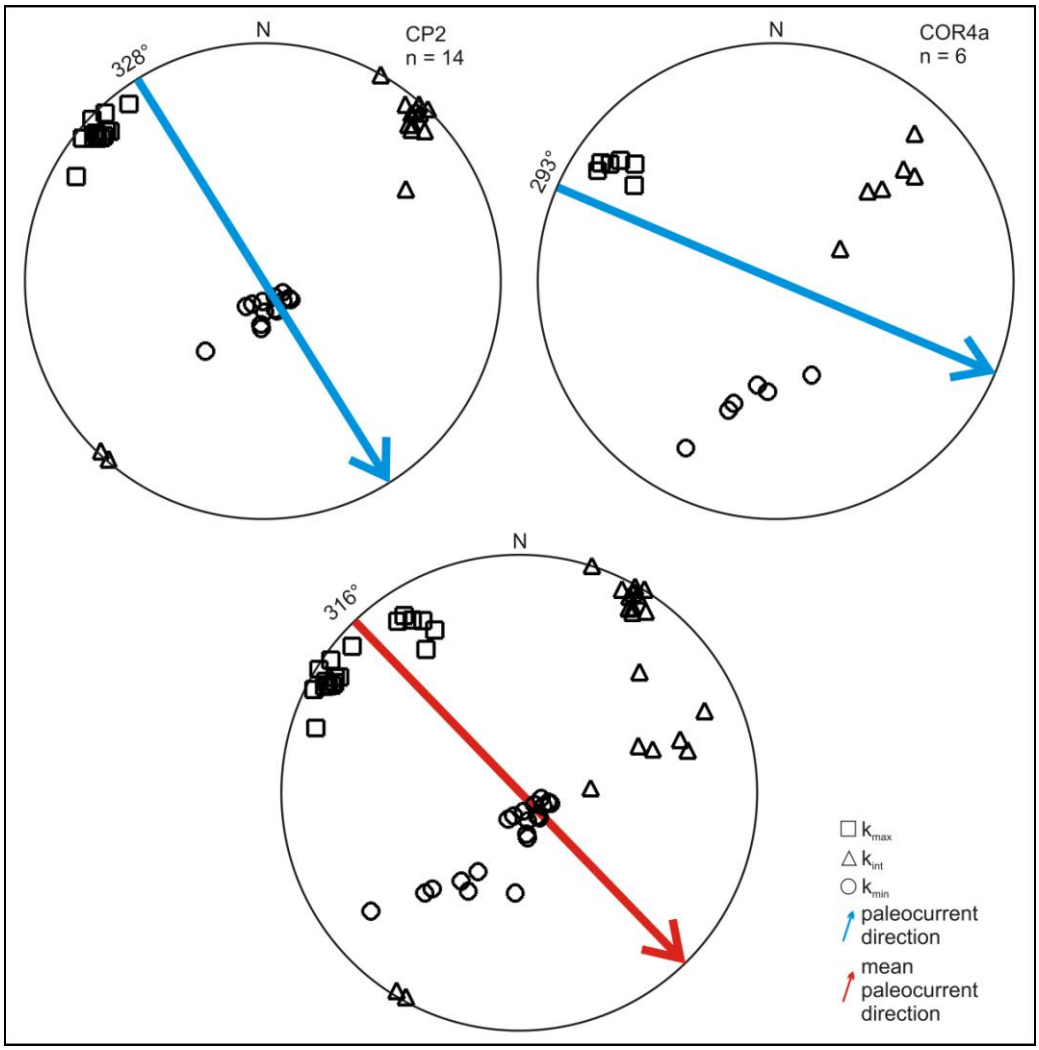

Fig. 2.4 – Example of procedure followed to rotate tilt-corrected AMS axes into a common reference direction to ease data comparison at the basin scale. Siliciclastic turbidite sites CP2 and COR4a are characterized by actual flow directions from flute-casts of 328°E and 293°E, respectively; the associated magnetic susceptibility axes have been rotated by 12° counter-clockwise and 23° clockwise, respectively, into the reference mean flow direction of 316°E. See text for discussion.

Massive sandstones (Bouma's T_a interval). *Siliciclastic massive sandstones* coming from the NW (Fig. 2.5A), sampled at 6 sites in 5 sections (n = 49 samples), are characterized by well clustered k_{max} axes with an overall mean direction (302°E) slightly departing (by ~14°) from the overall mean paleocurrent direction from flute-casts (316°E) (Fig. 2.5A). These features suggest relatively low density suspensions with clasts transported by traction and rapidly deposited in flow-aligned (slightly oblique) fabrics. Imbrication angles of ~10° and dipping up-current (i.e., to the NW) have been observed at a few sites (BO1c, CAB2b, COR4a, GIU1b; Fig. 2.6A, B, C, D). This feature confirms that these siliciclastic turbidites flowed from the NW to the SW. *Carbonatic and hybrid massive sandstones* coming from the SE (Fig. 2.5B), sampled at 3 sites in

3 sections (n = 31 samples), show a greater dispersion of the k_{max} axes if compared to the siliciclastic sandstones. An overall mean direction (307°E) departing (by ~20°) from the mean paleocurrent direction from flute-casts (327°E) has been measured (Fig. 2.5B). Similar disordered/oblique fabric has been described in many massive sandstones (Baas et al., 2007), and could be caused by high apparent viscosity due to high near-bed sediment concentrations combined with frequent clast collisions during rapid settling from suspension. The different behavior between siliciclastic and carbonatic sandstones is probably related to the different composition and concentration of the paleoflows.

Parallel-laminated sandstones (Bouma's T_b interval). *Siliciclastic parallel-laminated sandstones* coming from the NW (Fig. 2.5C), sampled at 14 sites in 7 sections (n = 141 samples), are characterized by well clustered k_{max} axes with an overall mean direction (301°E) slightly departing (by ~15°) from the overall mean paleocurrent direction from flute-casts (316°E) (Fig. 2.5C); imbrication angles ranging between 10° and 25° and dipping up-current (i.e., to the NW), have been observed only at sites CP5, GIU1a and PRE2 (Fig. 2.6E, F, G). *Carbonatic and hybrid parallel-laminated sandstones* coming from SE (Fig. 2.5D), sampled at 5 sites in 4 sections (n = 48 samples), show the same behavior. They are characterized by well clustered k_{max} axes with an overall mean direction (127°E) slightly departing (by ~20°) from the overall mean paleocurrent direction from flute-casts (147°E) (Fig. 2.5D).

The substantially flow-aligned magnetic fabric reflects the dominance of rapid sedimentation from suspension on tractional transport of clasts. The generation and preservation of plane-parallel laminations require bed load transport as well as suspension settling. Bed load particles are typically oriented with their major axes perpendicular to the main flow direction, whereas particles transported in suspension mostly have their major axis parallel to the main flow direction. Moreover, Rusnak (1957) found that bed load grains tend to pivot before coming to rest in a flow-aligned orientation.

Ripple cross-laminated sandstones (Bouma's T_c interval). These sandstones (Fig. 2.5E and F), sampled at 8 sites in 4 sections (n = 74 samples), are characterized by a dispersion on the horizontal plane of the k_{max} axes. The overall mean direction slightly departs (by ~39° for siliciclastic sandstones coming from the NW and by ~5° for the carbonatic and hybrid sandstones coming from SE) from the overall mean paleocurrent direction from flute-casts, but aboveall in the carbonatic and siliciclastic sandstones no clustering can be observed. These features reflect the dominance of grain avalanche processes on the leeward slip face of current ripples, associated with migrating bed forms. Avalanching involves particle transport in the form

of grain flows, which are known to produce deposits with flow-aligned fabric and relatively high imbrication angles (Rees, 1968; 1983; Allen, 1984). Concentrated suspensions were maintained by dispersive pressure caused by collisions (Lowe, 1982). In these circumstances, grains tend to align to minimize angular momentum transfer caused by collisions. This results in a preferred orientation with the long shape axes parallel to the movement direction and the short shape axes near the direction of maximum velocity gradient (Rees, 1968). Obviously, deposition of suspension load may also contribute to the dominance of flow-aligned fabric, particularly in intervals with steeply climbing ripples. Rolling grain transport is most frequent on the gentle stoss (up-current) side of ripples. In most cases, however, this part of the ripple profile is not preserved, hence the lack of flow-transverse fabric in Bouma's T_c divisions. Flow-aligned fabrics in Bouma's T_c divisions show relative high circular variance if compared with Bouma's T_a and T_b intervals as a result of local variations in flow direction over current ripples with sinuous and linguoid crest lines.

Some ripple cross-laminated sandstones sampled in the Castel del Rio section (CR in Fig. 2.1) and in the Passo Mandrioli section (PM in Fig. 2.1) show k_{max} axes aligned at high angles relative to the paleoflow direction measured by flute casts at the base of the turbidite beds. Figure 2.7 illustrates an example of such discrepancy in the Contessa carbonatic megabed at Castel del Rio. This discrepancy, confirmed by measurements of paleoflow direction from ripple crests alignment, can be related to a partial flow rebound as the result of successive deflections of turbidity currents against the basin margins or intrabasinal highs (Magalhaes and Tinterri; 2010).

***Undulated sandstones*.** These sandstones (Fig. 2.5G), sampled at 4 sites from 4 sections (n = 32 samples), are characterized by most of k_{max} axes oriented within ~15° from the overall mean paleocurrent direction (Fig. 2.5G); a subordinate mode occurs at ~90° of the mean paleocurrent direction, consistent with pronounced flow-transverse fabric. The gradual upward decrease in amplitude of undulations within the beds, and the continuity of lamination across undulations, indicate a gradually decreasing energy regime during deposition. This variation in flow velocity can explain the coexistence of a broad range of k_{max} orientations: a flow-aligned orientation is easily changed into a more stable flow-transverse orientation when the flow becomes strong enough to lift deposited grains and allow them to roll and jump on the bedding plane (Schwarzacher, 1963; Johansson, 1964; Hendry, 1976).

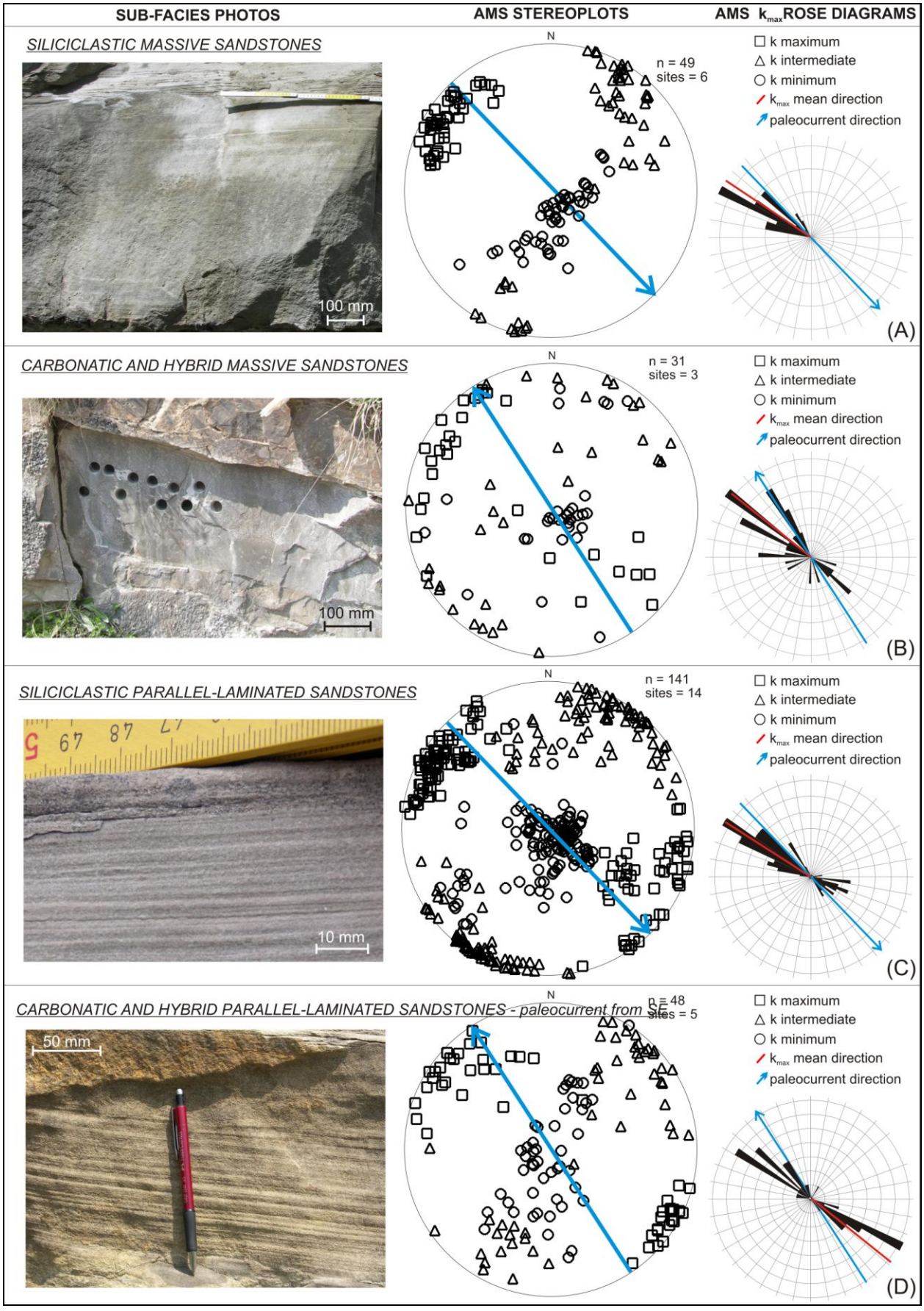
SUB-FACIES PHOTOS
AMS STEREOPLOTS
AMS k_{max} ROSE DIAGRAMS
SILICICLASTIC MASSIVE SANDSTONES
100 mm
N
n = 49
sites = 6
k maximum
k intermediate
k minimum
k_{max} mean direction
paleocurrent direction
(A)
CARBONATIC AND HYBRID MASSIVE SANDSTONES
100 mm
N
n = 31
sites = 3
k maximum
k intermediate
k minimum
k_{max} mean direction
paleocurrent direction
(B)
SILICICLASTIC PARALLEL-LAMINATED SANDSTONES
10 mm
N
n = 141
sites = 14
k maximum
k intermediate
k minimum
k_{max} mean direction
paleocurrent direction
(C)
CARBONATIC AND HYBRID PARALLEL-LAMINATED SANDSTONES - paleocurrent from SE
50 mm
N
n = 48
sites = 5
k maximum
k intermediate
k minimum
k_{max} mean direction
paleocurrent direction
(D)

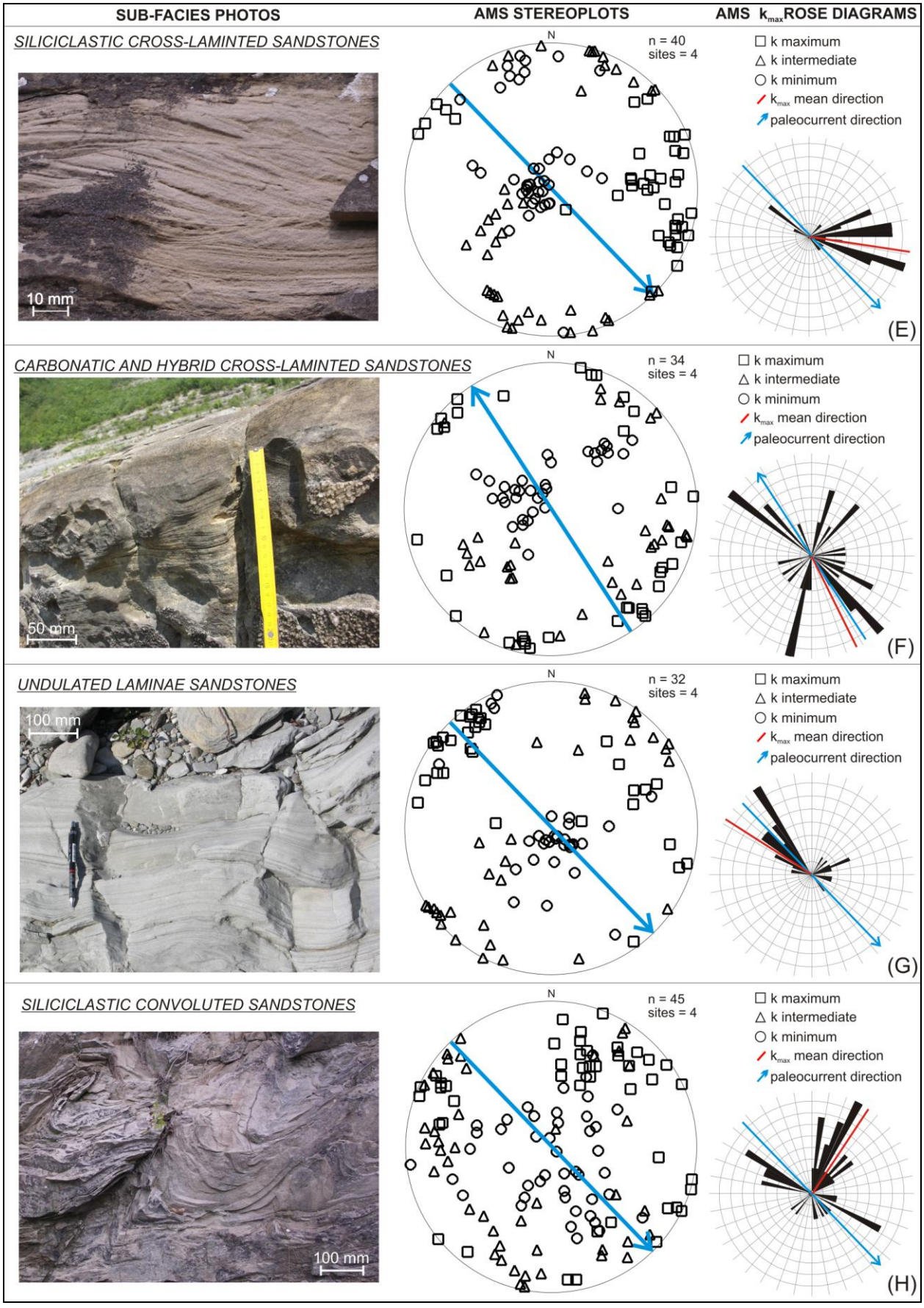
SUB-FACIES PHOTOS
AMS STEREOPLOTS
AMS k_{max} ROSE DIAGRAMS
SILICICLASTIC CROSS-LAMINTED SANDSTONES
10 mm
N
n = 40
sites = 4
k maximum
k intermediate
k minimum
k_{max} mean direction
paleocurrent direction
(E)
CARBONATIC AND HYBRID CROSS-LAMINTED SANDSTONES
50 mm
N
n = 34
sites = 4
k maximum
k intermediate
k minimum
k_{max} mean direction
paleocurrent direction
(F)
UNDULATED LAMINAE SANDSTONES
100 mm
N
n = 32
sites = 4
k maximum
k intermediate
k minimum
k_{max} mean direction
paleocurrent direction
(G)
SILICICLASTIC CONVOLUTED SANDSTONES
100 mm
N
n = 45
sites = 4
k maximum
k intermediate
k minimum
k_{max} mean direction
paleocurrent direction
(H)

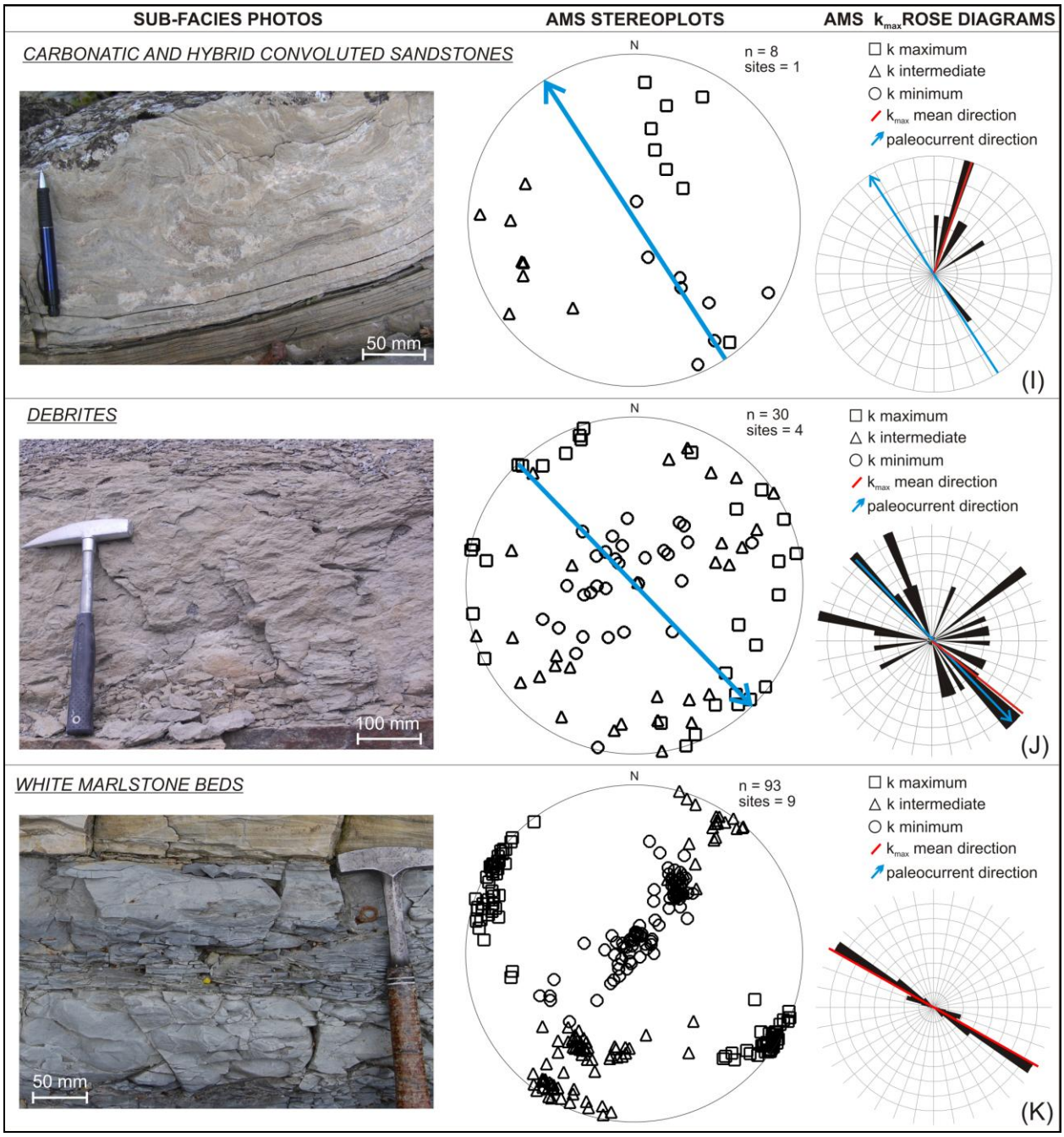

Fig. 2.5 – From left to the right: photographs of sampled turbiditic sub-facies, the associated AMS stereoplots, and rose diagrams with indication of the average direction of the maximum susceptibility axes (red lines) compared to the reference mean flow directions from flute-casts, which are from 316°E for siliciclastic turbidites and from 147°E for carbonatic and hybrid turbidites (blue arrows). The axes of magnetic susceptibility (kmax = squares, kint = triangles, kmin = circles) are plotted in tilt-corrected coordinates; N = geographic north; sites = number of sites; n = number of samples. (A) siliciclastic massive sandstones; (B) carbonatic and hybrid massive sandstones; (C) siliciclastic parallel-laminated sandstones; (D) carbonatic and hybrid parallel-laminated sandstones; (E) siliciclastic ripple cross-laminated sandstones; (F) carbonatic and hybrid ripple cross-laminated sandstones; (G) undulated sandstones; (H) siliciclastic convoluted sandstones; (I) carbonatic and hybrid convoluted sandstones; (J) debrites; (K) white marlstone beds.

Table 2.1 - AMS parameters of the sub-facies shown in Figure 2.5; n: number of samples per site; Kmean = mean susceptibility; kmax = maximum susceptibility; kint = intermediate susceptibility; kmin = minimum susceptibility; L = magnetic lineation; F = magnetic foliation; kmax direction: direction of the maximum axes on the stereoplot; σ = standard deviation.

SAMPLE	n	K_{mean} ± σ [+10E-6 SI]	k_{max} ± σ [+10E-6 SI]	k_{int} ± σ [+10E-6 SI]	k_{min} ± σ [+10E-6 SI]	L ± σ	F ± σ	k_{max} direction ± σ [°]
siliciclastic massive sandstones	49	134.71 ± 61.12	137.41 ± 62.90	134.87 ± 61.23	131.85 ± 59.26	1.017 ± 0.008	1.022 ± 0.014	302.67 ± 13.51
carbonatic and hybrid massive sandstones	31	134.71 ± 61.12	137.41 ± 62.90	134.87 ± 61.23	131.85 ± 59.26	1.017 ± 0.008	1.022 ± 0.014	259.29 ± 76.87
siliciclastic parallel laminated sandstones	141	134.71 ± 61.12	137.41 ± 62.90	134.87 ± 61.23	131.85 ± 59.26	1.017 ± 0.008	1.022 ± 0.014	237.44 ± 90.10
carbonatic and hybrid parallel laminated sandstones	48	134.71 ± 61.12	137.41 ± 62.90	134.87 ± 61.23	131.85 ± 59.26	1.017 ± 0.008	1.022 ± 0.014	222.74 ± 99.89
siliciclastic cross laminated sandstones	40	134.71 ± 61.12	137.41 ± 62.90	134.87 ± 61.23	131.85 ± 59.26	1.017 ± 0.008	1.022 ± 0.014	118.76 ± 73.37
carbonatic and hybrid cross laminated sandstones	34	134.71 ± 61.12	137.41 ± 62.90	134.87 ± 61.23	131.85 ± 59.26	1.017 ± 0.008	1.022 ± 0.014	162.10 ± 95.56
undulated sandstones	32	147.96 ± 56.41	151.70 ± 58.08	148.55 ± 56.54	143.64 ± 54.67	1.020 ± 0.008	1.033 ± 0.019	231.70 ± 113.78
siliciclastic convoluted sandstones	45	129.87 ± 39.79	132.70 ± 41.62	130.14 ± 40.64	126.17 ± 37.15	1.014 ± 0.006	1.031 ± 0.019	123.36 ± 111.02
carbonatic and hybrid convoluted sandstones	8	128.45 ± 32.43	131.43 ± 34.01	129.67 ± 33.42	124.25 ± 29.87	1.013 ± 0.005	1.040 ± 0.020	38.25 ± 45.13
debrites	30	152.79 ± 13.83	155.81 ± 14.21	152.99 ± 14.06	149.57 ± 13.30	1.019 ± 0.009	1.023 ± 0.010	188.05 ± 104.54
WM beds	93	157.73 ± 26.48	161.37 ± 27.70	158.45 ± 27.07	153.38 ± 24.75	1.018 ± 0.005	1.032 ± 0.018	214.11 ± 86.96

***Convoluted sandstones*.** These sandstones, sampled at 5 sites from 2 sections (n = 53 samples), are characterized by highly dispersed magnetic susceptibility axes (Fig. 2.5H and I). While highly scattered, the susceptibility axes are not randomly distributed whereby they tend to define a flow-transverse fabric with mean k_{max} direction rotated clockwise by ~90° in siliciclastic sandstones and by ~51° in carbonatic and hybrid sandstones from the reference mean paleoflow direction from flute casts (316°E in siliciclastic sandstones and 327° in carbonatic and hybrid sandstones) (Fig. 2.5H). A similar discrepancy in the same facies has been observed by Magalhaes and Tinterri (2010) between paleocurrent directions determined from flute casts and from the vergence of convoluted folds, and interpreted as the result of successive deflections of turbidity currents against the basin margins or intrabasinal highs. Imbrications of k_{max} axes by 10°–20° down-current observed in several sites (CAB2c, CR4, CR6, CR7; Fig. 2.6H, I, J, K) can be related to the presence of shear waves (i.e. cyclic wave loading related to shear stress caused by trains of moving internal waves in high-density turbidity currents; Magalhaes and Tinterri, 2010) that may affect the imbrication angle of elongated grains at or close to the bedding plane, even producing down current imbrications (Sakai et al., 2002).

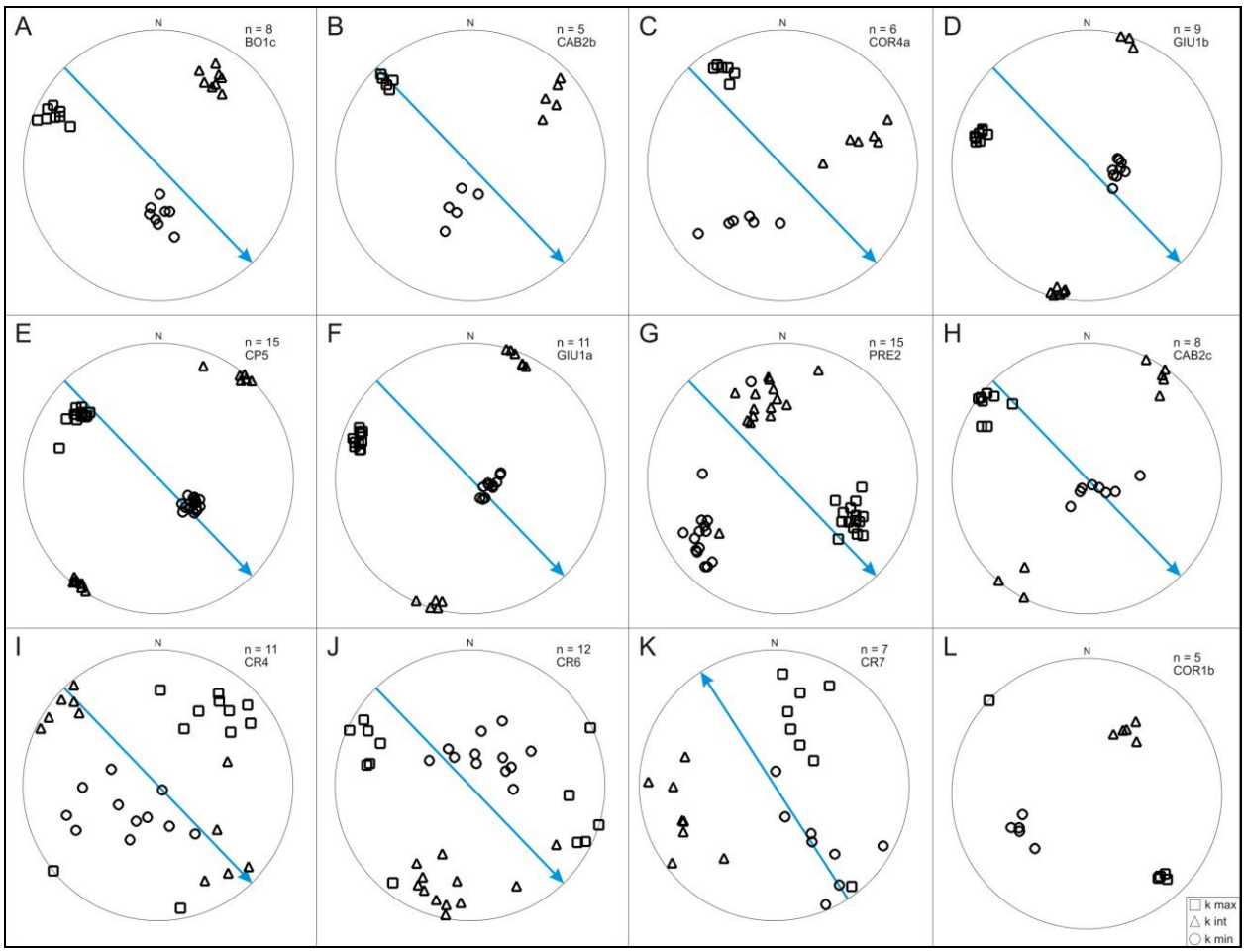

Fig. 2.6 – Stereographic projections of the principal axes of magnetic susceptibility (kmax = squares, kint = triangles, kmin = circles) in tilt-corrected coordinates of sites characterized by magnetic imbrication. The blue arrows represent the reference mean paleocurrent directions from flute casts (316°E for siliciclastic turbidites and 147°E for carbonatic and hybrid turbidites). [N = geographic north; n = number of samples; BO1c, etc. = site name].

Debrites have been sampled at 4 sites from 3 sections (n = 30 samples), and show AMS fabrics that are generally disordered or sometimes slightly flow-aligned (Fig. 2.5J). These results can be explained considering that in debrites (*sensu* Talling et al., 2004; Amy & Talling, 2006), clasts tend to be only weakly flow-aligned (e.g., Lindsay, 1968; Hiscott et al., 1997), particularly in the basal zone of shearing (Bouma and Pluenneke, 1975; Enos, 1977). A disordered fabric may arise from high flow viscosity combined with frequent clasts collisions during rapid settling from suspension. However, local hydraulic conditions govern whether grains can retain highly scattered to isotropic fabrics or can be reoriented into a more stable flow-aligned fabric before final settling.

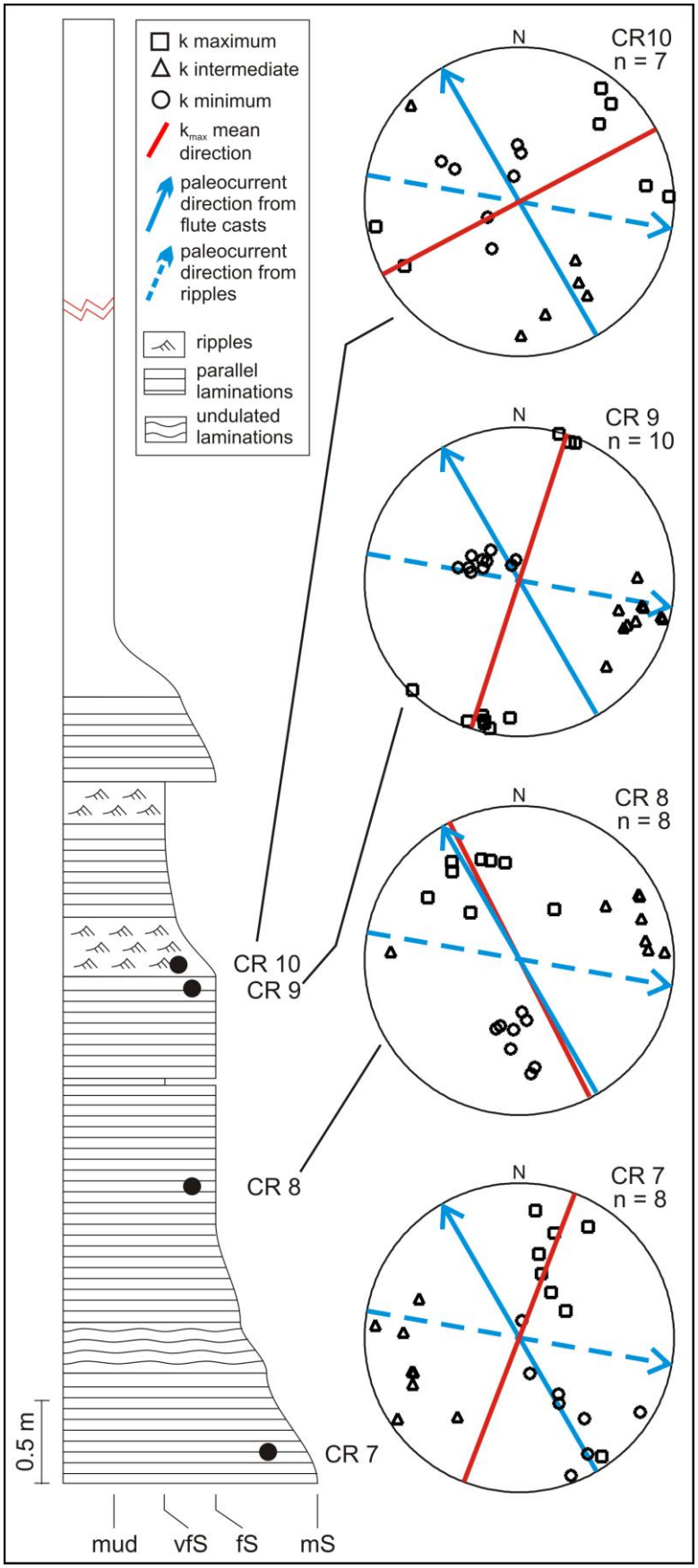

Fig. 2.7 – Stratigraphic log of the Contessa carbonatic megabed in the Castel del Rio section and the associated AMS stereoplots with indication of k_{max} orientation (red line) compared to the actual flow directions from flute-casts (150°E; blue arrow) as well as the paleoflow direction inferred from ripple marks (280°E, blue dashed arrow). Vertical variations in paleoflow directions throughout the megabed are apparent.

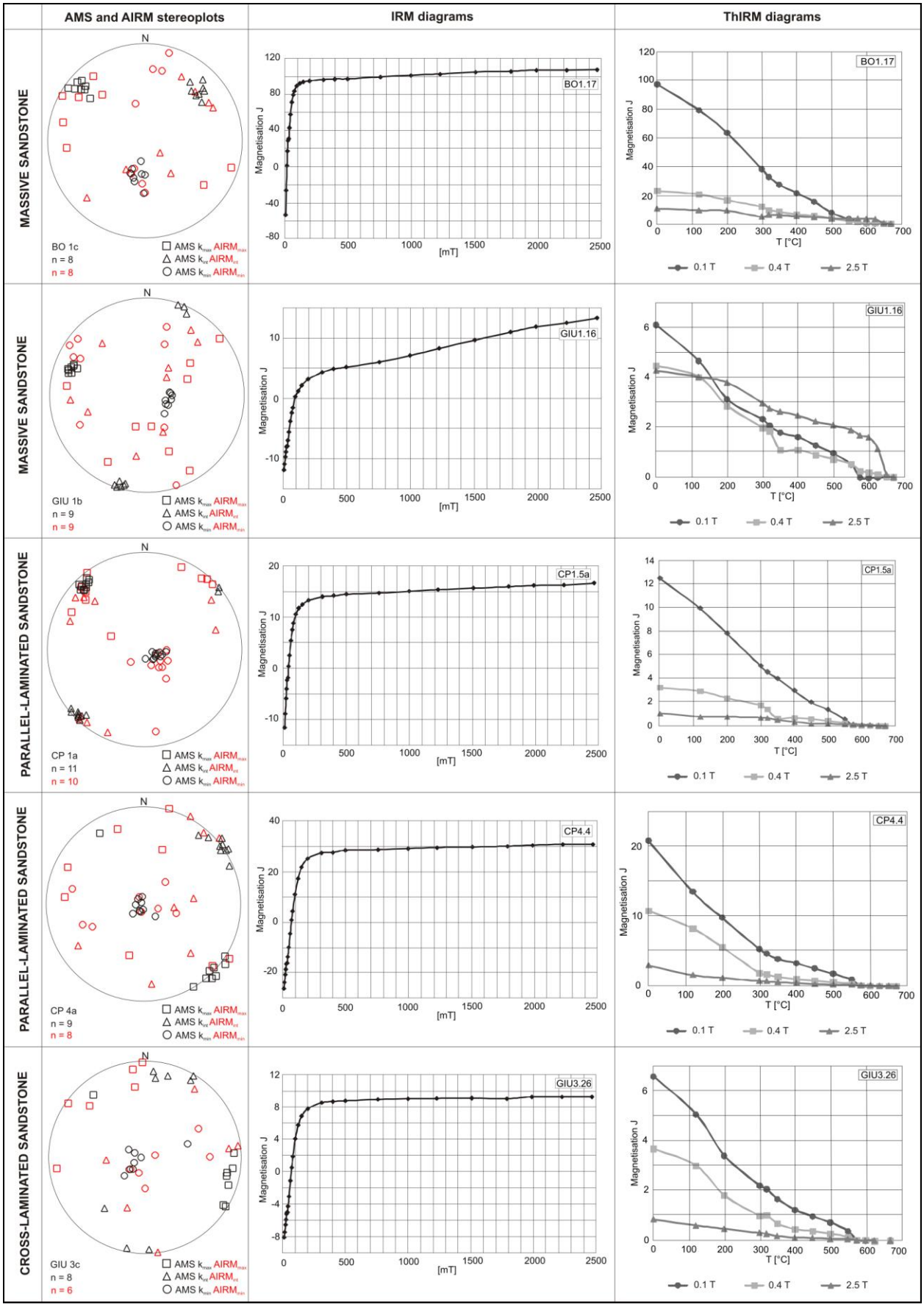
AMS and AIRM stereoplots
IRM diagrams
ThIRM diagrams
MASSIVE SANDSTONE
BO 1c
n = 8
n = 8
BO1.17
MASSIVE SANDSTONE
GIU 1b
n = 9
n = 9
GIU1.16
PARALLEL-LAMINATED SANDSTONE
CP 1a
n = 11
n = 10
CP1.5a
PARALLEL-LAMINATED SANDSTONE
CP 4a
n = 9
n = 8
CP4.4
CROSS-LAMINATED SANDSTONE
GIU 3c
n = 8
n = 6
GIU3.26
N
Magnetisation J
[mT]
T [°C]
0.1 T
0.4 T
2.5 T

Fig. 2.8 – AMS and AIRM data of selected samples plotted on common stereoplots and associated isothermal remanent magnetization (IRM) acquisition curves and thermal demagnetization of a 3-component IRM; AMS kmax = black squares, AMS kint = black triangles, AMS kmin = black circles; AIRMmax = red squares; AIRMint = red triangles; AIRMmin = red circles; N = geographic north; n = number of samples; BO1c, etc. = site name. See text for discussion.

Table 2.2 - AMS parameters of samples shown in Figure 2.8; n: number of samples per site; Kmean = mean susceptibility; kmax = maximum susceptibility; kint = intermediate susceptibility; kmin = minimum susceptibility; L = magnetic lineation; F = magnetic foliation; σ = standard deviation.

SAMPLE	n	K_{mean} ± σ [+10E-3 SI]	k_{max} ± σ [+10E-3 SI]	k_{int} ± σ [+10E-3 SI]	k_{min} ± σ [+10E-3 SI]	L ± σ	F ± σ
CP1a	10	29.82 ± 6.54	32.91 ± 7.50	29.88 ± 6.68	26.66 ± 5.51	1.101 ± 0.037	1.119 ± 0.052
CP4a	8	38.35 ± 6.20	42.40 ± 7.78	38.11 ± 6.65	34.54 ± 4.48	1.111 ± 0.056	1.010 ± 0.072
BO1c	8	378.23 ± 103.50	421.46 ± 121.79	380.12 ± 104.70	333.10 ± 85.25	1.108 ± 0.053	1.138 ± 0.049
GIU1b	9	14.82 ± 2.85	16.22 ± 4.98	14.90 ± 3.03	13.34 ± 1.01	1.074 ± 0.085	1.114 ± 0.185
GIU3c	6	9.12 ± 1.77	9.65 ± 1.81	9.19 ± 1.75	8.51 ± 1.76	1.050 ± 0.027	1.084 ± 0.025

Table 2.3 - AIRM parameters of samples shown in Figure 2.8; n: number of samples per site; Kmean = mean susceptibility; kmax = maximum susceptibility; kint = intermediate susceptibility; kmin = minimum susceptibility; L = magnetic lineation; F = magnetic foliation; σ = standard deviation.

SAMPLE	n	K_{mean} ± σ [+10E-6 SI]	k_{max} ± σ [+10E-6 SI]	k_{int} ± σ [+10E-6 SI]	k_{min} ± σ [+10E-6 SI]	L ± σ	F ± σ
GIU3c	8	116.83 ± 5.35	118.10 ± 5.54	116.94 ± 5.31	115.47 ± 5.20	1.010 ± 0.003	1.013 ± 0.004
GIU1b	9	134.80 ± 4.04	137.41 ± 4.08	134.53 ± 4.01	132.46 ± 4.05	1.021 ± 0.002	1.016 ± 0.002
BO1c	8	279.38 ± 48.07	286.34 ± 51.23	280.11 ± 48.23	271.71 ± 44.77	1.021 ± 0.007	1.030 ± 0.008
CP4a	9	76.56 ± 5.59	77.99 ± 5.92	76.92 ± 5.79	74.78 ± 5.07	1.074 ± 0.005	1.028 ± 0.011
CP1a	11	139.15 ± 4.67	143.49 ± 4.83	140.32 ± 4.81	133.66 ± 4.32	1.023 ± 0.001	1.050 ± 0.003

***White Marlstone (WM) beds*.** A well-preserved depositional anisotropic fabric with clustered k_{max}, k_{int} and k_{min} axes is evident in all WM beds (Fig. 2.5K). The k_{min} axes are consistently vertical or sub-vertical, i.e., perpendicular or sub-perpendicular to the bedding planes, whereas the k_{max} axes are consistently horizontal, i.e., parallel to the bedding planes, and oriented NW–SE. In one case (site COR 1b; Fig. 2.6L), an imbricated fabric with k_{max} axis plunging to the SE was observed. These results suggest that the WM beds deposited under weak velocity flows (Dall'Olio et al., submitted) that oriented the maximum susceptibility axis of paramagnetic grains, probably slightly elongated phyllosilicates, parallel to the mean current direction in the final stages of transport.

In summary, tilt-corrected AMS ellipsoids (Tab. 2.1) appear to be very well defined in massive, parallel laminated, and cross-laminated sandstones (Fig. 2.5) insofar as the mean k_{min} direction is vertical or sub-vertical (i.e., perpendicular or sub-perpendicular to bedding planes) whereas the mean k_{max} direction (red line in rose diagrams of Fig. 2.5) lies at low angles relative to the reference mean paleocurrent direction from flute-casts (blue arrow in stereonets and rose diagrams in Fig. 2.5). Within these substantially flow-aligned facies, a small but relatively

consistent offset of up to ~15–20° counterclockwise with respect to the mean paleoflow direction from flute casts has been observed (Fig. 2.5A, B, C, D and E). Excluding systematic measurement errors, the cause of the observed offset may be sought in small differences of flow directions between the erosive, flute cast-generating stage of turbidity currents and the subsequent depositional stages during which massive, planar, and cross stratifications are formed (assuming substantial flow alignment of kmax axes in these facies). Taira and Scholle (1979) and Clark and Stanbrook (2001) found upward changes in mean orientation of sand grains in Bouma-type turbidites that seems to support our observations. Processes such as local changes in current direction due to current meandering, or that take into account the effects of currents interaction, lateral confining slopes (Magalhaes and Tinterri, 2010), or the Coriolis force on decelerating flows (e.g., Scott, 1967, Colburn, 1968; Parkash and Middleton, 1970; Yagishita and Jopling, 1983), may all have contributed to the observed offset, which is presently under investigation.

In order to understand which minerals contribute to the susceptibility signal, the anisotropy of the isothermal remanent magnetization (AIRM) (Tab. 2.2) has been studied on a selected set of samples from sites characterized by well-defined AMS ellipsoids (Tab. 2.3). To ease comparison, AMS and AIRM data have been plotted on common equal-area steroplots in Figure 2.8. Sites CP1a (parallel laminated sandstones) and BO1c (massive sandstones) show clustered maximum, intermediate, and minimum AIRM axes (red symbols in Fig. 2.8) that broadly coincide with the maximum, intermediate, and minimum susceptibility axes of the AMS ellipsoid (black symbols in Fig. 2.8), suggesting a clear contribution to the AMS by ferromagnetic (*sensu latu*) minerals. The AIRM and AMS of site GIU3c (cross-laminated sandstones) also show some degree of similarity, whereas in site GIU1b (massive sandstones), the AIRM axes appear scattered relative to the AMS axes. From these analyses we conclude that in the investigated facies there is a variable contribution of ferromagnetic (*sensu latu*) grains to the AMS.

The nature of these grains has been determined by means of isothermal remanent magnetization (IRM) curves and thermal demagnetization of a 3-component IRM (Fig. 2.8). These analyses reveal the presence of a dominant low coercivity phase with maximum unblocking temperature of ~570 °C interpreted as magnetite coexisting with an intermediate coercivity phase with unblocking temperature of ~320 °C interpreted as a sulfide phase. Hematite with high coercivity and maximum unblocking temperature of ~680 °C is also occasionally present in sample GIU1.16 from site GIU1b).

Image analysis has been conducted on thin sections in massive sandstones (site CP; Fig. 2.1). Phyllosilicates (muscovite), magmatic lithics, quartz, feldspars have been recognized in abundant carbonate matrix (Fig. 2.9). Minerals with an anisotropic shape have been selected and divided in three different classes of orientation (red objects oriented up-current, blue object sub-horizontal, green objects oriented down-current; Fig. 2.9). According to our analysis, paramagnetic phyllosilicates and magmatic lithics, likely containing magnetite, dominate the current-induced AMS and AIRM signals.

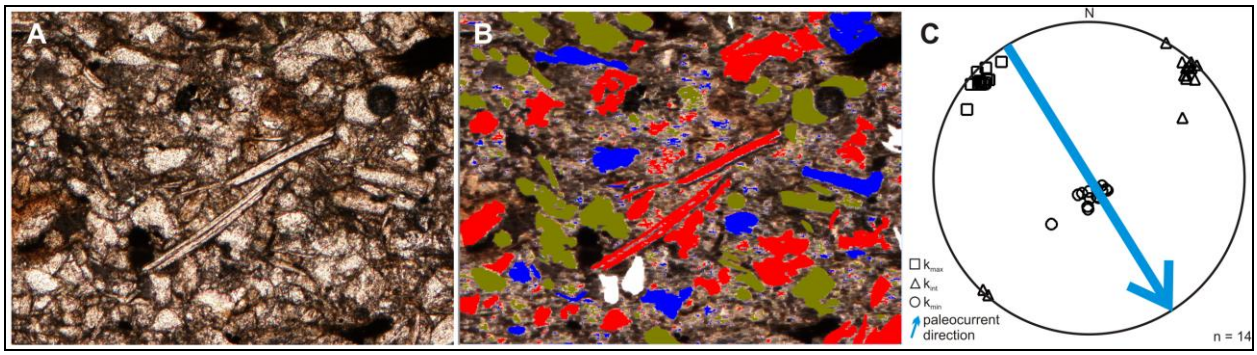

Fig. 2.9 – Thin section of sample CP2: (A) original photo; (B) photo elaborated throughout Image Analysis techniques (red is what, blue is what, green is what); (C) AMS steroplot of site CP2 (kmax = squares, kint = triangles, kmin = circles; N = geographic north; n = number of samples; blue arrow = actual flow direction from flute-casts at the base of the sampled bed [328°E]).

Thermal demagnetization of the natural remanent magnetization (NRM) conducted on a total of 157 fresh samples revealed the presence in 46 samples of an initial magnetic component isolated between room temperature and 250–300 °C and broadly aligned along the present-day field direction in *in situ* coordinates (average MAD = 5°) (Fig. 2.10A). Removal of these initial magnetizations revealed the presence of scattered components with no linear trending to the origin of the demagnetization axes. IRM acquisition curves and thermal demagnetization of a 3-component IRM confirm the presence of variable mixtures of magnetite and hematite as magnetic carriers of the NRM (Fig. 2.10B and C). The initial magnetic components are better grouped before than after bedding tilt correction (Fig. 2.10D), with the Fisher precision parameter k decreasing by a factor of ~7 upon full (100%) correction for tilting, and are therefore interpreted as sub-recent remagnetization overprints. The apparent absence of primary (i.e., Miocene) magnetic component directions in the studied samples prompted us to adopt NRM data from the literature in order to correct the flow directions for Apennine thrust sheets-rotations since the time of sediment deposition (see discussion below).

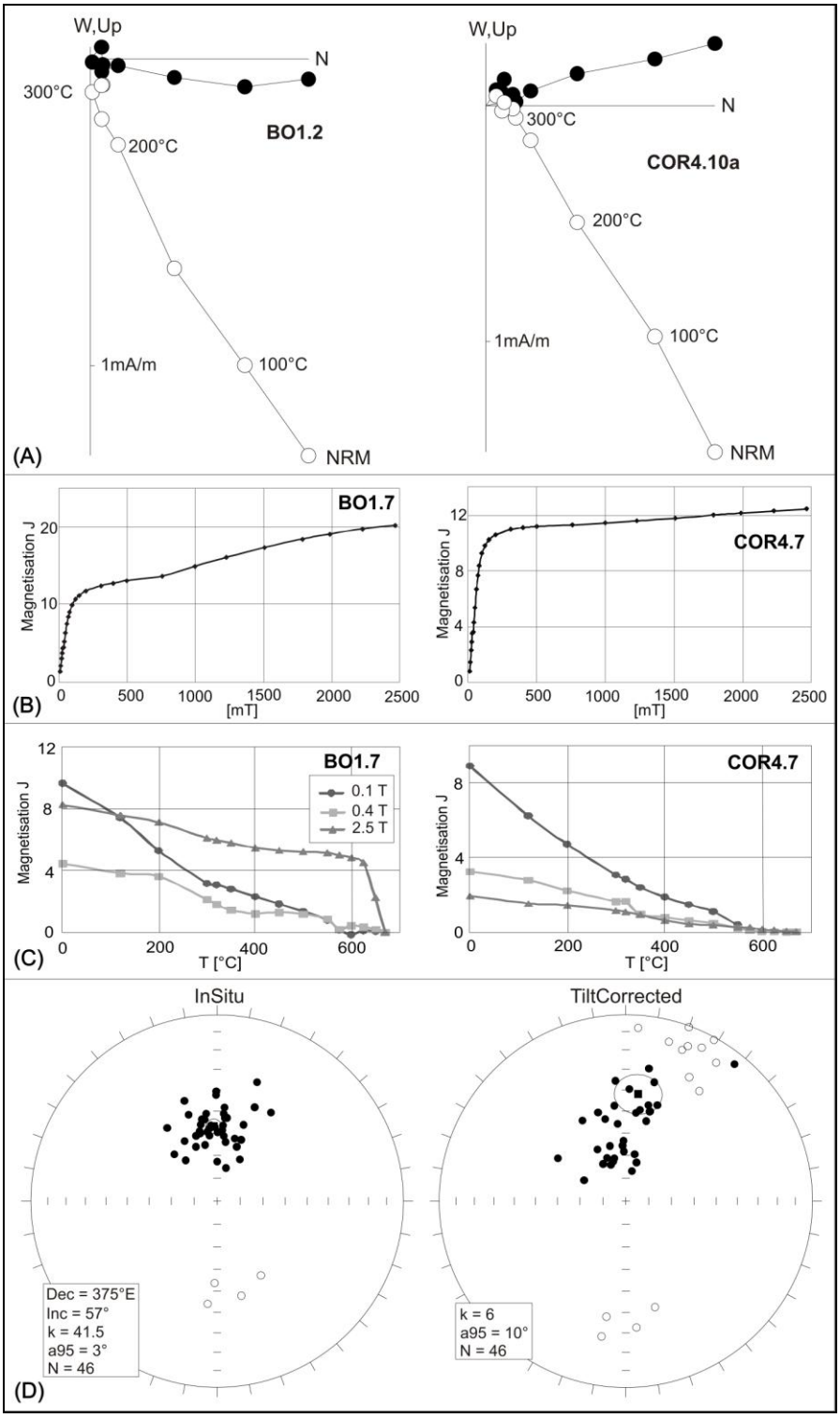

Fig. 2.10 – (A) Zijderveld demagnetization diagrams of two representative samples (BO1.2 and COR 4.10a) from the Marnoso Arenacea Formation; closed (open) circles are projections onto the horizontal (vertical) plane in in situ coordinates; (B) isothermal remanent magnetization (IRM) acquisition curves and (C) thermal demagnetization of a 3-component IRM of two samples (BO1.4 and COR 4.7) from the same sites of samples in panel (A); (D) equal-area projections before and after bedding tilt correction of the

initial magnetic component directions isolated in 46 samples (out of a total of 157) of the Marnoso Arenacea Formation; closed (open) symbols represent down-pointing (up-pointing) directions. See text for discussion.

Miocene paleogeography of the Marnoso Arenacea basin

We used our AMS-determined flow directions in conjunction with paleomagnetic and geologic data from the literature to reconstruct the geometry of the MA basin from its present-day configuration (Fig. 2.1) to its Miocene configuration (Fig. 2.11). In order to correct for the general counterclockwise rotation of the Apennine thrust sheets since the time of sediment deposition, we applied to the flow directions a clockwise rotation of 29° ± 8° as suggested by Speranza et al. (1997) and Muttoni et al. (1998; 2000) for the same general area of this study, after acknowledging that our NRM data yielded inconclusive results (see above). This correction yielded a N–S direction of elongation of the foredeep associated with the eastward migration of the Apennine thrust fronts (di Biase & Mutti, 2002) during the deposition of the MA Formation (Fig. 2.11).

Within this regional setting, the MA basin can be subdivided into a shallow-marine Alpine Basin in the north, and a deep-marine Apennine Basin in the south, separated by the Valle Salimbene-Bagnolo Ridge (Fig. 2.11), which is a roughly ESE-trending, buried feature interpreted as a wrench zone acting as the kinematic transfer between the N–S compression in the Alps and the SW–NE compression in the Apennines (di Biase & Mutti, 2002). Large volumes of sand coming from the southern and western Alps in the north (Gandolfi et al., 1983; Ricci Lucchi, 1986; Roveri et al., 2002) were able to enter the adjacent and deeper Apennine Basin through turbidity currents that crossed the Valle Salimbene-Bagnolo Ridge possibly along fault-controlled depressions. These turbidity currents moved then southward within the confined foredeep (di Biase & Mutti, 2002), while at the same time minor volumes of carbonatic and hybrid turbidites moved northward upon entering the foredeep from shallow-water carbonate platforms located along the southern and south-eastern margins of the basin (Gandolfi et al., 1983) (Fig. 2.11).

In addition to southward-flowing siliciclastic turbidites and northward-flowing carbonatic and hybrid turbidites, the MA basin was also characterized by the presence of N–S contour currents, which left their testimony in the white marlstone (WM) beds. These deposits have frequently been interpreted as due to hemipelagic settling of fine-grained particles, but according to AMS analysis (this study; Dall'Olio et al., submitted) they are interpreted as deposited under weak velocity currents. These results prompted Dall'Olio et al. (submitted) to suggest that the WM

beds may have deposited under the effect of contour currents and should therefore be referred to as muddy contourites.

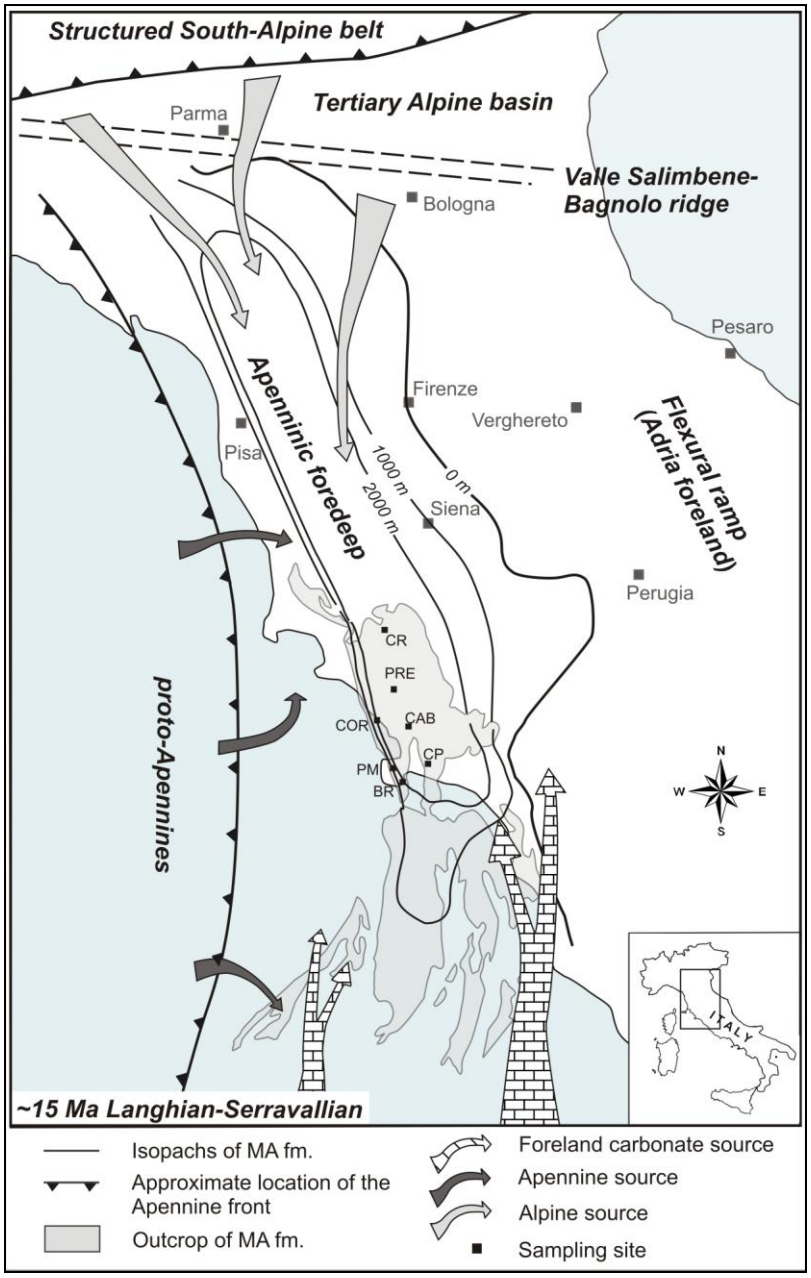

Fig. 2.11 - Paleogeographic map of the studied area during the middle Miocene showing the main sources and dispersal patterns of sediment within the Marnoso Arenacea foredeep basin. See text for details and discussion.

Conclusions

The following conclusions can be reached from this study on the MA Formation:

1) the AMS is a very useful fabric analysis technique for quantifying flow directions in turbiditic sandstones provided it is performed in appropriate depositional intervals selected by means of detailed sedimentological analyses and is cross-validated by direct estimates of flow directions

from sedimentological indicators (before attempting extrapolations to cases where sedimentological indicators are absent, e.g., in drill cores). Particular advantages of this technique are the significantly faster measurement time compared to standard petrographic fabric analysis and its capability to characterize the orientation of the entire population of (magnetic) grains in three dimensions, whereas standard image analysis on orthogonal thin sections is intrinsically limited to two-dimensional estimates of grains' orientations.

2) Massive, parallel-laminated, and cross-laminated beds containing paramagnetic phyllosilicates show well-clustered AMS data with a single dominant fabric type; AIRM data are substantially similar to AMS data suggesting a contribution to the AMS by ferromagnetic grains (mainly magnetite probably contained in lithic grains). A robust correlation between magnetic fabric and paleocurrent directions from sedimentological indicators (e.g., flute casts) has been found in these facies, albeit a small but relatively consistent offset of up to ~15–20° counterclockwise has been observed and tentatively explained as due to small variations of flow directions (of as yet unknown origin) between the erosive, flute cast-generating stage of turbidity currents and the subsequent deposition of massive, planar, and cross stratifications.

4) Fabrics oriented at high angle (~40–60°) relative to the paleocurrent direction from sedimentological indicators (flow-transverse fabric) have been observed only in a few samples and can be interpreted as the result of successive deflections of turbidity currents against the margins of the basin and/or of intrabasinal highs, or due to flow accelerations (triggered by, e.g., interactions with floor topography) able to lift grains from the depositional plane and roll them over it before attaining a more stable flow-transverse orientation. The difficulty to identify a unique transport mode in these depositional intervals makes the reconstruction of paleocurrent directions from AMS data more challenging, if compared to massive, parallel-laminated and cross-laminated divisions.

5) Highly dispersed AMS fabrics are apparently common in convoluted and undulated sandstones as well as in debrites, suggesting depositional processes that partially prevented grains' orientation (e.g., *en masse* freezing) or post-depositional processes that disrupted the original current-induced fabric (e.g., post-depositional dewatering).

6) Our AMS analysis coupled with paleomagnetic and geologic data from the literature helped reconstructing the complex paleogeography of the Marnoso Arenacea foredeep prior to rotational deformation of the Apennines since the Miocene.

ACKNOWLEDGMENTS

G. Malgesini is warmly acknowledged for his help during field work. Financial support was provided by FIRB 2006–2009 funds to F. Felletti, and IAS grant to E. Dall'Olio.

References

Agico KLY-3 User's Guide (Ver. 2.2 Nov. 1998) Modular system for measuring magnetic susceptibility, anysotropy of magnetic susceptibility, and temperature variation of magnetic susceptibility. AGICO Advanced Geoscience Instruments CO. Brno, Czech Republic.

Allen, J.R.L. (1964) Primary current lineation in the lower Old Red Sandstone (Devonian), Anglo-Welsh Basin. *Sedimentology*, **3**, 89-108.

Allen, J.R.L. (1984). Sedimentary Structures: their Character and Physical Basis. *Developments in Sedimentology*,. **30A/B**, Elsevier, Amsterdam, 593-663.

Allen, J.R.L. (1991) The Bouma division A and the possible duration of turbidity currents. *Journal of Sedimentary Petrology*, **61**, 2, 291-295.

Amy, L.A. and Talling, P.J (2006). Anatomy of turbidites and linked debrites based on long distance (120 x 30 km) bed correlation, Marnoso Arenacea Formation, Northern Apennines, Italy. *Sedimentology*, **53**, 161-212.

Argenton, H., Bobier, C. and Polveche, J. (1975). La mésure de l'anisotropie de susceptibilité magnetique dans les flysches; application à la recherche des directions des paleocourants. *Sedimentary Geology*, **14**, 2, 149-167.

Argnani, A. and Ricci Lucchi, F. (2001) Tertiary siliciclastic turbidite systems of the Northern Apennines. In: Apennines and Adjacent Mediterranean Basins (Vai, G.B. and Martini, P. Eds.), Kluwer Academic Publishers, 327-350.

Arnott, R.W.C. and Hand, B.M. (1989) Bedforms, primary structures and grain fabric in the presence of suspended sediment rain: *Journal of Sedimentary Petrology*, **59**, 1062-1069.

Baas, J.H., Hailwood, E.A., McCaffrey, W.D., Kay, M., and Jones, R. (2007) Directional petrological characterisation of deep-marine sandstones using grain fabric and permeability anisotropy: Methodologies, theory, application and suggestions for integration. *Earth-Science Reviews*, **82**, 101-142.

Boccaletti, M., Calamita, F., Deiana, G., Gelati, R., Massari, F., Moratti, G. and Ricci Lucchi, F. (1990) Migrating foredeep-thrust belt system in the northern Apennines and southern Alps. *Palaeogeography Palaeoclimatology Palaeoecology*, **77**, 1, 3-14.

Borradaile, G.J., Fralick, P.W. and Lagroix, F. (1999) Acquisition of anhysteretic remanence and tensor subtraction from AMS isolates true palaeocurrent grain alignments. In: Palaeomagnetism and Diagenesis in Sediments (Tarling, D.H. and Turner, P. Eds), Geological Society, London, Special Publications, **151**, 139-145.

Bouma, A.H. and Pluenneke, J.L. (1975) Structural characteristics of debrites from the Philippine Sea. *Initial Reports of the Deep Sea Drilling Project*, **31**, 497-505.

Clark, J.D. and Stanbrook, D.A. (2001) Formation of large-scale shear structures during deposition from high-density turbidity currents, Grès d'Annot Formation, south-east France. In: Particulate Gravity Currents (McCaffrey, W.D., Kneller, B.C. and Peakall, J. Editors). International Association of Sedimentologists, Special Publication, **31**, 219-232.

Colburn, I.P. (1968) Grain fabrics in turbidite sandstone beds and their relationship to sole mark trends on the same beds. *Journal of Sedimentary Petrology*, **38**, 146-158.

Costa, E., Pialli, G. and Plesi, G. (1998) Foreland basins of the Northern Apennines; relationships with passive subduction of the Adriatic lithosphere. *Memorie della Societa Geologica Italiana*, **52**, 595-606.

Dall'Olio, E., Felletti, F., and Muttoni, G. (submitted) Constraints on mechanisms of deep-water mudstone deposition in the Marnoso Arenacea Formation (Miocene, Italy) through magnetic fabric analysis. *Journal of Sedimentary Research.*

di Biase, D. and Mutti, E. (2002) The "Proto Adriatic Basin". In: Revisiting Turbidites of the Marnoso Arenacea Formation and their Basin-Margin Equivalents: Problems with Classic Models (Mutti, E., Ricci Lucchi, F. and Roveri, M. Eds). Excursion Guidebook. Università di Parma and Eni-Agip Division, 64th EAGE Conference and Exhibition, Florence, Italy, I 1–I 4.

Dondi, L., Mostardini, F. and Rizzini, A. (1982) Evoluzione sedimentaria e paleogeografica nella Pianura Padana. Translated Title: Sedimentary and paleogeographic evolution of the Po Plain. In: Guida alla geologia del margine Appenninico-Padano. Translated Title: Geologic guide to the Apennine-Po margin, 47-58.

Ellwood, B.B. (1980) Induced and remanent magnetic properties of marine sediments as indicators of depositional processes. *Marine Geology*, **38**, 233-244.

Enos, P. (1977) Flow regimes in debris flow. *Sedimentology*, **24**, 1, 133-142.

Galehouse, J.S. (1968) Anisotropy of magnetic susceptibility as a paleocurrent indicator; a test of method. *Geological Society of America Bulletin*, **79**, 3, 387-390.

Gandolfi, G., Paganelli, L. and Zuffa, G.G. (1983) Petrology and dispersal directions in the Marnoso Arenacea Formation (Miocene, northern Apennines). *Journal of Sedimentary Petrology*, **53**, 493–507.

Ghibaudo, G. (1992) Subaqueous sediment gravity flow deposits: practical criteria for their field description and classification. *Sedimentology*, **39**, 423-454.

Hamilton, N. and Rees, A.I. (1970) The use of magnetic fabric in paleocurrent estimation. In: Paleogeophysics (Runcorn, S.K. Ed.). London, Academic Press, 445-464.

Harms, J.C. (1975) Depositional environments as interpreted from primary sedimentary structures and stratification sequences. Society of Economic Paleontologists and Mineralogists. 161 pp.

Hendry, H.E. (1976) The orientation of discoidal clasts in resedimented conglomerates, Cambro-Ordovician, Gaspé, eastern Quebec. *Journal of Sedimentary Petrology*, **46**, 48-55.

Hiscott, R.N. and Middleton, G.V. (1980) Fabric of coarse deep-water sandstones, Tourelle Formation, Quebec, Cananda. *Journal of Sedimentary Petrology*, **50**, 703-722.

Hiscott, R.N., Hall, F.R. and Pirmez, C. (1997) Turbidity-current overspill from the Amazon channel: texture of the silt/sand load, paleoflow from anisotropy of magnetic susceptibility and implications for flow processes. *Proceedings of the Ocean Drilling Program, Scientific Results*, **155**, 53-78.

Johansson, C.E. (1964) Orientation of pebbles in running water: a laboratory study *Geografiska Annaler*, **45A**, 85–112.

Kneller, C. and Branney, M.J. (1995) Sustained high-density turbidity currents and the deposition of thick massive sands. *Sedimentology*, **42**, 4, 607-616.

Knode, T.L., Vickers, K.V. and Edmiston, C. (1990) Determination and cross verification of paleodip/paleocurrents directions. In: AAPG annual convention with DPA/ EMD divisions and SEPM, an associated society; technical program with abstracts. *AAPG Bulletin*, **74**, 5, 696 pp.

Kuenen, P.H.H. (1957) Sole markings of graded greywacke beds. *The Journal of Geology*, **65**, 3; 231-258.

Ledbetter, M.T. and Ellwood, B.B. (1980) Spatial and temporal changes in bottom-water velocity and direction from analysis of particle size and alignment in deep-sea sediment. *Marine Geology*, **38**, 245-261.

Lindsay, J.F. (1968) The Development of Clast Fabric in Mudflows. *Journal of Sedimentary Research*, **38**, 4, 1242-1253.

Liu, B., Saito, Y., Yamazaki, T., Abdeldayem, A., Oda, H., Hori, K. and Zaho, Q. (2001) Paleocurrent analysis for the Late Pleistocene-Holocene incised-valley fill of the Yangtze delta, China by using anisotropy of magnetic susceptibility data. *Marine Geology*, **176**, 175-189.

Liu, B., Saito, Y., Yamazaki, T., Abdeldayem, A., Oda, H., Hori, K. and Zhao, Q. (2005) Anisotropy of magnetic susceptibility (AMS) characteristics of tide-influenced sediments in the Late Pleistocene-Holocene Changjiang incised valley fill, China. *Journal of Coastal Research*, **21**, 5, 1031–1041.

Lowe, D.R. (1982) Sediment gravity flows II: Depositional models with special reference to the deposits of high-density turbidity currents. *Journal of Sedimentary Petrology*, **52**, 279-298.

Lowrie, W. (1990) Identification of ferromagnetic minerals in a rock by coercivity and unblocking temperature properties. *Geophysical Research Letters*, **17**, 2, 159-162

Lowrie, W. and Hirt, A.M. (1987) Anisotropy of magnetic susceptibility in the Scaglia Rossa pelagic limestone. *Earth and Planetary Science Letters*, **82**, 349-356.

Malgesini, G., Talling, P. and Felletti, F. (2009) Bed-by-bed correlations as a test for depositional models of sediment dispersal into the deep ocean: Marnoso Arenacea formation (Miocene – Northern Apennines). In: 27th IAS Meeting – Sedimentary of Mediterranean island(s) - Abstracts Book, (Edited by Pascucci, V. and Andreucci, S., Editrice Democratica Sarda), 586.

McBridge, E. and Picard, D. (1991) Facies implications of Trichichnus and Chondrites in turbidites and hemipelagites, Marnoso Arenacea Formation (Miocene), northern Apennines, Italy. *Palaios*, **6**, 281–290.

Monaco, P. and Checconi, A. (2008) Stratinomic indications by trace fossils in Eocene to Miocene turbidites and hemipelagites of the Northern Apennines (Italy). *Studi Trentini di Scienze Naturali, Acta Geologica*, **83**, 133–163.

Monaco, P. (2008) Taphonomic features of Paleodictyon and other graphoglyptid trace fossils in Oligo-Miocene thin-bedded turbidites, northern Apennines, Italy. *Palaios*, **23**, 667-682.

Mulder, T. and Alexander, J. (2001) The physical character of subaqueous sedimentary density currents and their deposits. *Sedimentology*, **48**, 269–299.

Mutti, E. (1977) Distinctive thin-bedded turbidite facies and related depositional environments in the Eocene Hecho Group (South-Central Pyrenees, Spain). *Sedimentology*, **24**, 107–131.

Mutti, E. (1979) Turbidites et cones sous-marins profonds. In: Sédimentation Détritique (Fluviatile, Littorale et Marine), (Homewood, P. ed.), Université de Fribourg, Institut de Géologie, 353–419.

Mutti, E. (1992) Turbidite Sandstones. Ente Nazionale Idrocarburi (ENI) – Università di Parma, 275 pp.

Mutti, E., Bernoulli, D., Lucchi, F. R. and Tinterri, R. (2009) Turbidites and turbidity currents from Alpine 'flysch' to the exploration of continental margins. *Sedimentology*, **56,** 267–318.

Mutti, E. and Johns, D.R. (1979) The role of sedimentary by-passing in the genesis of basin plain and fan fringe turbidites in the Hecho Group System (South-Central Pyrenees). *Società Geologica Italiana, Memorie*, **18**, 15–22.

Mutti, E. and Ricchi Lucchi, F. (1972) Le torbiditi dell'Apennino settentrionale: introduzione all'analisi di facies. *Società Geologica Italiana, Memorie*, **11,** 161–199.

Mutti, E. and Ricchi Lucchi, F. (1975) Field Trip A-11: Turbidite facies and facies associations. In: Examples of Turbidite Facies Associations from Selected Formations of Northern Apennines: International Association of Sedimentologists (Mutti, E., Parea, G.C., Ricci Lucchi, F., Sagri, M., Zanzucchi, G., Ghibaudo, G. and Iaccarino, I. Eds), 9th International Congress, Nice, France, 21–36.

Muttoni, G., Argnani, A., Kent, D.V., Abrahamsen, N. and Cibin, U. (1998) Paleomagnetic evidence for Neogene tectonic rotations in the Northern Appennines, Italy. *Earth and Planetary Science Letters*, **154**, 25-40.

Muttoni, G., Argnani, A., Kent, D.V., Abrahamsen, N. and Cibin, U. (2000) Paleomagnetic evidence for a Neogene two-phase counterclockwise tectonic rotation in the Northern Apennines (Italy). *Tectonophysics*, **326**, 241-253.

Muzzi Magalhaes, P. and Tinterri, R. (2010) Stratigraphy and depositional setting of slurry and contained (reflected) beds in the Marnoso Arenacea Formation (Langhian-Serravallian) Northern Apennines, Italy. *Sedimentology*, **57**, 7, 1685-1720.

Nilsen, T.H., Shew, R.D., Steffens, G.S. and Studlick, J.R.J. (2008) Atlas of Deep-water Outcrops. *AAPG Studies in Geology*, **56**, 504 pp.

Parés, J.M., Hassold, N.J.C., Rea, D.K. and van der Pluijm, B.A. (2007) Paleocurrent directions from paleomagnetic reorientation of magnetic fabrics in deep-sea sediments at the Antarctic Peninsula Pacific margin (ODP Sites 1095, 1101). *Marine Geology*, **242,** 261–269.

Parkash, B. and Middleton, G.V. (1970) Downcurrent textural changes in Ordovician turbidite greywackes. *Sedimentology*, **14**, 259–293.

Pickering, K.T., Hiscott, R.N., Kenyon, N.H., Ricci Lucchi, F. and Smith, R.D.A. (1995) Atlas of Deep Water Environments: Architectural Style in Turbidite Systems. (Chapman & Hall, New York), 303–306.

Rees, A.J. (1965) The use of anisotropy of magnetic susceptibility in the estimation of sedimentary fabric. *Sedimentology*, **4**, 257-283.

Rasband, W. S. (2008) ImageJ. US National Institutes of Health, Bethesda, Maryland,USA. http://rsb.info.nih.gov/ij/index.html

Rees, A.J. (1968) The production of preferred orientation in a concentrated dispersion of elongated and flattened grains. *Journal of Geology*, **76**, 457–465.

Rees, A.J. (1983) Experiments on the production of transverse grain alignment in a sheared dispersion. *Sedimentology*, **30**, 437–448.

Ricci Lucchi, F. (1975) Depositional cycles in two turbidite formations of northern Apennines (Italy). *Journal of Sedimentary Petrology*, **45**, 1, 3-43.

Ricci Lucchi, F. (1986) The Oligocene to recent foreland basins of the Northern Apennines. In: Foreland Basins (Allen, P.A. and Homewood, P. Eds), *IAS Spec. Publ*., **8**, 105–139. Blackwell Scientific, Oxford.

Ricci Lucchi, F. and Valmori, E. (1980) Basin-wide turbidites in a Miocene, over-supplied deep-sea plain: a geometrical analysis. *Sedimentology*, **27**, 241–270.

Rich, J.L. (1950) Flow markings, grooving, and intra-stratal crumpling as a criteria for recognition of slope deposits, with illustrations from Silurian rocks of Wales. *Bulletin of the American Association of Petroleum Geologists*, **34**, 4,. 717-741.

Roveri, M., Ricci Lucchi, F., Lucente, C.C., Manzi, V. and Mutti, E. (2002) Stratigraphy, facies and basin fill history of the Marnoso Arenacea Formation. In: Revisiting Turbidites of the Marnoso Arenacea Formation and their Basin-Margin Equivalents: Problems with Classic Models (Mutti, E., Ricci Lucchi, F. and Roveri, M. Eds). Excursion Guidebook. Università di Parma and Eni-Agip Division, 64th EAGE Conference and Exhibition, Florence, Italy, III 1–III 15.

Rupke, N.A. (1976) Sedimentology of very thick calcarenite-marlstone beds in a flysch succession, southwestern Pyrenees. *Sedimentology*, **23**, 1, 43-65.

Rusnak, G.A. (1957) The orientation of sand grains under conditions of "unidirectional" fluid flow: 1. Theory and experiment. *Journal of Geology*, **65**, 384–409.

Sagnotti, L. and Meloni, A. (1993) Pleistocene rotations and strain in southern Italy: the example of the Sant'Arcangelo Basin. *Annali di Geofisica*, **XXXVI**, 2, 83-95.

Sakai, T., Yokokawa, M., Kubo, Y., Endo, N. and Masuda, F. (2002) Grain fabric of experimental gravity flow deposits. Sedimentary Geology 154, 1–10.

Schieber, J. and Ellwood, B.B. (1993) Determination of basinwide paleocurrent patterns in a shale succesion from anisotropy of magnetic susceptibility (AMS): a case of study of the Mid-Proterozoic Newland Formation, Montana. *Journal of Sedimetary Petrology*, **63**, 878-880.

Schwarzacher, W. (1963) Orientation of crinoids by current action. *Journal of Sedimentary Petrology*, **33**, 580–586.

Scott, K.M. (1967) Intra-bed palaeocurrent variations in a Silurian flysch sequence, Kirkcudbrightshire, Southern Uplands of Scotland. *Scottish Journal of Geology*, **3**, 268–281.

Shanmugam, G. (1996) High-density turbidity currents; are they sandy debris flows? *Journal of Sedimentary Research*, **66**, 1, 2-10.

Shor, A.N., Kent, D.V. and Flood, R.D. (1984) Contourite or turbidite? Magnetic fabric of fine-grained Quaternary sediments, Nova Scotia continental rise. In: Fine-Grained Sediments; Deep- Water Processes and Facies (Stow, D.A.V. and Piper, D.J.W. Eds.). *Geological Society of London, Special Publication*, **15**, 257-273.

Speranza, F., Sagnotti, L. and Mattei, M. (1997) Tectonics of the Umbria–Marche–Romagna arc (central-northern Apennines, Italy): new paleomagnetic constraints. *Journal of Geophysical Research*, **102**, B2, 3153–3166.

Taira, A. (1989) Magnetic fabric and depositional processes. In: Sedimentary facies in the Active Plate Margin (Taira, A. and Masuda, F. Eds). Tokyo, Terra Scientific Publishing, 44-77.

Taira, A. and Scholle, P.A. (1979) Deposition of resedimented sandstone beds in the Pico Formation, Ventura Basin, California, as interpreted from magnetic fabric measurements. *Bulletin Geological Society of America*, **90**, 952-962.

Talling, P.J, Amy, L.A., Wynn, R.B., Peakall, J. and Robinson M. (2004) Beds comprising debrite sandwiched within co-genetic turbidite: origin and widespread occurrence in distal depositional environments. *Sedimentology*, **51**, 163–194.

Talling P.J., Amy, L.A., Wynn, R.B., Blackbourn, G. and Gibson, O. (2007) Evolution of Turbidity Currents Deduced from Extensive Thin Turbidites: Marnoso Arenacea Formation (Miocene), Italian Apennines. *Journal of Sedimentary Research*, **77**, 3, 172-196.

Tarling, D.H. and Hrouda, F. (1993) The Magnetic Anisotropy of Rocks. Chapman & Hall, London.

Vai, G.B. (2001) GSSP, IUGS and IGC; an endless story toward a common language in the earth sciences. *Episodes*, **24**, 1, 29-31.

Veloso, E.E., Anma, R., Ota, T., Komiya, T., Kagashima, S. and Yamazaki, T. (2007) Paleocurrent patterns of the sedimentary sequence of the Taitao ophiolite constrained by anisotropy of magnetic susceptibility and paleomagnetic analyses. *Sedimentary Geology*, **201**, 446–460.

Yagishita, K. and Jopling, A.V. (1983) Grain fabric of planar cross-bedding formed by lateral accretion, Caledon outwash, Ontario, Canada. *Journal of Geology*, **91**, 599–606.

Walker, R.G. (1967) Upper Flow Regime Bed Forms in Turbidites of the Hatch Formation, Devonian of New York State. *Journal of Sedimentary Research*, **37**, 1052-1058.

Walker, R.G. (1984) Shelf and shallow marine sands. In: Facies Models 2nd edition (Walker, R.G. Ed.). Geoscience Canada, Reprint Series 1, 141-170.

Chapter 3

Paper #2

Constraints on mechanisms of deep-water mudstone deposition in the Marnoso Arenacea Formation (Miocene, Italy) through magnetic fabric analysis

Eleonora Dall'Olio[1*], Fabrizio Felletti[1] and Giovanni Muttoni[1]

1 Dipartimento di Scienze della Terra "Ardito Desio". Università degli Studi di Milano. Via Mangiagalli 34, 20133 Milano, Italy.

* e-mail: eleonora.dallolio@unimi.it

Paper submitted to *Journal of Sedimentary Research.*

Abstract

Mudstones represent prominent rock types of marine successions, yet a full understanding of their depositional processes is often hampered by a lack of generally accepted diagnostic criteria to distinguish between hemipelagic settling and deposition from a flowing medium. The Marnoso-Arenacea Formation, which is a turbiditic unit of Miocene age outcropping in the northern Apennines (Italy), offers the possibility to address some of these uncertainties. A relatively small (~10%) but distinctive portion of the Marnoso-Arenacea Formation is comprised of white marlstone beds (WM beds) that have frequently been interpreted as due to the hemipelagic settling of fine-grained particles (hemipelagites). The analysis of the anisotropy of magnetic susceptibility (AMS) revealed the presence in the WM beds of maximum susceptibility axes clustered within the depositional plane along the average palaeoflow direction inferred from flute casts at the base of turbidite beds, whereas the minimum susceptibility axes are oriented perpendicular to the bedding plane. We interpret this fabric as largely sedimentary in origin and due to the alignment within the bedding plane of paramagnetic grains (e.g., muscovite) and possibly also ferromagnetic grains (magnetite) under weak velocity currents. The trend of the maximum susceptibility axes, and hence of the palaeoflow direction, is approximately oriented NNW–SSE after correction for Apennines thrust-sheet rotation since the Miocene. These results suggest that the WM beds cannot be entirely due to hemipelagic settling, as often quoted in the literature. A discussion on alternative depositional mechanisms leads us to conclude that the WM beds may have deposited under the effect of contour currents and should therefore be referred to as muddy contourites.

Key words

white marlstone beds; Marnoso Arenacea Fm.; hemipelagites; muddy contourites; anisotropy of magnetic susceptibility

Introduction

Mudstones are a major component of marine sedimentation and play a fundamental role in hydrocarbon exploration and exploitation (Viana, 2008). Mechanisms accountable for deep sea mudstone accumulation include gravity-induced turbidity currents, thermohaline-induced bottom contour currents, and hemipelagic suspension settling (Rebesco and Camerlenghi, 2008). Distinguishing among muddy turbidites (hemiturbidites sensu Stow and Wetzel, 1990), contourites, and hemipelagites is not trivial (Stow and Faugères, 2008; Mulder et al., 2008; 2009) as these deposits share several common sedimentological features (Stow and Wetzel, 1990). The distinction is further hampered by interaction processes whereby bottom currents may incorporate and redistribute particles originated by hemipelagic-pelagic settling (Stow et al., 1998); for example, Reeder et al. (2002) and Dennielou (1997) interpreted the Sicily Channel and North Atlantic deposits, respectively, as the result of bottom-current lofting and re-suspension of hemipelagic muds.

The Miocene Marnoso Arenacea turbidite system from the northern Apennines, Italy, provides the opportunity to address uncertainties concerning mechanisms of mudstone deposition in the deep sea. In the Marnoso Arenacea, distinctive white marlstone beds (hereafter WM beds) overlie mudstone layers derived from the deposition of the tail of turbidity currents (Bouma's Te divisions). Several authors (Mutti and Ricci Lucchi, 1972, 1975; Mutti, 1977, 1979; Mutti and Johns, 1979; Talling et al., 2007) referred to the WM beds as hemipelagites, often using the term "hemipelagic" with reference to composition rather than to a specific depositional process. Mutti and Ricci Lucchi (1972) contemplated three possible genetic processes to account for the WM beds associated with deep-water turbidites: turbidity currents, intermediate currents (i.e. bottom currents) and "normal" settling from standing water. Later, Mutti et al. (2002) and Muzzi Magalhaes and Tinterri (2010) suggested that the WM beds could derive from the settling of suspension clouds produced from fading turbidity currents (hemiturbidites sensu Stow and Wetzel, 1990).

It is therefore fair to say that despite an ever-growing body of knowledge regarding the sedimentology and depositional characteristics of the WM beds, the issue of their origin is virtually unsolved. This is reminiscent of uncertainties regarding the origin of similar white marlstone deposits from other well-studied sedimentary basins worldwide (Kuenen, 1964; Van der Lingen, 1969; Hesse, 1975; Rupke, 1975; Stow and Piper, 1984; Stanley, 1988; Stow and Wetzel, 1990; Stow and Tabrez, 1998; Mutti et al., 2002; Remacha et. al., 2005; Stow and Faugères, 2008; Mulder et al., 2008; Rebesco and Camerlenghi, 2008). An ultimate

understanding of the sedimentary processes responsible for the deposition of the WM beds of the Marnoso Arenacea Formation, as well as of similar sediments deposited elsewhere, is hampered by conflicting interpretations on the origin of the sedimentary structures that they contain (Stow and Faugères, 2008; Mulder et al., 2008).

In this paper, we attempt to decipher the origin of the WM beds by integrating sedimentological observations with the study of the anisotropy of magnetic susceptibility (AMS), which is a relatively inexpensive and highly effective technique to discriminate between hemipelagic and current-induced depositional fabrics. Still water deposition produces a magnetic fabric with minimum susceptibility axes clustered around the pole to the depositional plane within which maximum and intermediate susceptibility axes are uniformly dispersed, defining a planar, near-horizontal, gravity-induced settling fabric, whereas the magnetic fabric of sediments deposited from flowing water is typified by a current-oriented magnetic foliation plane (e.g., Ellwood, 1980; Lowrie and Hirt, 1987; Taira, 1989; Sagnotti and Meloni, 1993; Pares et al., 2007).

Geological setting

The Marnoso Arenacea Formation (hereafter MA) crops out extensively over an area of ~7.2 x 103 km2 in the northern Apennines from Emilia to Umbria (Fig. 3.1A), and is partly buried under tectonic or sedimentary units both to the W and to the NE of its present outcrop area (Fig. 3.1A). The MA is a wedge-shaped, non-channelized, and mainly siliciclastic turbidite system (Ricci Lucchi, 1969, 1975, 1978, 1979; Ricci Lucchi and Valmori, 1980; Ricci Lucchi, 1981; Mutti and Ricci Lucchi, 1972; Mutti et al., 2002; Amy and Talling, 2006; Muzzi Magalhaes and Tinterri, 2010) that represents the final stages of filling of an Early to Late Miocene migrating Apennine foredeep complex, accumulated between the Langhian and the Tortonian (Ricci Lucchi and Valmori, 1980; Fig. 3.1B).

Palinspastic restorations indicate an original width of the MA basin of about 90–140 km and a sediment thickness of up to 3 km (Ricci Lucchi, 1975, 1981, 1986; Boccaletti et al., 1990; Costa et al., 1998; Vai, 2001). The 1 km-isopach (Dondi et al., 1982; Argnani and Ricci Lucchi, 2001) defines an elongated basin running at least 400 km along the Apennine front (Fig. 3.1A). Two depocenters, comprising slightly thicker sequences of strata, have been identified in previous studies (Ricci Lucchi and Valmori 1980; Amy and Talling 2006). These depocenters are separated by a bathymetric feature near Verghereto (Fig. 3.1A) termed “Verghereto High” (Ricci

Lucchi and Valmori 1980). To the SE, the thickness of the MA decreases rapidly (Fig. 3.1A), suggesting the presence of an additional structural high in the Gubbio area (Argnani and Ricci Lucchi, 2001).

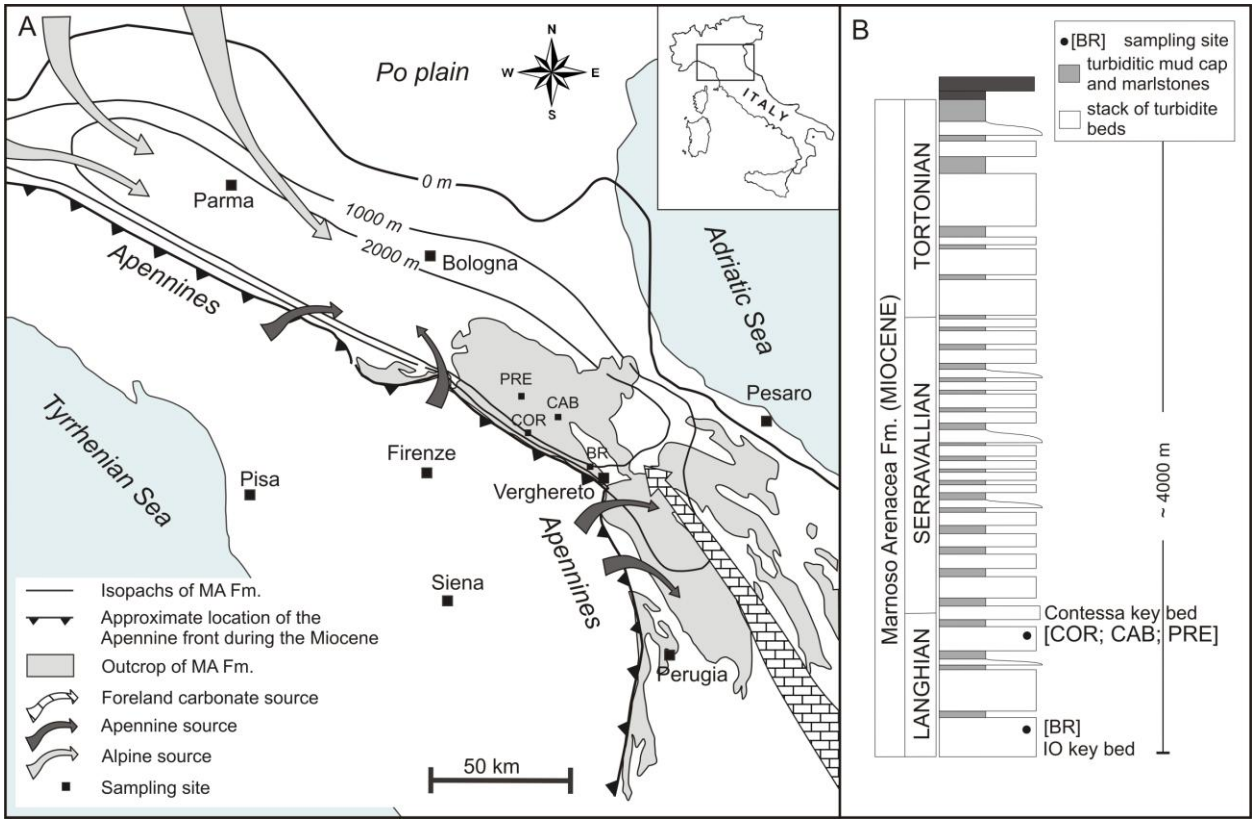

Fig. 3.1 – A) Map showing the outcrop area and thickness of the Marnoso-Arenacea Formation (after Argnani and Ricchi Lucchi, 2001; isopachs in the Po plain subsurface from Dondi et al., 1992) and location of the sampling sites. Marnoso-Arenacea sediment sources were located mainly in the Alps but also the Apennines including foreland carbonate ramps in the south. B) Schematic stratigraphical log of the Marnoso-Arenacea Formation (modified after Mutti et al., 2002). Solid circles indicate sampling sites: COR, CAB, GIU, PRE, BR.

Palaeogeographic reconstructions (Mutti and Ricci Lucchi, 1972; Mutti et al., 2002) coupled with petrographic (Gandolfi et al., 1983) and palaeocurrent (Amy and Talling 2006; Muzzi Magalhaes and Tinterri, 2010) analyses revealed that the elongated MA basin was fed mainly by Alpine (crystalline) sediments through multiple entry points located to the N and W, and flowing axially from the NW to the SE (in present-day coordinates) as revealed by paleocurrent directions measured at the base of turbidite beds (Fig. 3.1A). In addition, minor volumes of carbonate and hybrid turbidites derived from shallow-water carbonate platforms located along the southern and south-eastern margins of the basin, in the Gubbio area and central Italy, are also present (Gandolfi et al., 1983; Talling et al., 2007). These carbonate and hybrid turbidites flowed

from the SE to the NW (in present-day coordinates), i.e., in the opposite direction of the aforementioned siliciclastic turbidites, and comprise key marker beds such as the Contessa and Colombine megaturbidites that allow high-resolution stratigraphic correlations at the basin scale. Furthermore, slumps and turbidite flows have been reported coming also from active thrust fronts located to the west of the basin (Ricci Lucchi, 1975). The ability of flows to traverse the basin in opposite directions implies low sea-floor gradients (Ricci Lucchi and Valmori 1980; Amy and Talling 2006). Paleobathymetric estimates from δ18O on benthic foraminifera from the MA indicate a wide range of upper to mid bathyal water depths (Aharon and Sen Gupta, 1994).

The White Marlstones beds (WM beds)

The WM beds consist of < 20 cm (rarely >50 cm) admixtures of cohesive clay and silt (generally ranging from 0.5 to 50 µm in size; Talling et al., 2007). They overlie in rapid vertical transition dark blue-gray Bouma's Te intervals of the MA siliciclastic turbidites, from which they can be distinguished by their texture, lighter color (Fig. 3.2), greater carbonate content (25–45%), as well as lesser total organic content (~1 % T.O.C versus ~2 % T.O.C of the Bouma's Te divisions). The carbonate content of the WM beds is chiefly represented by planktonic foraminifera and coccoliths, and rare benthic foraminifera (Fig. 3.3, white arrows); mica (Fig. 3.3, black arrows), illite, and dolomite have also been observed. This overall composition is reminiscent of the composition of mudstone intervals of carbonate and hybrid turbidites derived from shallow-water carbonate platforms located along the southern and south-eastern margins of the basin, in the Gubbio area and central Italy (Fig. 3.1A) (Gandolfi et al., 1983; Talling et al., 2007).

Our observations indicate that the WM beds are characterized by a massive, ungraded, speckled, and generally featureless aspect with rare 0.2–1.0 mm-thick parallel laminations picked out by concentrations of silt of modal size of 10 µm or by the occurrence of irregular shelly concentrations. Laminae can also be arranged in cm- to dm-thick stacks of alternating fine silt and clayey silt. The vertical distribution of laminae, as well as of bed thickness, composition and color variability, appears to be random throughout the WM beds. Primary sedimentary structures have been partly destroyed by moderate but relatively continuous bioturbation, indicating sedimentation rates sufficiently low to prevent major disturbances to the infauna (McBridge and Picard, 1991; Monaco and Checconi, 2008; Monaco 2008). Numerous published stratigraphical

sections (Ricci Lucchi and Valmori, 1980, Talling, 2001; Mutti et al., 2002) and basin-scale high-resolution correlations (Amy and Talling 2006; Talling et al., 2007; Muzzi Magalhaes and Tinterri, 2010) clearly indicate an apparently random distribution of thickness and frequency of the WM beds compared to the thickness and frequency distribution of the associated MA turbidites. The general down-current (i.e., southward) thinning of turbidites and of Bouma's Te divisions is accompanied by a thickening of the WM beds. The maximum cumulative thickness of the WM beds occurs on the down-flow side of the Verghereto High (Talling et al., 2007).

Fig. 3.2 – A) and B) Examples of Marnoso-Arenacea Formation outcrops showing fine- to medium-grained turbidides (*), the associated Bouma's Te divisions (**), and the WM beds. (***); the WM beds can be distinguished from Bouma's Te divisions by their lighter color as a result of greater carbonate content and lesser total organic carbon content.

The average rate of sediment accumulation inferred from biostratigraphically-dated sections from the literature (Ricci Lucchi and Valmori, 1980, Talling, 2001; Mutti et al., 2002; Amy and Talling 2006; Talling at al., 2007; Muzzi Magalhaes and Tinterri, 2010) is of about 3 cm/kyr. These values are similar to sedimentation rates of generally <2 cm/kyr for compacted pelagic sediments (Solomon Islands; Colwell and Exon, 1988), of 5–15 cm/kyr for compacted hemipelagic sediments (Oman margin; Stow and Tabrez, 1998), of 3–10 cm/kyr for contouritic sheeted drifts (Stow and Tabrez, 1998), and are relatively lower than rates of 20 cm/kyr for modern and uncompacted hemipelagic muds (East Japan Sea; Park et al., 2006).

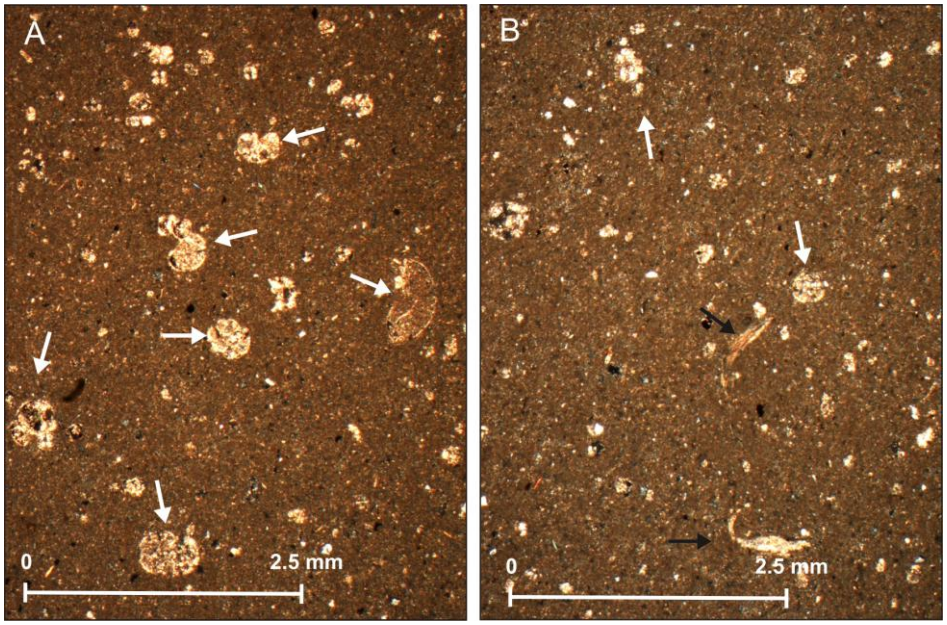

Fig. 3.3 – A) and B) Microfabric of the WM beds, characterized by high carbonate content (~45%; chiefly pelagic foraminifers) and grain size comprised between mud and silt. White arrows indicate pelagic foraminifers (Globigerinoides), whereas black arrows indicate muscovite minerals of the mica group, probably representing the main source of the (para)magnetic susceptibility signal.

The anisotropy of magnetic susceptibility

The magnetic susceptibility is a second-rank symmetric tensor, k_{ij}, which relates the magnetization J_i induced in a sample by a field H_i, according to the formula $J_i = k_{ij} H_j$. The anisotropy of magnetic susceptibility (AMS) can be specified by six quantities, three relating to the magnitude of the principal susceptibility axes (k_{max}, k_{int} and k_{min}) and three relating to their directions, which are mutually orthogonal.

In sedimentologic analyses, the AMS is considered to be a proxy for the preferred alignment of natural magnetic particles attained in the final stages of sediment transport, with the maximum susceptibility axis, k_{max}, and the minimum susceptibility axis, k_{min}, representing the preferred orientation of the longest and shortest magnetic grain axes, respectively (e.g., Hamilton and Rees, 1970; Taira and Scholle, 1979). This method is based on the fact that a current is able to orient paramagnetic grains (e.g., phyllosilicates, olivines, pyroxenes, anphiboles), diamagnetic grains (e.g., quartz, calcite, feldspars), and ferromagnetic (sensu lato) grains (e.g., magnetite, goethite, hematite), and that the resulting AMS ellipsoid reflects the orientation imparted by the current to such grains (Parés et al., 2007).

AMS in sediments may develop during and after deposition. During settling of grains, e.g., phyllosilicates, on the sea floor, their short shape axes usually fall perpendicular to the bedding plane. As a result, an oblate fabric develops (well-developed foliation). The AMS fabric mimics this sedimentologic fabric because in phyllosilicates, the short shape axis corresponds to the crystallographic c-axis as well as to the minimum susceptibility direction, and, therefore, a magnetic foliation (defined by the plane containing k_{max} and k_{int} axes) develops parallel to the depositional surface.

When currents are present, hydraulic forces control grains' alignment (current-induced fabric; Shor et al., 1984). Elongated particles suspended in a moderate velocity flow typically travel in upright (vertical) position until they touch ground and rotate parallel to the flow direction. Flow-aligned fabrics arise when grains are subjected to minimal drag forces and negative lift forces that result in pushing particles down onto the seabed (Pettijohn, 1975; Collinson and Thompson, 1982; Allen, 1984). Such flow-aligned orientations can sometime evolve into flow-transverse orientations when strong currents are capable to lift and displace grains after initial deposition (Schwarzacher, 1963; Johansson, 1964; Hendry, 1976). Contrary to suspended particles, bed-load particles typically roll on the seabed with the long shape axis perpendicular to the main flow direction (Baas et al., 2007), producing what is often called a "rolling" fabric (Harms et al., 1982).

The AMS fabric reflects the orientation of elongated paramagnetic as well as large ferromagnetic grains either parallel or perpendicular to the current direction because in such elongated grains, the maximum susceptibility axis commonly lies broadly along (or at small angle with) the particle length. Consequently, a magnetic lineation can develop as revealed by a clustering of the k_{max} axes either parallel or perpendicular to the current direction depending on the hydrodynamic boundary conditions. After deposition, the fabric may be affected by compaction, bioturbation, and disruption by migration of trapped fluids and/or gas, or tectonic deformation. Thus, studies of the AMS fabric can also provide information on post-depositional processes.

Materials and methods

AMS analyses have been carried out on 93 cylindrical (10.3 cm3) oriented samples collected in 9 distinct WM beds from 4 selected stratigraphic sections (Fig. 3.1) with a water-cooled drill, and oriented with a magnetic compass. All sampled WM beds overlie Bouma's Te intervals of MA siliciclastic turbidites flowing axially from the NW to the SE (in present-day coordinates). The

susceptibility of each specimen was measured in 15 directions with a KLY-3 Kappabridge adopting the standard measurement scheme of the Agico KLY-3 User's Guide (1998). A susceptibility tensor was then fit to the data by means of least square analysis, and the errors of the fit were calculated using multivariate statistics (Agico KLY-3 User's Guide, 1998). Each susceptibility tensor was subsequently rotated into tilt-corrected coordinates using site-mean bedding attitudes, and plotted on stereographic projections. AMS data were also used to obtain for each site the magnetic lineation $L = k_{max}/k_{int}$ (Balsely and Buddington, 1960) and the magnetic foliation $F = k_{int}/k_{min}$ (Stacey et al., 1960). Oblate (foliated) and prolate (lineated) fabrics were plotted on Flinn-type diagrams (Hrouda, 1982; Tarling and Hrouda, 1993).

To determine the ferromagnetic mineralogy of the sediments potentially contributing to the AMS, representative samples were subjected to stepwise acquisition of an isothermal remanent magnetization (IRM) up to 2.5 T with an ASC Pulse Magnetizer. Samples were then subjected to thermal demagnetization of a three-component IRM imparted in 2.5 T, 1.0 T, and 0.1 T orthogonal fields (Lowrie, 1990). A second suite of fresh samples was subjected to thermal demagnetization of the natural remanent magnetization (NRM) in order to isolate magnetic component directions potentially present in the WM beds. IRM and NRM measurements were made on a 2G DC SQUID cryogenic magnetometer placed in a magnetically shielded room in the Alpine Laboratory of Paleomagnetism of Peveragno, Italy.

Results

Equal-area stereographic projections of the samples' susceptibility axes are plotted in Figure 3.4A after correction for bedding tilt, whereas the susceptibility values plus additional parameters discussed in the text, averaged at the site level, are reported in Table 3.1. A well-preserved anisotropic fabric with clustered k_{max}, k_{int} and k_{min} axes is evident in all sites (Fig. 3.4A; entire dataset plotted in Fig. 3.5A). The k_{min} axes are consistently vertical, i.e., perpendicular to the bedding planes, whereas the k_{max} axes are consistently horizontal, i.e., parallel to the bedding planes, and oriented NW–SE (in present-day coordinates, i.e., without correction for Apennine thrust-sheet rotation; see below) (Fig. 3.5B). In one case (site COR 1b; Fig. 3.4A), an imbricated fabric with k_{max} axes plunging to the SE was observed. The anisotropy degree is generally low and the Flinn-type plot shows that the AMS ellipsoids tend to be only

slightly prolate (L>F) or oblate (F>L) (Fig. 3.5C). Notably, purely foliated fabrics with k_{max} and k_{int} axes scattered in the depositional plane (Parés et al., 2007) have not been observed.

Table 3.1 - AMS parameters of the WM beds: n: number of samples per site; Kmean = mean susceptibility; kmax = maximum susceptibility; kint = intermediate susceptibility; kmin = minimum susceptibility; L = magnetic lineation; F = magnetic foliation; σ = standard deviation from the mean.

	n	K_{mean} ± σ [*10E-6 SI]	k_{max} ± σ [*10E-6 SI]	k_{int} ± σ [*10E-6 SI]	k_{min} ± σ [*10E-6 SI]	L ± σ	F ± σ
COR1a	17	146.7 ± 39.90	149.7 ± 40.72	146.0 ± 39.69	144.4 ± 39.28	1.0253 ± 0.0023	1.0113 ± 0.0029
COR1b	5	161.7 ± 2.05	165.4 ± 2.14	161.5 ± 2.06	158.4 ± 1.96	1.0244 ± 1.0010	1.0197 ± 0.0015
COR3	16	189.2 ± 8.45	195.7 ± 8.55	191.6 ± 8.37	180.4 ± 8.52	1.0213 ± 0.0019	1.0625 ± 0.0102
CAB1	4	163.6 ± 11.85	166.9 ± 12.14	164.0 ± 11.86	159.7 ± 11.55	1.0174 ± 0.0005	1.0269 ± 0.0030
GIU2	7	153.7 ± 6.89	157.0 ± 6.99	154.3 ± 6.99	149.7 ± 6.71	1.0178 ± 0.0012	1.0309 ± 0.0043
PRE1	2	156.6 ± 4.09	160.2 ± 4.04	157.8 ± 4.40	151.8 ± 3.84	1.0151 ± 0.0027	1.0392 ± 0.0027
BR4	16	141.8 ± 4.78	144.3 ± 4.65	142.0 ± 4.59	138.9 ± 4.81	1.0161 ± 0.0033	1.0223 ± 0.0046
BR5	14	138.9 ± 5.06	141.7 ± 5.30	139.7 ± 5.18	135.4 ± 4.71	1.0143 ± 0.0007	1.0316 ± 0.0040
BR6	12	173.7 ± 23.64	177.1 ± 24.96	175.2 ± 24.39	168.7 ± 21.61	1.0109 ± 0.0020	1.0374 ± 0.0118
BR7	11	105.7 ± 7.48	107.6 ± 7.87	106.4 ± 7.94	103.0 ± 6.71	1.0121 ± 0.0055	1.0323 ± 0.0170

The observed magnetic fabric could be due to the presence of paramagnetic and/or ferromagnetic (s.l.) grains. Slightly elongated paramagnetic phyllosilicates (muscovite; Fig. 3.3B, black arrows) have been frequently observed in thin sections in association with abundant diamagnetic carbonates. The analyses of the IRM acquisition and of the thermal demagnetization of a three-component IRM reveal the presence of a low coercivity ferromagnetic phase with maximum unblocking temperatures of ~570 °C interpreted as magnetite (Fig. 3.6A, B). The thermal demagnetization of the NRM reveals that this magnetite carries no stable magnetic component directions saved for an initial (low temperature) viscous overprint broadly oriented along the present-day field direction in in situ coordinates. Hence, we conclude that paramagnetic muscovite and possibly also magnetite grains control the observed AMS fabric.

The NW–SE-oriented k_{max} axes of the WM beds are virtually parallel to the average flow direction measured by sedimentological markers (e.g., flute casts) at the base of MA turbidite beds. They are also parallel to the basin axis (corresponding to the elongation of the Miocene Apennine foredeep), to the bathymetric contours, and to the lateral confining slopes of the MA basin. The substantial parallelism between k_{max} orientation and average flows direction from flute casts tends to suggest a sedimentological, current-induced origin for the magnetic fabric.

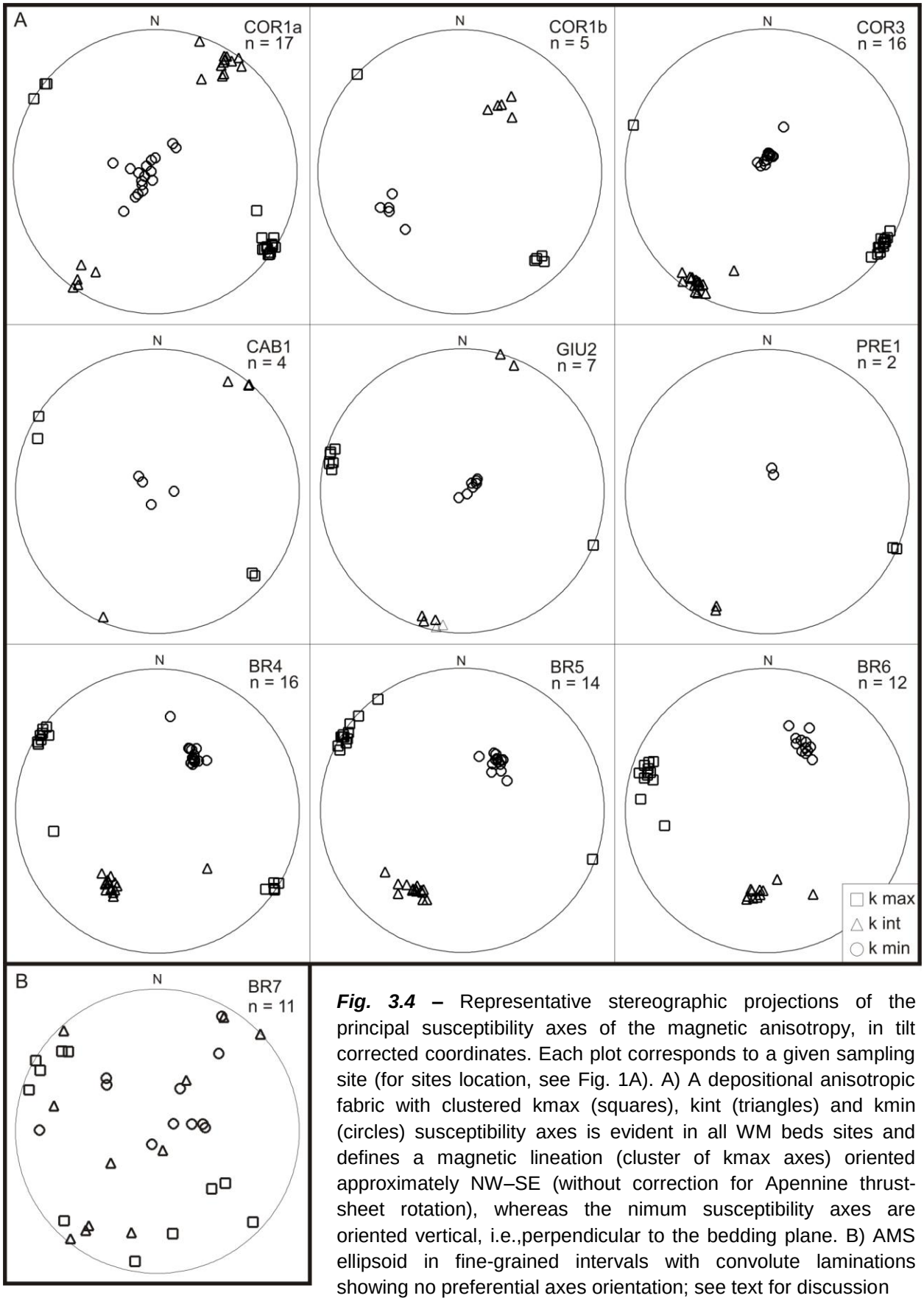

Fig. 3.4 – Representative stereographic projections of the principal susceptibility axes of the magnetic anisotropy, in tilt corrected coordinates. Each plot corresponds to a given sampling site (for sites location, see Fig. 1A). A) A depositional anisotropic fabric with clustered kmax (squares), kint (triangles) and kmin (circles) susceptibility axes is evident in all WM beds sites and defines a magnetic lineation (cluster of kmax axes) oriented approximately NW–SE (without correction for Apennine thrust-sheet rotation), whereas the nimum susceptibility axes are oriented vertical, i.e.,perpendicular to the bedding plane. B) AMS ellipsoid in fine-grained intervals with convolute laminations showing no preferential axes orientation; see text for discussion (COR1a,COR1b, COR3, CAB1, GIU2, PRE1, BR4, BR5, BR6, BR7: sampling sites; n = number of samples per site).

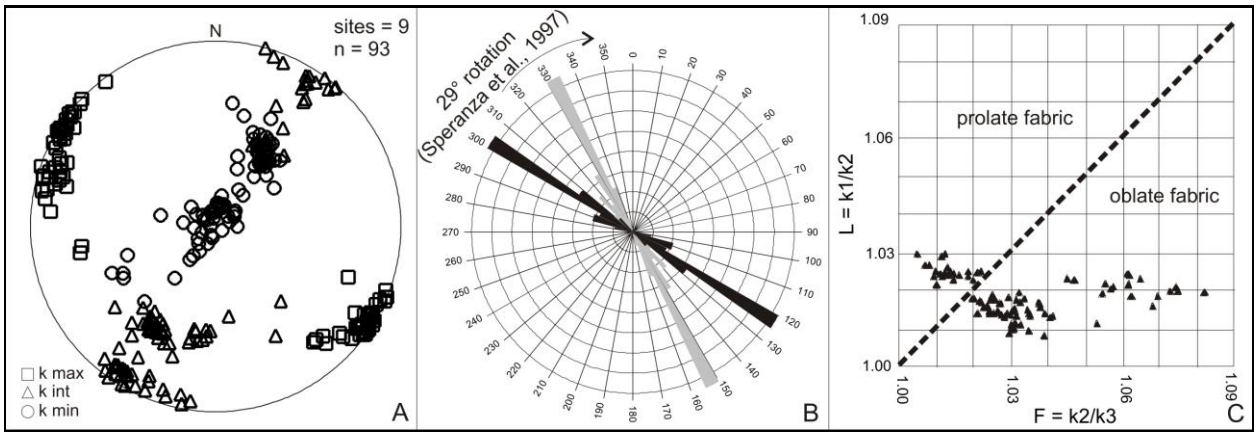

Fig. 3.5 – A) Stereographic projection of principal axes of magnetic susceptibility (kmax = squares, kint = triangles, kmin = circles) for the entire WM beds dataset (N = geographic north; sites = number of sites; n = number of samples) plotted in tilt-corrected coordinates. B) Rose diagram showing in black the preferred kmax orientation of the entire WM beds dataset in tilt-corrected coordinates; a general NW–SE trend (without correction for Apennine thrust-sheet rotation) is clearly evident. The same preferred kmax orientation corrected for Apennine thrust-sheet rotation of 29±8° counterclockwise since the Oligo–Miocene (Speranza et al., 1997) is indicated in grey. C) Flinn-type plot showing the depositional magnetic fabrics of the studied samples. The dashed line separates samples with prolate fabric from samples with oblate fabrics (L = magnetic lineation; F = magnetic foliation).

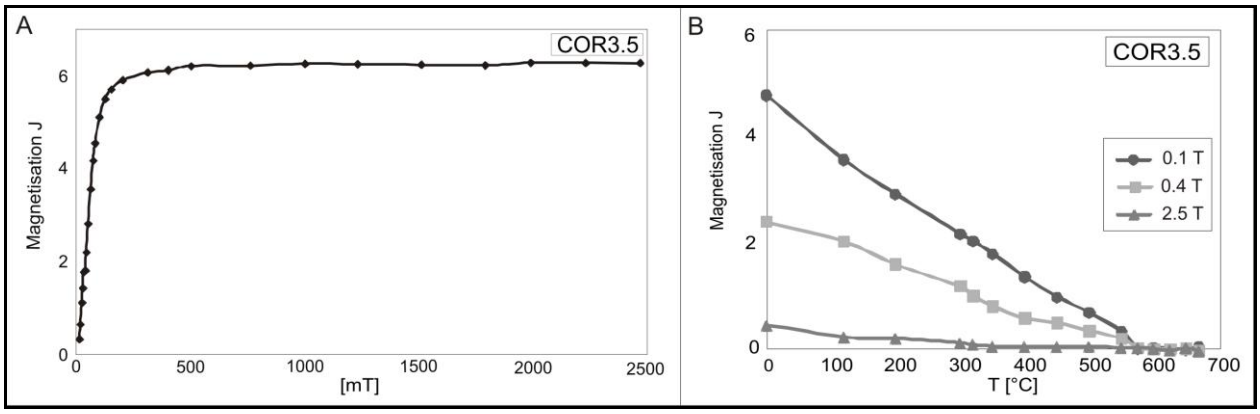

Fig. 3.6 – Isothermal remanent magnetization (IRM) acquisition curve (left panel) and thermal decay of a three-component IRM (righ panel) for sample COR3.5 of the WM beds indicating the presence of magnetite.

Finally, we placed the current-induced AMS fabric of the WM beds in paleogeographic coordinates by correcting the mean k_{max} direction (Fig. 3.5B) for the counterclockwise rotation of Apennine thrust-sheets since the Miocene using primary NRM data from the literature (as our NRM demagnetization experiments yielded inconclusive results). We applied to the mean k_{max} direction a clockwise rotation of 29° ± 8° as suggested by Speranza et al. (1997) and Muttoni et al. (1998, 2000) for Oligo–Miocene sediments from the same general area of this study,

obtaining a corrected NNW–SSE direction (330°E) that approximates the Miocene palaeoflow direction (Fig. 3.5B; grey area).

Discussion and conclusions

The previous analyses indicate the presence in the WM beds of a well-preserved magnetic fabric with k_{max} axes clustered within the depositional plane and broadly parallel to the average flow direction measured by flute casts at the base of turbidite beds. This fabric is interpreted as sedimentary rather than tectonic in origin and suggests that weak velocity flows oriented the maximum susceptibility axes of paramagnetic grains (muscovite) and possibly also ferromagnetic grains (magnetite) parallel to the mean current direction in the final stages of transport. The trend of the k_{max}, and hence of the inferred palaeoflow direction, is oriented NNW–SSE after correction for Apennine thrust-sheet rotation.

A current-induced AMS fabric implies that the WM beds cannot be explained considering simply hemipelagic settling of deep-sea mud because hemipelagic deposition of, e.g., phyllosilicates gives rise to purely foliated fabrics with no preferred k_{max} and k_{int} orientation (e.g., Ellwood, 1980; Lowrie and Hirt, 1987; Taira, 1989; Sagnotti and Meloni, 1993; Pares et al., 2007). Our results suggest that the WM beds were deposited under the effect of weak velocity currents, as previously contemplated (but not proved) by Mutti and Ricci Lucchi (1972). Excluding hemipelagic settling, the WM beds could arise from two alternative depositional mechanisms: turbidity currents or bottom currents.

Turbidity currents

The WM beds could derive from the settling of suspension clouds produced from fading turbidity currents (hemiturbidites sensu Stow and Wetzel, 1990). During a turbidity event, thick and relatively diluted turbulent flows (flowing axially from the NNW to the SSE in tectonic-corrected coordinates; Fig. 3.7A) could have detached from the basal and denser part of the flow at gentle bends along the axial flow path (as described for the Navy Fan of the California borderland; Normark and Piper, 1972). These diluted flows may have moved high along basin-bordering slopes where they eroded and incorporated carbonate-rich sediments, to be eventually deflected and forced to rejoin the axial zone farther down-current after deposition of the dense axial flow (Mutti et al., 2002); Muzzi Magalhaes and Tinterri, 2010). In this interpretation,

sketched in Figure 3.7A, a single large-volume turbidity event can generate a stack of several delayed, ponded WM beds above its main axial deposit of medium-grained sand.

A turbiditic origin implies that the flows, after dropping the heavier terrigenous load, began depositing lighter particles, e.g., abundant carbonate shells and phyllosilicates. This indicates that the WM beds may have resulted from hydraulic sorting of the finer and lighter particles toward the upper part of the flow, and may constitute the distal end members of turbiditic facies tracts (end of Bouma's Te division). Calcite is much denser than clay minerals but clay minerals flocculate more effectively than carbonates (Piper 1978; Stow et al. 1984), forming flocs 10–50 μm in size in a muddy turbulent flow. They are thus much larger hydrodynamically (despite their lower density) than 1–3 μm sized micritic carbonates (Piper 1978; Stow et al. 1984). Thus, when large amounts of fine carbonates are present, their concentration increase near the top of a turbidity current because they have lower tendency to form large flocs, and they will therefore tend to concentrate at the top of graded mud beds.

The settling of a suspension cloud at the end of a turbidity flow may have been facilitated by bathymetric gradient reductions and flow ponding toward the southern part of the basin, or by the presence of intrabasinal topographic highs and/or slope changes that triggered flow deceleration and mud-erosion processes (Muzzi Magalhaes and Tinterri, 2010). Similar depositional mechanisms have been proposed by Remacha et al. (2005) for basin-plain calcilutites in the Hecho Basin (south-central Pyrenees, Spain).

Bottom currents

The WM beds could represent muddy contourites deposited from semi-permanent bottom currents flowing parallel to the basin axis (Fig. 3.7B), similarly to what observed along slope settings elsewhere (Stow and Lovell, 1979; Stow, 1982; Gonthier et al., 1984; Howe, 1995, 1996; Stow and Tabrez, 1998). Light particles such as carbonate shells and phyllosilicates could have been incorporated into bottom currents by particle lofting and re-suspension. The AMS analysis indicates that these currents were relatively constant in direction, whereas sedimentological indicators (sorting, homogenization by bioturbation, and absence of erosional surfaces) point to weak intensities, in the range of 0.05–0.15 ms-1 as derived from the "bedform-velocity matrix" proposed by Stow et al. (2009). The WM beds commonly contain bimodal admixtures of cohesive silt and clay characterized by poor sorting. These characteristics are all commensurate with transport of a mixed-composition load followed by deposition directly from suspension. The occurrence of irregular shelly concentrations and of alternating fine silt and mud

laminae, some of which showing internal grading, possibly indicates small fluctuations in current strength during WM beds deposition.

As the WM beds show a composition similar to the turbidites derived from the carbonate platforms located along the south-eastern margin of the basin (Gandolfi et al., 1983; Talling et al., 2007), we infer that the bottom currents also originated in the south-east and flowed northwestward (Fig. 3.7B) parallel to the basin axis and in the opposite direction of the MA siliciclastic turbidites (Fig. 3.7A). The imbricated magnetic fabric observed in site COR 1b (Fig. 3.4A), with k_{max} axis plunging to the SE, supports this interpretation.

We favour the hypothesis that the WM beds represent muddy contourites based on the following arguments.

(i) The vertical distribution of thickness and frequency of the WM beds appears to be random compared to the bedding thickness distribution of the associated turbidites (Talling, 2001; Amy and Talling, 2006; Talling et al., 2007). In particular, thick WM beds frequently overlie very thin and fine-grained MA turbidites, whereas thick turbidites may underlie thin WM beds. This evidence suggests that the MA turbidites and the WM beds are not related statistically (and presumably also genetically); consequently, the WM beds can hardly represent the distal end members of turbiditic facies tracts.

(ii) The vertical distribution of laminae, sedimentary structures, composition, and color appear to be random throughout the WM beds. Instead, if the WM beds were derived from the settling of suspension clouds produced from fading turbidity currents, we would expect systematic vertical variations of the aforementioned features as described by Piper (1978) and Mulder et al. (2008; 2009).

(iii) Several sedimentological features of the WM beds seem to be more consistent with standard contourite models (Piper, 1978, Stow and Lovell, 1979; Stow, 1982; Gonthier et al., 1984; Howe, 1995, 1996; Stow and Tabrez, 1998, Mulder et al., 2008; 2009; Stow and Faugères, 2008) than with turbidite models (Piper, 1978; Stow and Faugères, 2008; Mulder et al., 2008; 2009). These features include the occurrence of (1) relatively continuous, moderate bioturbation, indicating sedimentation rates sufficiently low to prevent major disturbances to the infauna, (2) parallel laminations, and (3) irregular shelly concentrations.

Our interpretation of the WM beds as muddy contourites does not exclude in any case the effects of pirating by contour currents of fine-grained material originally supplied by turbidity currents,

as demonstrated in similar depositional systems elsewhere (Rebesco et al., 1996, 1997; Pudsey, 2000; Knutz et. al., 2002; Escutia et al., 2000).

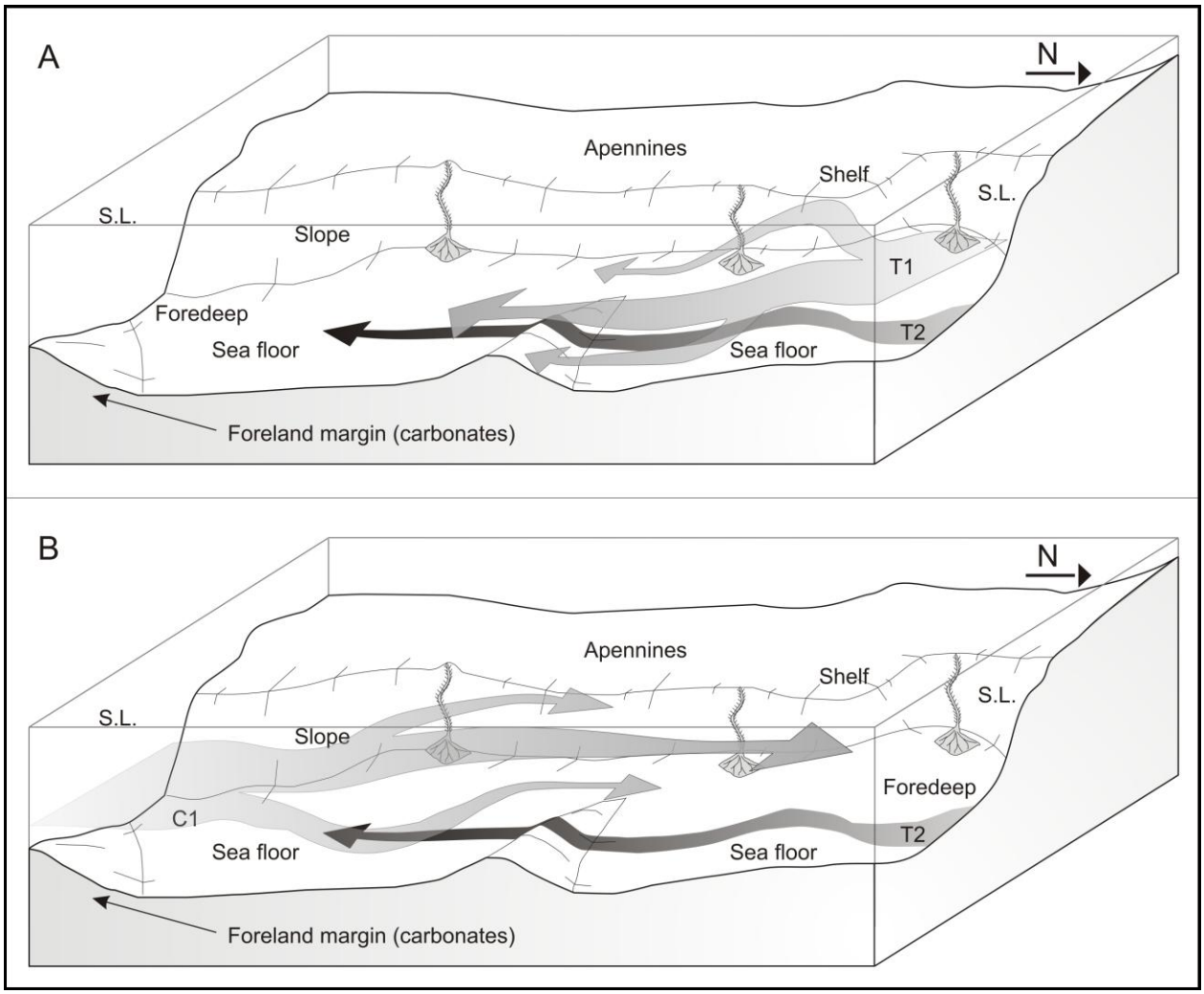

Fig. 3.7 – Alternative mechanisms to explain the WM beds. A) The WM beds could have deposited from an essentially stationary suspension cloud (T1) that is produced from a fading turbidity current (T2), implying that the WM beds resulted from hydraulic sorting of the finer and lighter particles (e.g., carbonates, phyllosilicates) toward the upper part of the flow, and constitute the distal end members of a turbiditic facies tract (end of Bouma's Te division). B) Alternatively, the WM beds could represent muddy contourites deposited from semi-permanent bottom currents (C1) flowing parallel to the basin-axis, which is our preferred option as discussed in the text. (S.L. = sea level; N = geographic north)

ACKNOWLEDGMENTS

G. Malgesini is warmly acknowledged for his help during field work. Financial support was provided by FIRB 2006–2009 funds to F. Felletti, and IAS grant to E. Dall'Olio.

References

Agico Kly-3 User's Guide (Ver. 2.2 Nov. 1998) Modular system for measuring magnetic susceptibility, anysotropy of magnetic susceptibility, and temperature variation of magnetic susceptibility. AGICO Advanced Geoscience Instruments CO. Brno, Czech Republic

Aharon P, Sen Gupta BK (1994) Bathymetric reconstructions of the Miocene-age 'calcari a Lucina' (Northern Apennines, Italy) from oxygen isotopes and benthic Foraminifera. Geo Mar. Lett. 14(2/3): 219–230.

Allen JRL (1984) Sedimentary Structures: their Character and Physical Basis Developments in Sedimentology 30A/B: 593-663

Amy L, Talling PJ (2006) Anatomy of turbidites and linked debrites based on long distance (120 × 30 km) bed correlation, Marnoso Arenacea Formation, Northern Apennines, Italy. Sedimentology 53 (1): 161-212

Argnani A, Ricci Lucchi F (2001) Tertiary siliciclastic turbidite systems of the Northern Apennines. In: Vai GB, Martini P (Eds.) Apennines and Adjacent Mediterranean Basins. Kluwer Academic Publishers:327– 350

Baas JH, Hailwood EA, McCaffrey WD, Kayc M and Jones R (2007) Directional petrological characterisation of deep-marine sandstones using grain fabric and permeability anisotropy: methodologies, theory, application and suggestions for integration. Earth-Sci Rev 82(1-2): 101-142

Balsley JR, Buddington AF (1960) Magnetic susceptibility anisotropy and fabric of some Adirondack granites and orthogneisses. American Journal of Science 258-A:6-20

Boccaletti M, Calamita F, Deiana G, Gelati R, Massari F, Moratti G, Ricci Lucchi F (1990) Migrating foredeep-thrust belt system in the northern Apennines and southern Alps. Palaeogeography Palaeoclimatology Palaeoecology 77(1):3-14

Cifelli F, Mattei M, Chadima M, Lenser S, Hirt AM (2009) The magnetic fabric in "undeformed clays": AMS and neutron texture analyses from the Rif Chain (Morocco). Tectonophysics 466:79–88

Costa E, Pialli G, Plesi G (1998) Foreland basins of the Northern Apennines; relationships with passive subduction of the Adriatic lithosphere. Memorie della Societa Geologica Italiana 52:595-606

Collinson JD, Thompson DB (1982) Sedimentary Structures. George Allen and Unwin, London:194

Colwell JB, Exon NF (1988) Quaternary hemipelagic sedimentation in the basins flanking the Solomon Islands volcanic arc. Geo-marine Letters 8(3): 139-147

Ellwood BB (1980) Induced and remanent magnetic properties of marine sediments as indicators of depositional processes. Marine Geology 38:233-244

Dennielou B (1997) Dynamique sédimentaire sur le plateau des Açores pour les derniers 400 ka. Thèse de doctorat. Université de Bretagne Occidentale: 341

Dondi L, Mostardini F, Rizzini A (1982) Evoluzione sedimentaria e paleogeografica nella Pianura Padana. Translated Title: Sedimentary and paleogeographic evolution of the Po Plain. In: Guida alla geologia del margine Appenninico-Padano Translated Title: Geologic guide to the Apennine-Po margin:47-58

Escutia C, Eittreim SL, Cooper AK, Nelson CH (2000) Morphology and acoustic character of the Antarctic Wilkes Land turbidite systems: ice-sheets-sourced versus river-sourced fans. Journal of Sedimentary Research 70(1):84–93

Gandolfi G, Paganelli L, Zuffa GG (1983) Petrology and dispersal pattern (Miocene, Northern Apennines). J. Sed. Petrol., 53: 493–507.

Gonthier EG, Faugeres JC, Stow DAV (1984) Contourite facies of the Faro drift, Gulf of Cadiz. In: Stow DAV, Piper DJW Editors (1984) Fine grained sediments, deep-water processes and facies. Geological Society Special Publication 15:275–292

Hamilton N, Rees AI (1970) The use of magnetic fabric in paleocurrent estimation. In: Runcorn SK Editor (1970) Palaeogeophysics. Academic Press, New York:445–464

Harms JC, Southard JB, Walker RG (1982) Structures and Sequences in Clastic Rocks. SEPM Short Course vol. 9:249 pp

Hendry HE (1976) The orientation of discoidal clasts in resedimented conglomerates, Cambro-Ordovician, Gaspé, eastern Quebec. Journal of Sedimentary Petrology 46:48–55

Hesse R (1975) Turbiditic and non-turbiditic mudstone of Cretaceous flysch sections of the East Alps and other basins. Sedimentology 22:387–416

Howe JA (1995) Sedimentary processes and variations in slope current activity during the last glacial-interglacial episode on the Hebrides Slope, Northern Rockall Trough, North Atlantic Ocean. Sedimentary Geology 96:201–230

Howe JA (1996) Turbidite and contourite sediment waves in the northern Rockall Trough, North Atlantic Ocean. Sedimentology 43:219–234

Hrouda F (1982) Magnetic anisotropy of rocks and its application in geology and geophysics. Surveys in Geophysics 5(1):37-82

Johansson CE (1964) Orientation of pebbles in running water: a laboratory study. Geografiska Annaler 45A:85–112

Knutz PC, Jones EJW, Austin WEN, van Weering TCE (2002) Glacimarine slope sedimentation, contourite drifts and bottom current pathways on the Barra Fan, UK North Atlantic margin. Marine Geology 188:129–146

Kuenen PH (1964) Deep-sea sands and ancient turbidites. In Bouma AH, Brouwer A (Eds.) Turbidites. Amsterdam, Elsevier:3–33

Lowrie W (1990) Identification of ferromagnetic minerals in a rock by coercivity and unblocking temperature properties. Geophysical Research Letters 17, 2: 159-162

Lowrie W, Hirt AM (1987) Anisotropy of magnetic susceptibility in the Scaglia Rossa pelagic limestone. Earth and Planetary Svience Letters 82:349–356

Mattei M, Funicello R, Kissel C (1995) Paleomagnetic and structural evidence for Neogene block rotations in the Central Apennines, Italy. Journal of Geophysical Research 100 (B9):17863-17883

McBridge E, Picard D (1991) Facies implications of Trichichnus and Chondrites in turbidites and hemipelagites, Marnoso-arenacea Formation (Miocene), northern Apennines, Italy. Palaios 6:281–290

Monaco P, Checconi A (2008) Stratinomic indications by trace fossils in Eocene to Miocene turbidites and hemipelagites of the Northern Apennines (Italy). Studi Trent. Sci. Nat., Acta Geol., 83:133–163

Monaco P (2008) Taphonomic features of Paleodictyon and other graphoglyptid trace fossils in Oligo-Miocene thin-bedded turbidites, northern Apennines, Italy. Palaios 23:667-682

Mulder T, Faugères JC, Gonthier E (2008) Mixed turbidite-contourite systems. In: Rebesco M, Camerlenghi A (eds) Contourites. Developments in Sedimentology 60:435–456

Mulder T, Zaragosi S, Razin P, Grelaud C, Lanfumey V, Bavoil F (2009) A new conceptual model for the deposition process of homogenite; application to a Cretaceous megaturbidite of the western Pyrenees (Basque region, SW France) Sedimentary Geology 222(3-4):263-273

Mutti E (1977) Distinctive thin-bedded turbidite facies and related depositional environments in the Eocene Hecho Group (South-Central Pyrenees, Spain). Sedimentology 24:107–131

Mutti E (1979) Turbidites et cones sous-marins profonds. In Homewood P (ed.) Sédimentation Détritique (Fluviatile, Littorale et Marine): Université de Fribourg, Institut de Géologie:353–419

Mutti E, Johns DR (1979) The role of sedimentary by-passing in the genesis of basin plain and fan fringe turbidites in the Hecho Group System (South-Central Pyrenees). Società Geologica Italiana, Memorie 18:15–22

Mutti E, Ricchi Lucchi F (1972) Le torbiditi dell'Apennino settentrionale: introduzione all'analisi di facies Società Geologica Italiana, Memorie 11:161–199

Mutti E, Ricchi Lucchi F (1975) Field Trip A-11: Turbidite facies and facies associations. In Mutti E, Parea GC, Ricci Lucchi F, Sagri M, Zanzucchi G, Ghibaudo G, Iaccarino I (Eds) Examples of Turbidite Facies Associations from Selected Formations of Northern Apennines: International Association of Sedimentologists, 9th International Congress, Nice, France:21–36

Mutti E, Ricci Lucchi F, Roveri M (2002) Revisiting Turbidites of the Marnoso-arenacea Formation and their Basin-Margin Equivalents: Problems with Classic Models. Excursion Guidebook. Workshop organized by Dipartimento di Scienze della Terra (Universita` di Parma) and Eni- Divisione Agip, 64th EAGE Conference and Exhibition, Florence, Italy, May 27–30, 120 pp.

Muttoni G, Argnani A, Kent DV, Abrahamsen N, Cibin U (1998) Paleomagnetic evidence for Neogene tectonic rotations in the Northern Appennines, Italy. Earth and Planetary Science Letters 154:25-40

Muttoni G, Argnani A, Kent DV, Abrahamsen N, Cibin U (2000) Paleomagnetic evidence for a Neogene two-phase counterclockwise tectonic rotation in the Northern Apennines (Italy). Tectonophysics 326:241-253

Muzzi Magalhaes P, Tinterri R (2010) Stratigraphy and depositional setting of slurry and contained (reflected) beds in the Marnoso-arenacea Formation (Langhian-Serravallian) Northern Apennines, Italy. Sedimentology 57,7:1685-1720

Normark WR, Piper DJW (1972) Sediments and growth pattern of Navy deep-sea fan, San Clemente Basin, California borderland. The Journal of Geology 80,2:198-223

Park MH, Kim JH, Ryu BJ, Kim IS, Chang HW (2006) AMS radiocarbon dating of the marine late Pleistocene–Holocene sediment cores from the western Ulleung Basin, East/Japan Sea. Nuclear Instruments and Methods in Physics Research Section B: Beam Interactions with Materials and Atoms 243 (1): 211-215

Parés JM, Hassold NJC, Rea DK, van der Pluijm BA (2007) Paleocurrent directions from paleomagnetic reorientation of magnetic fabrics in deep-sea sediments at the Antarctic Peninsula Pacific margin (ODP Sites 1095, 1101). Marine Geology 242:261-269.

Pettijohn FJ (1975) Sedimentary Rocks, Third Edition. Harper and Row Publishers, New York: 628

Piper DJW (1978) Turbidite muds and silts on deepsea fans and abyssal plains. In Stanley DJ, Kelling G (Eds.) Sedimentation in Submarine Canyons, Fans and Trenches: Stroudsburg, Pennsylvania, Dowden, Hutchinson and Ross:163–176

Pudsey CJ (2000) Sedimentation on the continental rise west of the Antarctic Peninsula over the last three glacial cycles. Marine Geology 167:313–338

Rebesco M, Camerlenghi A (2008) Contourites, Developments in Sedimentology 60, Elsevier, Amsterdam:663 pp

Rebesco M, Larter RD, Barker PF, Camerlenghi A, Vanneste LE (1997) The history of sedimentation on the continental rise west of the Antarctic Peninsula. In: The American Geophysical Union (Ed.), Geology and Seismic Stratigraphy of the Antarctic Margin: Part 2. Antarctic Research Series 71:29–49

Rebesco M, Larter RD, Camerlenghi A, Barker PF (1996) Giant sediment drifts on the continental rise west of the Antarctic Peninsula. Geo-Marine Letters 16:65–75

Reeder MS, Rothwell G, Stow DAV (2002) The Sicilian gateway: Anatomy of the deep-water connection between East and West Mediterranean basins. In: Stow DAV, Pudsey CJ, Howe JA, Viana AR (eds) Deep-water contourite systems: Modern drifts and ancient series, seismic and sedimentary characteristics: Geological Society of London, Memoirs 22:171-190.

Remacha E, Fernández LP, Maestro E (2005) The Transition Between Sheet-Like Lobe and Basin-Plain Turbidites in the Hecho Basin (South-Central Pyrenees, Spain). Journal of Sedimentary Research 75(5):798-819

Ricci Lucchi F (1969) Recherches stratonomiques et sédimentologiques sur le Flysch Miocène de la Romagna (Formation Marnoso-arenacea). Proc. IV Sess. Comm. Medit. Neog. Strat. Giorn. Geol. 36:163-198

Ricci Lucchi F (1975) Depositional cycles in two turbidite formations of northern Apennines (Italy). Journal of Sedimentary Petrology 45(1):3-43

Ricci Lucchi F (1978) Turbidite dispersal in a Miocene deep-sea plain. Geol. Mijnbouw 57:559-576

Ricci Lucchi F (1979) Ricostruzione geometrica parziale di un lobo di conoide sottomarina. Mem. Soc. Geol. It. 18:125–133

Ricci Lucchi F (1981) The Marnoso arenacea turbidites, Romagna and Umbria Apennines. In: Excursion guidebook, with contribution on sedimentology of some italian basins (Ed. F. Ricci Lucchi), 2nd IAS Eur. Meeting, Bologna:229-303

Ricci Lucchi F (1986) The Oligocene to Recent foreland basins of the Northern Apennines. In Allen PA, Homewood P (Eds.) Foreland Basins. International Association of Sedimentologists, Special Publication 8:105–139

Ricci Lucchi F, Valmori E (1980) Basin-wide turbidites in a Miocene, over-supplied deep-sea plain: a geometrical analysis. Sedimentology 27:241-270

Rupke NA (1975) Deposition of fine-grained sediments in the abyssal environment of the Algero-Balearic Basin, western Mediterranean Sea. Sedimentology 22:95–109

Sagnotti L, Meloni A (1993) Pleistocene rotations and strain in southern Italy: the example of the Sant'Arcangelo Basin. Annali di Geofisica XXXVI,2:83-95

Schwarzacher W (1963) Orientation of crinoids by current action. Journal of Sedimentary Petrology 33:580–586

Shor AN, Kent DV, Flood RD (1984) Contourite or turbidite? Magnetic fabric of fine-grained Quaternary sediments, Nova Scotia continental rise. In Stow DAV, Piper DJW (Eds.) Fine-Grained Sediments; Deep- Water Processes and Facies. Geological Society of London, Special Publication 15:257-273

Speranza F, Sagnotti L, Mattei M (1997) Tectonics of the Umbria–Marche–Romagna arc (central-northern Apennines, Italy): new paleomagnetic constraints. Journal of Geophysical Research 102(B2):3153–3166

Stacey FD, Joplin G, Lindsay J (1960) Magnetic anisotropy and fabric of some foliated rocks from SE. Australia Geofis Pura Appl 47:30–40

Stanley DJ (1988) Turbidities reworked by bottom currents: Upper Cretaceous examples from St. Croix, US Virgin Islands. Smithsonian Contributions to the Marine Science 33:79 pp

Stow DAV (1982) Bottom currents and contourites in the North Atlantic. Bull. Inst. Geol. Bassin d'Aquitaine 31:151–166

Stow DAV, Faugères JC (2008) Contourites facies and facies model. In: Rebesco M, Camerlenghi A (eds) Contourites. Developments in Sedimentology 60:223–250

Stow DAV, Faugères JC, Viana AR, Gonthier E (1998) Fossil contourites; a critical review. Sedimentary Geology 115(1-4):3-31

Stow DAV, Hernandez-Molina FJ, Llave E, Sayago-Gil M, Diaz del Rio V, Branson A (2009) Bedform-velocity matrix; the estimation of bottom current velocity from bedform observations. Geology Boulder 37(4):327-330

Stow DAV, Lovell JPB (1979) Contourites: their recognition in modern and ancient sediments. Earth Science Reviews 14:251–291

Stow DAV, Piper DJW (1984) Fine-Grained Sediments; Deep- Water Processes and Facies. Geological Society of London, Special Publication 15:659 p

Stow DAV, Tabrez AR (1998) Hemipelagites: processes, facies and model. In: Stoker MS, Evans D, Cramp A (Eds) Geological processes on continental margins. Geological Society (London) Special Publication 129, Blackwell Scientific, Oxford:317–337

Stow DAV, Wetzel A (1990) Hemiturbidite: a new type of deep-water sediment. In Cochran JR, Stow DAV (Eds.) Proceedings of the Ocean Drilling Program, Scientific Results: College Station, Texas, U.S.A. 116:25–34

Stow DAV, Wezel FC, Savelli D, Rainey SRC, Angell G (1984) Depositional model for calcilutites: Scaglia Rossa limestones, Umbro–Marchean Apennines. In Stow DAV, Piper DJW (Eds.) Fine-Grained Sediments; Deep- Water Processes and Facies. Geological Society of London, Special Publication 15:223–241

Taira A (1989) Magnetic fabric and depositional processes. In: Taira A., Masuda F. (Eds) Sedimentary facies in the Active Plate Margin. Tokyo, Terra Sci.Publ.:44-77

Taira A, Scholle PA (1979) Deposition of resedimented sandstone beds in the Pico Formation, Ventura Basin, California, as interpreted from magnetic fabric measurements. Bulletin of the Geological Society of America 90:952–962

Talling PJ (2001) On the frequency distribution of turbidite thickness. Sedimentology 48:1297-1329

Talling PJ, Amy LA, Wynn RB, Blackbourn G, Gibson O (2007) Evolution of Turbidity Currents Deduced from Extensive Thin Turbidites: Marnoso Arenacea Formation (Miocene), Italian Apennines. Journal of Sedimentary Research 77(3):172-196

Tarling DH, Hrouda F (1993) The Magnetic Anisotropy of Rocks. Chapman and Hall:212 p

Vai GB (2001) GSSP, IUGS and IGC; an endless story toward a common language in the earth sciences. Episodes 24(1):29-31

Van Der Lingen GJ (1969) The turbidite problem: New Zealand. Journal of Geology and Geophysics 12:7–50

Viana AR (2008) Economic relevance of Conturites. In: Rebesco M, Camerlenghi A (eds) Contourites. Developments in Sedimentology 60:493-510

Chapter 4

Paper #3

The anisotropy of magnetic susceptibility as a tool to discriminate flow dynamics in a confined turbidite system (Castagnola Formation, NW Italy)

Eleonora Dall'Olio[1*], Fabrizio Felletti[1] and Giovanni Muttoni[1]

1 Dipartimento di Scienze della Terra "Ardito Desio". Università degli Studi di Milano. Via Mangiagalli 34, 20133 Milano, Italy.

Abstract

This paper details the impact of basin topography on flow behavior and deposition of a well-exposed confined turbiditic succession, evaluating the use of the anisotropy of magnetic susceptibility (AMS) as a tool to investigate the effects of basin confinement on turbidity flow dynamics. The study succession (~300 m thick) crops out in the eastern part of the Tertiary Piedmont Basin (Castagnola Basin, northern Italy) and occurs in the lower member of an Upper Oligocene–Lower Miocene turbidite system (Castagnola Formation). This small and confined turbidite system hosts sheet-like turbidite sandstone beds with a variable degree of morphological confinement.

A well-preserved anisotropy of magnetic susceptibility (with an overall flow-aligned fabric) has been observed in many sites and is due to the presence of paramagnetic and/or ferromagnetic (s.l.) grains. The AMS stereoplots were associated to the different depositional intervals in which they were collected. Anyway the correlation between AMS fabric and depositional intervals reveals to be not straightforward. By contrast, we observed a strong correlation between magnetic fabric and bed-thickness distribution: (a) beds thicker than ~1.20 m show a wide range of variability of magnetic fabrics, whereas (b) beds thinner than ~1.20 m show a developed flow-oriented magnetic fabric. The thickness of ~1.20 m represents a threshold that marks the minimum thickness of a specific group of beds generated by flows that, because of the volume transported, were able to cover the entire basin floor, to be reflected or deflected and to aggrade vertically, generating a continuous interaction of flows, that are recorded in the AMS stereoplots. AMS fabric and bed thickness distribution are deeply investigated to support the hypothesis of their primarily relationship in the organization of grains in confined basins.

Key words

Anisotropy of magnetic susceptibility, Castagnola Formation, confined turbidite system

Introduction

Deposition derived from sediment gravity flows in deep-marine confined basins is strongly controlled by the interactions among flow magnitude and/or duration, flow efficiency, size and morphology (i.e., degree of confinement, irregularities of bottom and marginal slopes) of the depocenters (Mutti, 1979; Kneller,1995; Winker,1996; Prather et al.,1998; Kneller and McCaffrey, 1999; Mutti et al.,1999; Sinclair and Tomasso, 2002; Sinclair and Cowie, 2003; Kneller and McCaffrey, 2004; Lomas and Joseph, 2004; Smith, 2004 among many others). Understanding how these variables combine to modify facies distribution is an important and complex issue.

This study aims to evaluate the use of the anisotropy of magnetic susceptibility (AMS) as a tool to investigate the effects of basin confinement on turbidity flow dynamics, i.e., changes in paleocurrent intensity and direction (e.g. flow ponding, reflection and/or deflection) related to basin geometry. The AMS is a highly effective technique that investigates the magnetic fabric directly correlated to gravity flows. In standing water deposition, the minimum susceptibility axes are clustered around the pole, whereas the maximum and the intermediate susceptibility axes are uniformly dispersed, defining a planar, near-horizontal, gravity-induced settling fabric (Fig. 4.1A). Instead, the magnetic fabric of sediments deposited from flowing water is typified by a current-oriented magnetic foliation plane (e.g., Ellwood, 1980; Lowrie and Hirt, 1987; Taira, 1989; Sagnotti and Meloni, 1993; Pares et al., 2007)that could highlight a flow oblique fabric (Fig. 4.1B), a flow transverse fabric (Fig. 4.1C) or a flow-aligned fabric (Fig. 4.1D).

Our case study focuses on the well-exposed Castagnola Formation, which represents the deepest and most confined depocenter of an Upper Oligocene–Lower Miocene turbidite system cropping out in the eastern part of the Tertiary Piedmont Basin (NW Italy) (Baruffini et al., 1994; Di Giulio and Galbiati, 1998; Mutti, 1992). The basin hosts sheet-like turbidite sandstone beds that provide analogues for several deepwater clastic reservoirs with a variable degree of morphological confinement. Good exposures facilitate direct observations of different types of terminations of the turbidite sandstone bodies, together with their corresponding equivalent successions at the depocenter (Baruffini et al., 1994; Felletti, 2002).

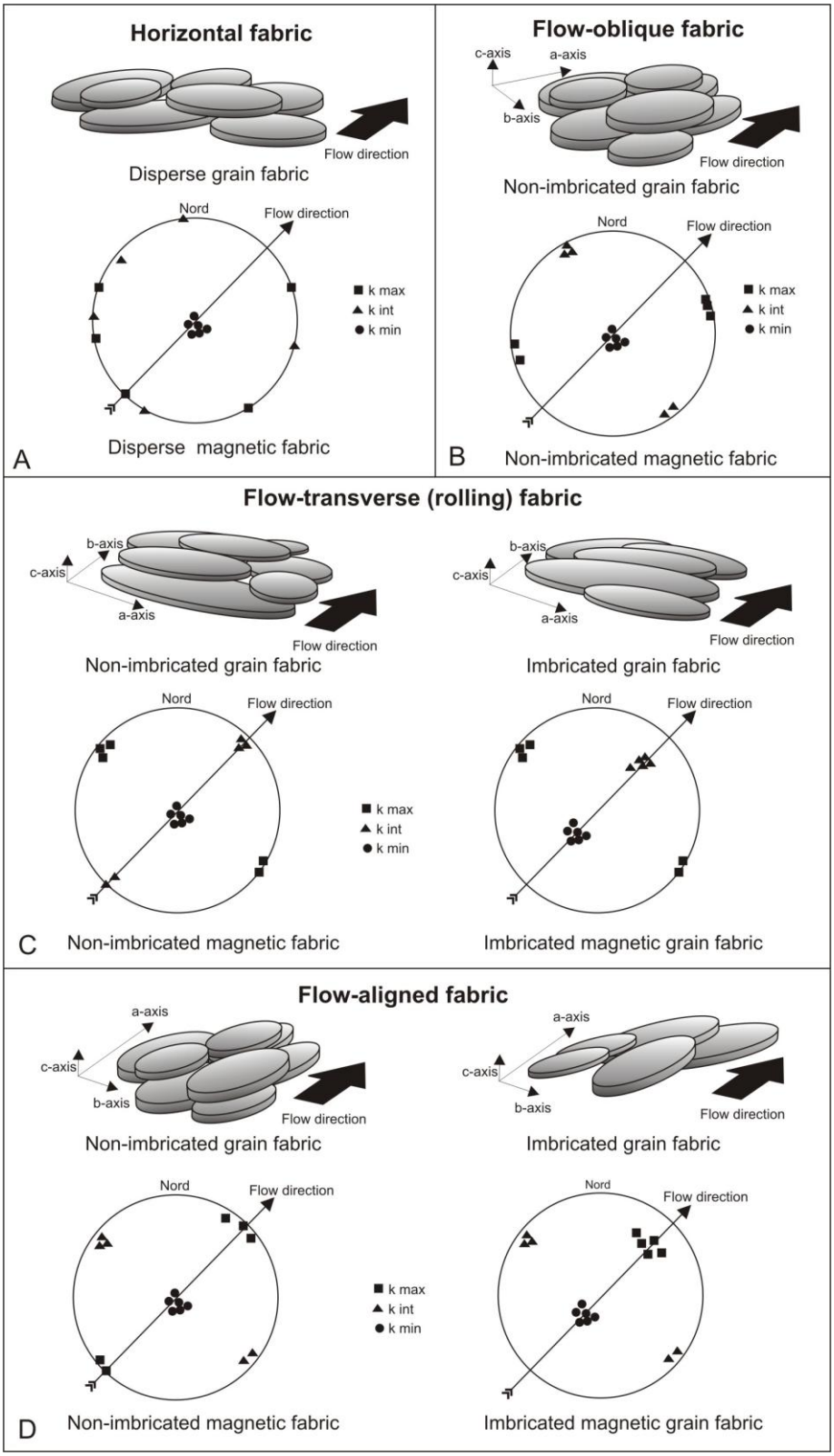

Fig. 4.1 – Main types of anisotropic grain shape fabrics, presented by schematic drawings of the orientation of elongated grains and by the orientation of the three principal orthogonal axes in upper hemisphere stereograms. Horizontal fabric (A) and flow-oblique fabric (B) are non-imbricated by definition. For the flow-transverse (C) and flow-aligned (D) fabrics, non-imbricated and imbricated subtypes are shown on the left- and right-hand side, respectively. a=long grain axis; b=grain axis of intermediate length; c=short grain axis

Geological setting and facies-stratigraphy

The study area, located in NW Italy, belongs to the Tertiary Piedmont Basin (hereafter TPB – Fig. 4.2A), which is a relatively undeformed episutural basin that developed unconformably over the Alpine and Apenninic fold-and-thrust belts (Biella et al., 1992). A thick sequence of predominantly terrigeneous sediments of Oligocene to Miocene age (Gelati and Falletti, 1996; Mutti et al., 2002 – Fig. 4.2B) was deposited in the TPB during phases of major Alpine and Apenninic orogenic deformation. In the easternmost part of the TPB, an almost 3000 m-thick turbidite succession crops out , ranging from late Eocene to early Miocene in age (Baruffini et al., 1994). Several unconformities are present within the succession. The major ones correspond to regional tectonic events that induced important changes in basin size and configuration, as well as variations of sediment dispersal pattern and facies distribution (Cavanna et al., 1989; Di Giulio and Galbiati, 1993). The turbidite deposits record morphological variations on the sea floor due to the activity of the Villalvernia-Varzi Line (VVL; Fig. 4.2C), a crustal-scale lineament active at Oligo-Miocene times (Biella et al., 1992; Laubscher et al., 1992).

The Castagnola Formation

A Chattian–Aquitanian phase of transpressive motion along the VVL produced a structural depression in the easternmost part of the TPB (Castagnola Basin - Fig. 4.2C), that was progressively filled by the siliciclastic turbidites of the Castagnola Formation (Baruffini et al., 1994; Di Giulio and Galbiati, 1998; Mutti, 1992). The basin axis is oriented ENE–WSW (in modern-day coordinates) and it is approximately parallel to the VVL trend. The basin geometry exerted a structural and morphological control on the shape of turbidite bodies, on their facies distributions, and on stacking patterns (Baruffini et al., 1994). The Castagnola turbidite system, consisting of at least 800 m of deepwater sediments, appears to pinch out with onlap relationships (‘infill’ of Hurst et al., 1999) onto the underlying, tectonically deformed slope marls of the Rigoroso Formation (Cavanna et al., 1989; Di Giulio and Galbiati, 1993). According to some authors (Cavanna et al., 1989; Stocchi et al., 1992; Baruffini et al., 1994), the Castagnola Formation consists of large volume gravity flows charged with fine-grained sediment that evolved from high-density to low-density turbidity currents during their run-out. The tabular geometry of these sediments is a product of the relatively large volumes of the gravity flows with respect to the size of the depocenter. The main dispersion of paleocurrents is toward the NE (in modern-day coordinates) as revealed from sedimentological indicators at the base of the Castagnola Formation.

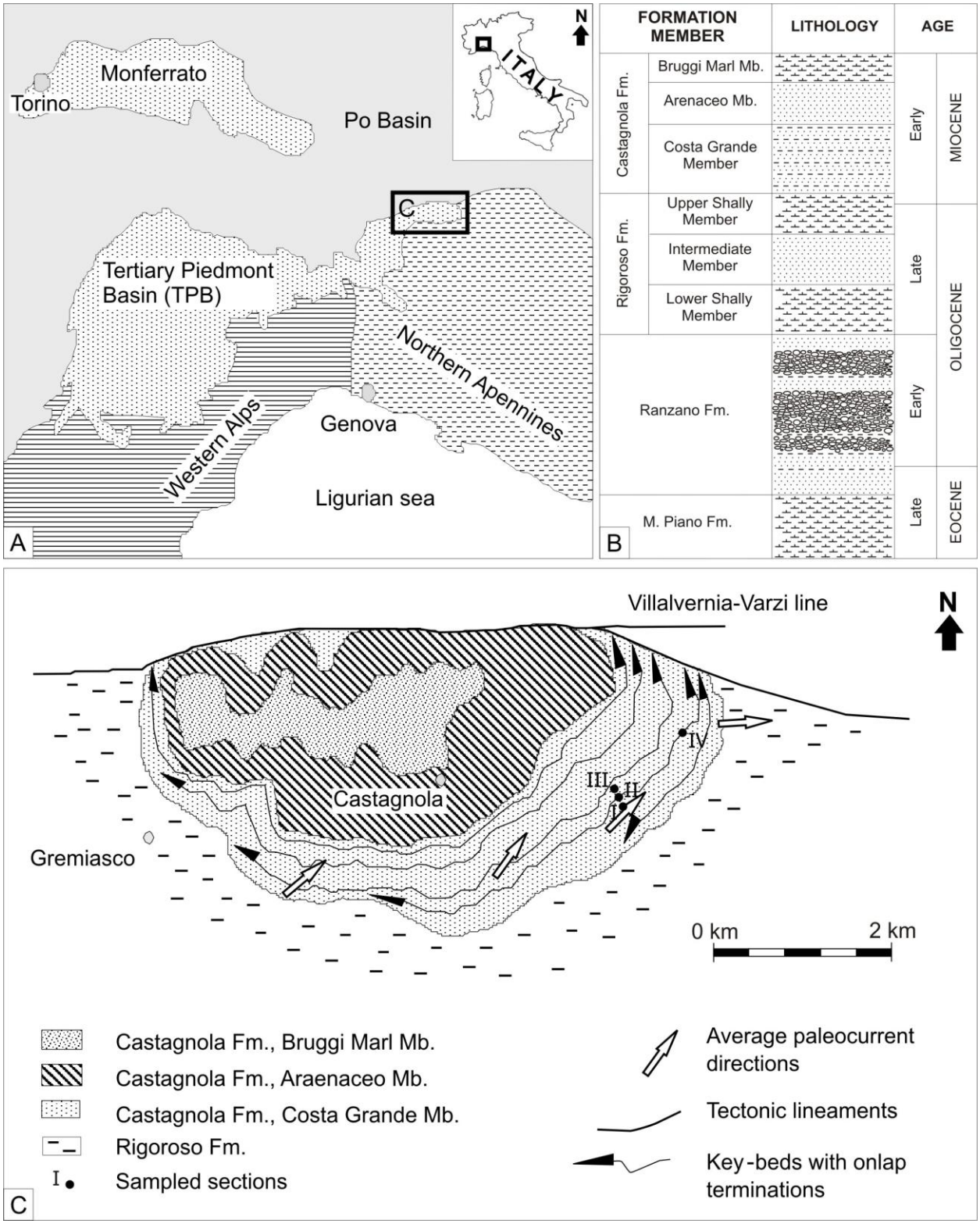

Fig. 4.2 – (A) Location of the Tertiary Piedmont Basin (Italy); (B) stratigraphic column for the eastern sector of the Tertiary Piedmont Basin (after Andreoni et al.,1981); (C) geological sketch map of the Castagnola Basin (redrawn and modified after Stocchi et al., 2002) with the sampling sections (dots)

Table 4.1 – Features of the sampled basin

	CASTAGNOLA TURBIDITE SYSTEM
Basin size (present time)	Max length ~ 6 km SW-NE Max width ~ 4 km NW-SE
Max thickness of the system	900 m (Baruffini et al., 1994)
Average palaeocurrent trends	From SW to NW (dispersion up to 180°)
Volume sediment entrapped	5 x 109 m3 (total), 1.3 x 109 m3 (sand) (Baruffini et al., 1994)
Depositional style	Flat and aggradational
Shape of sandstones bodies	Almost tabular
Geometry of beds	Tabular. Sandstone beds fine upward into mudstones. Rare erosional surfaces
Max. lateral extension of individual beds	6 km, corresponding to the width of the basin
Stacking patterns	Small-scale cycles of bed thick
Terminations	1) Rapid pinch-outs (average angle of onlap: 10°, generally flows impinged the palaeoslope at high angle); 2) Gradual pinch-outs (average angle of onlap: 5°, generally flows impinged the palaeoslope at low angle)
Facies association	- classical Tc-e/Td-e Bouma sequences (dilute turbulent flows); - massive and graded sandstone beds, frequent delayed grading (concentrated flows with aggradational depositional features); - sandstone beds and sandstone/mudstone couplets, formed by repetitions of massive, plane-parallel laminated and cross-laminated sandstone depositional divisions (mildly concentrated flows with complex internal organization).

Facies and facies associations

The studied sequence (Tab. 1 - Fig. 4.3A and B) comprises the oldest turbidite sandstones of the Castagnola Basin (Fig. 4.2C), cropping out over a ~4 km-long transect where sediment thickness ranges from ~300 m in the local depocenter to 0 m at the northern and southern terminations (Baruffini et al., 1994). This succession is bounded at the base by key-bed 1, which is the lowermost megabed of the Castagnola Formation, characterized by a thickness of up to 5 m, and at its top by another megabed termed key-bed 3 (Cavanna et al., 1989). The study succession shows an increase of the sand/mud ratio towards its northern pinch-out termination.

The facies and facies associations that can be observed in the studied succession are: (i) the classical Tc-e/Td-e Bouma sequences (dilute turbulent flows); (ii) massive and graded sandstone beds, frequent delayed grading (concentrated flows with aggradational depositional features); (iii) sandstone beds and sandstone/mudstone couplets, formed by repetitions of massive, plane-parallel laminated and cross-laminated sandstone depositional divisions (mildly concentrated flows with complex internal organization).

In order to evaluate changes in flow direction and intensity, different depositional intervals (sensu Harms, 1975; Walker, 1984) have been vertically sampled in the same bed (e.g. massive division, parallel-laminated division cross-laminated division, etc.). A description of the sampled deposition intervals and of the fabric patterns is provided hereafter.

Massive sandstones (Bouma's Ta interval) (Fig. 4.3C). These intervals are characterized by lack of stratification and normal grading. They are commonly interpreted as the product of deposition at rates of suspended load fallout high enough to suppress tractional transport (Ghibaudo, 1992; Arnott and Hand, 1989 Allen, 1991). Under these circumstances, quick dumping of sediment may occur in highly depletive flows (sensu Kneller and Branney, 1995) or rapidly waning flows. Although the massive beds used in the present study were selected carefully, it cannot be ruled out that some samples were collected from depositional intervals that appear massive by eye, but were formed in upper plane-bed or current ripple flow regimes.

In massive basal Ta-divisions, both flow-aligned and disordered fabrics have been found, although some of these should better be termed oblique fabrics (e.g. Sestini and Pranzini, 1965; Scott, 1967; Rees et al., 1968; Hiscott and Middleton, 1980). The disordered/oblique fabric may be caused by high apparent viscosity due to high near-bed sediment concentrations combined with frequent clast collisions during rapid settling from suspension (Rees, 1983). Imbrication angles are highly variable, but published values of up to 30°–40° tend to be higher than for Tb-divisions (Bouma, 1962; Hiscott and Middleton, 1980).

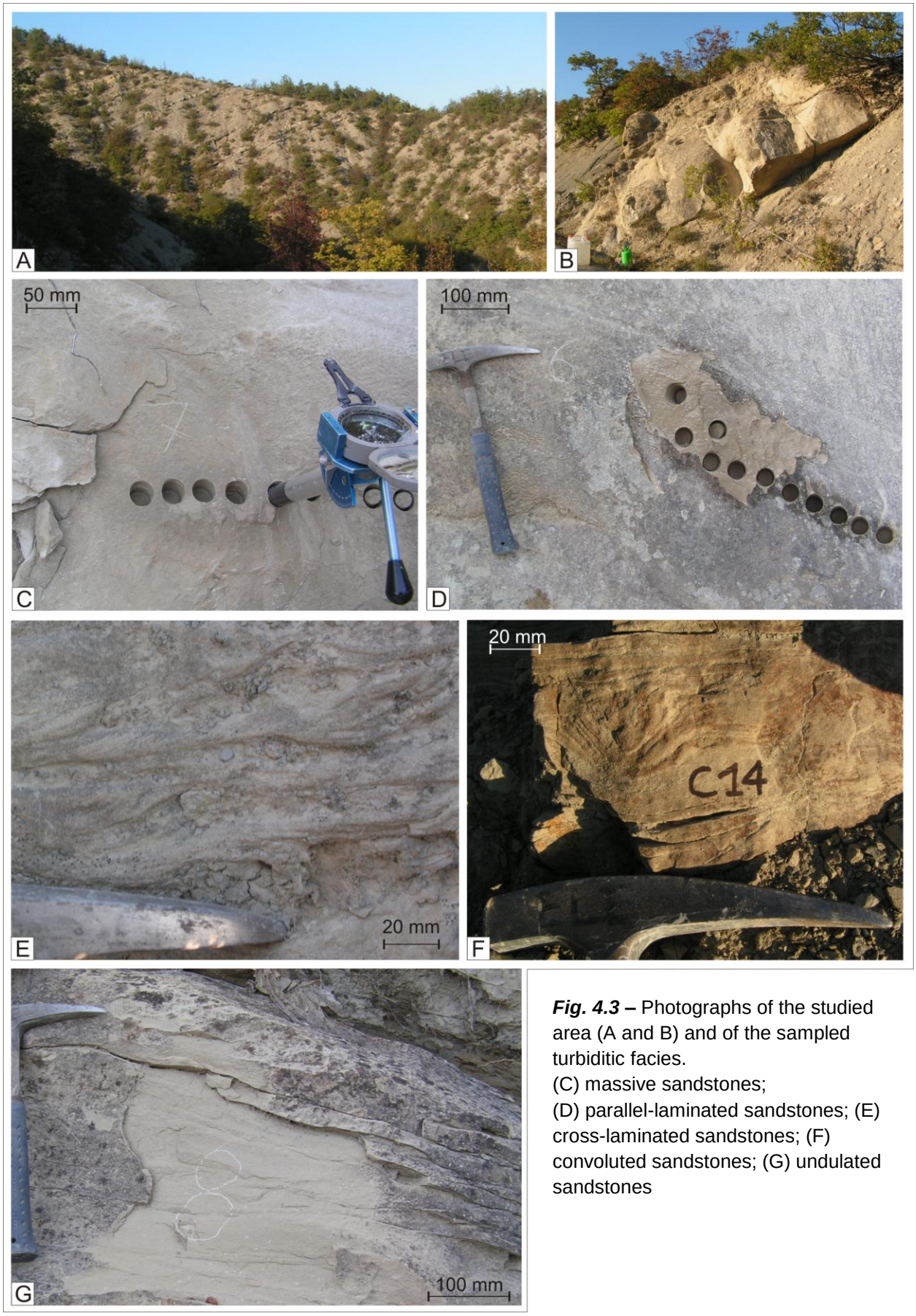

Fig. 4.3 – Photographs of the studied area (A and B) and of the sampled turbiditic facies.
(C) massive sandstones;
(D) parallel-laminated sandstones; (E) cross-laminated sandstones; (F) convoluted sandstones; (G) undulated sandstones

Parallel-laminated sandstones (Bouma's Tb interval) (Fig. 4.3D). These sandstones comprise alternations of laminae of different grain size, usually present at the top of stratified planar beds or massive beds with normal grading. Laminae formation is related to traction coupled with fall-out in upper flow regimes (Lowe, 1982; Ghibaudo, 1992).

Flow-aligned fabric is apparently most common in plane-parallel laminated intervals (Crowell, 1955; Stanley, 1963; Scott, 1967; Walker, 1967; Clark and Stanbrook, 2001), but flow-transverse fabric has been observed as well (Bouma, 1962; Stanley, 1963; Parkash and Middleton, 1970; Clark and Stanbrook, 2001). Rapid sedimentation from suspension favors a flow-aligned fabric. At relatively low suspended sediment concentrations; clasts can be transported along the bottom by traction and attain a flow-transverse fabric. Imbrication angles for Tb-divisions usually range between 5° and 20°. The highest imbrication angles have been found on upper stage plane beds below flows with high suspended fallout rate (Arnott and Hand, 1989) and high Froude number (Yagishita et al., 2004).

Cross-laminated sandstones (Bouma's Tc interval) (Fig. 4.3E). These sandstones are characterized by ripple-cross laminations related to traction coupled with fall-out under lower flow regimes conductive to ripples formation. They represent the final flow stages, in which flow density and velocity are sufficiently low for bed-form development (Lowe, 1982; Ghibaudo, 1992).

Grain avalanches associated with migrating bed forms theoretically generate flow-aligned fabrics. This is confirmed by measurements in rippled Tc-divisions (Taira and Scholle, 1979). However, Bouma (1962) found flow-transverse fabric, Von Rad (1970) obtained a wide spread in grain orientations, and Ballance (1964) found flow-transverse fabric in mud ripples. Current ripples in Tc-divisions dominantly have linguoid crest lines accompanied by highly variable flow directions at the sediment surface (Baas, 1999). Hence, a relatively large offset from a flow-aligned fabric is expected in sections on either side of the center line through a linguoid ripple. This may account for the observed variation in fabric patterns in the Tc-divisions. Mean imbrication angles in Tc-divisions are similar to those in Tb-divisions, but the variance is larger (McBride, 1962; Von Rad, 1970; Taira and Scholle, 1979).

Undulated sandstones (Fig. 4.3F). These medium-grained sandstones consist of a series of broad, symmetrical undulations, between 20 and 50 cm in wavelength and 2 to 4 cm in amplitude. The undulations are ~10 cm-thick, and generally occur above a graded basal division. They grade upward with decreasing amplitude into parallel laminae. The crests of the

undulations are roughly parallel to the sole mark directions. They are interpreted as longitudinal features and generated by upper flow regimes (Walker, 1967).

Few previous studies concentrated on this fabric patterns. A flow-aligned fabric is apparently most common (Scott, 1967; Parkash and Middleton, 1970), but flow-transverse fabric has been observed as well. Rapid sedimentation from suspension favors a flow-aligned fabric. The different behavior can be explained with a variation of flow velocity that allows the grains to roll and jump on the bedding plane. At relatively low suspended sediment concentrations, clasts can be transported along the bottom by traction and attain a flow-transverse fabric.

Convoluted sandstones (Fig. 4.3G). These medium- to fine-grained sandstones are characterized by the presence of convolute laminae with load structures.

In convolute deposits, clasts are weakly flow-aligned (Hiscott et al., 1997), and the grain fabric is highly variable to isotropic (Bouma and Pluenneke, 1975).

Debrites. These depositional intervals are characterized by a poorly sorted and/or chaotically structured muddier sand or sandy mud with a dark color, easily distinguishable by the lower and upper portions of the bed (Haughton et al., 2009). Debrites are characteristic of hybrid events, in which an initial turbulent flow is succeeded by a debris flow because of a change in flow rheology (Haughton et al., 2009).

In debris flow deposits (sensu Middleton and Hampton, 1973, 1976), clasts are weakly flow-aligned (Hiscott et al., 1997), particularly in the basal zone of shearing or the grain fabric is highly variable to isotropic (Bouma and Pluenneke, 1975). Imbrication is either absent or low angle and dipping up-current (Bouma and Pluenneke, 1975).

Turbidite mud/Hemipelagites. In this category we include turbidite muddy divisions and hemipelagic shales; we have no objective sedimentological elements to separate the two category within the studied succession. They are muddy sediments that deposited by slow settling of particles or are formed by suspension fallout at low flow velocities (Taira and Scholle, 1979).

Methods and sampling

Data collection

Four detailed stratigraphical sections were studied to represent the typical basin center sequence (sections I, II, III) and basin margin sequence (section IV) (Fig. 4.2C and Fig. 4.4). Logs measured record for each bed its total thickness as well as the thickness and sedimentological characteristics (grain size, presence of erosional surfaces, mud clasts, etc.) of its internal

subdivisions (i.e., depositional divisions or bed intervals, sensu Ghibaudo, 1992). Partially amalgamated beds were measured as individual layers by detecting the subtle grain-size changes that are associated with amalgamation surfaces. Paleocurrent sedimentological indicators (*flute marks*), present at the base of the sampled turbidite beds, were measured with a magnetic compass in order to validate (and compare) flow directions estimated by AMS analyses. Samples for paleomagnetic analyses were collected in the field (302 oriented samples) with a water-cooled rock drill and oriented with a magnetic compass. Cylindrical samples have been reduced in the laboratory to standard dimension (2.5 cm in diameter and 2.22 cm in height for a total volume of ~10 cm^3).

Laboratory analysis

Anisotropy of magnetic susceptibility (AMS). AMS analyses have been carried out on 302 oriented samples. The magnetic susceptibility of each specimen was measured in 15 directions with a KLY-3 Kappabridge adopting the standard measurement scheme illustrated in the Agico KLY-3 User's Guide (1998). A susceptibility tensor was then fit to the data by means of least square analysis, and the errors of the fit were calculated using multivariate statistics (Agico KLY-3 User's Guide, 1998). Susceptibility tensors were subsequently rotated into tilt-corrected coordinates using site-mean bedding attitudes, and then plotted on stereographic projections. AMS is considered to be a proxy for the preferred alignment of natural magnetic particles attained in the final stages of sediment transport, with the maximum susceptibility axis, k_{max}, and the minimum susceptibility axis, k_{min}, approximating the preferred orientation of the longest and shortest magnetic grain axes, respectively (e.g., Hamilton and Rees, 1970; Taira and Scholle, 1979; Tarling and Hrouda, 1993; Borradaile et al., 1999). This method is based on the fact that a current is able to orient paramagnetic grains (e.g., phyllosilicates, olivines, pyroxenes, anphiboles), diamagnetic grains (e.g., quartz, calcite, feldspars), and ferromagnetic (sensu lato) grains (e.g., magnetite, goethite, hematite), and that the resulting AMS ellipsoid reflects the orientation imparted by the current to such grains (e.g., Ellwood, 1980; Lowrie and Hirt, 1987; Taira, 1989; Sagnotti and Meloni, 1993; Parés et al., 2007). When currents are present, hydraulic forces control grains alignment (current-induced fabric; Shor et al., 1984). The AMS fabric lines up either parallel or perpendicular to the current direction in case of moderate or high hydrodynamic regimes, respectively. Conversely, settling in standing water produces an horizontal fabric with minimum susceptibility axes clustered around the pole to the depositional plane within which maximum and intermediate susceptibility axes are uniformly dispersed, defining a planar, near-horizontal, gravity-induced settling fabric (Ellwood, 1980; Tarling and

Hrouda, 1993; Pares et al., 2007). After deposition, the fabric may be affected by compaction, bioturbation, and disruption by migration of trapped fluids and/or gas, or by tectonic deformation. Thus, studies of the AMS fabric can also provide information on post-depositional processes.

Isothermal remanent magnetization (IRM) and thermal demagnetization of a three-component IRM (ThIRM) are the paleomagnetic analyses that permit to define the ferromagnetic content of the sediments. IRM have been carried out on a total of 16 cylindrical samples by imparting a magnetizing field progressively increasing from 10 mT to 2470 mT with a ASC Scientific Pulse Magnetizer IM 10-30, and measuring the induced remanence after each magnetizing step with a 2G Enterprises 755 DC-SQUID cryogenic magnetometer. 10 samples have been subjected to the ThIRM (Lowrie, 1990) obtained in fields of 0.1 T, 0.4 T and 2.5 T, with the intensity of each orthogonal IRM component plotted as a function of temperature.

AMS, IRM and ThIRM analyses were carried out at the Alpine Laboratory of Paleomagnetism of Peveragno (Cuneo, Italy).

Image analysis was performed on thin sections from selected intervals with the aim to optically isolate minerals or grains potentially responsible for the observed AMS. This analysis was conducted using the ImageJ software (Rasband, 2008).

Statistical analysis

As confined basins have characteristic flow processes that can modify significantly the bed-thickness population (Malinverno, 1997, Felletti and Bersezio, 2010), AMS study has been combined with a statistical analysis of bed-thickness distribution. It is general agreed that the bed-thickness within turbidite systems is, in some ways, related to basin geometry and to the magnitude and duration of depositional events.

Analysis of bed-thickness distribution. Bed-thickness distribution is the statistical analysis on the frequency of sand beds in the studied turbidite succession. Throughout the paper, "bed thickness" is equivalent to the thickness of the sandstones plus siltstones divisions in a single bed, because no objective sedimentological elements could be used to separate turbidite mud from hemipelagic shale. In order to exclude hemipelagic intervals from the thickness distribution of turbidite beds, we applied our statistical analysis only to the thickness of the coarse-grained divisions of the beds. The data were organized in a database suitable for statistical computation that includes codification and thickness of all the depositional intervals, total thickness of the single beds (sandstones + siltstones + mudstones + hemipelagites), and coarse-grained division thickness (sandstone + siltstone).

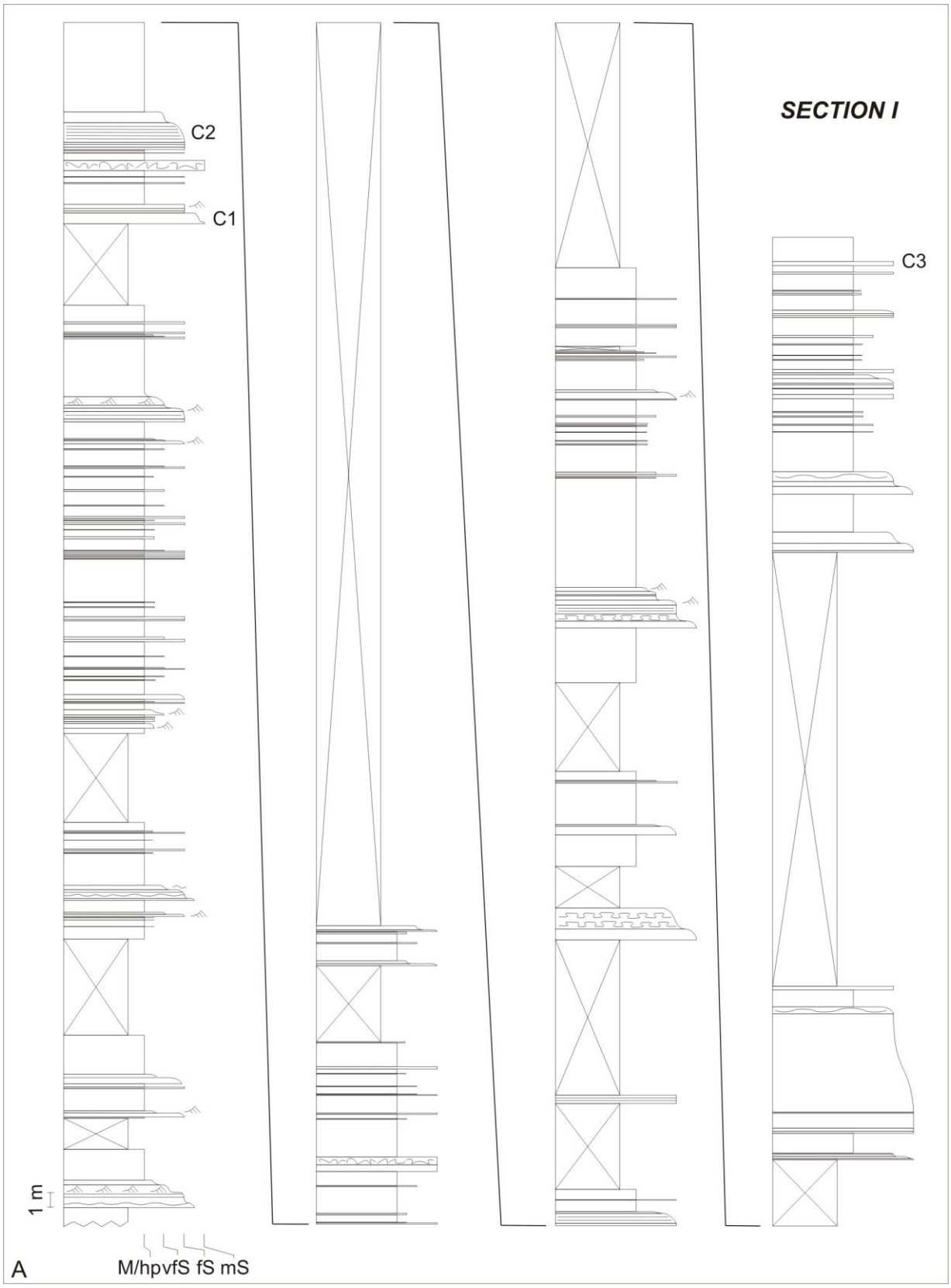
SECTION I
C2
C1
C3
1 m
A
M/hpvfS fS mS

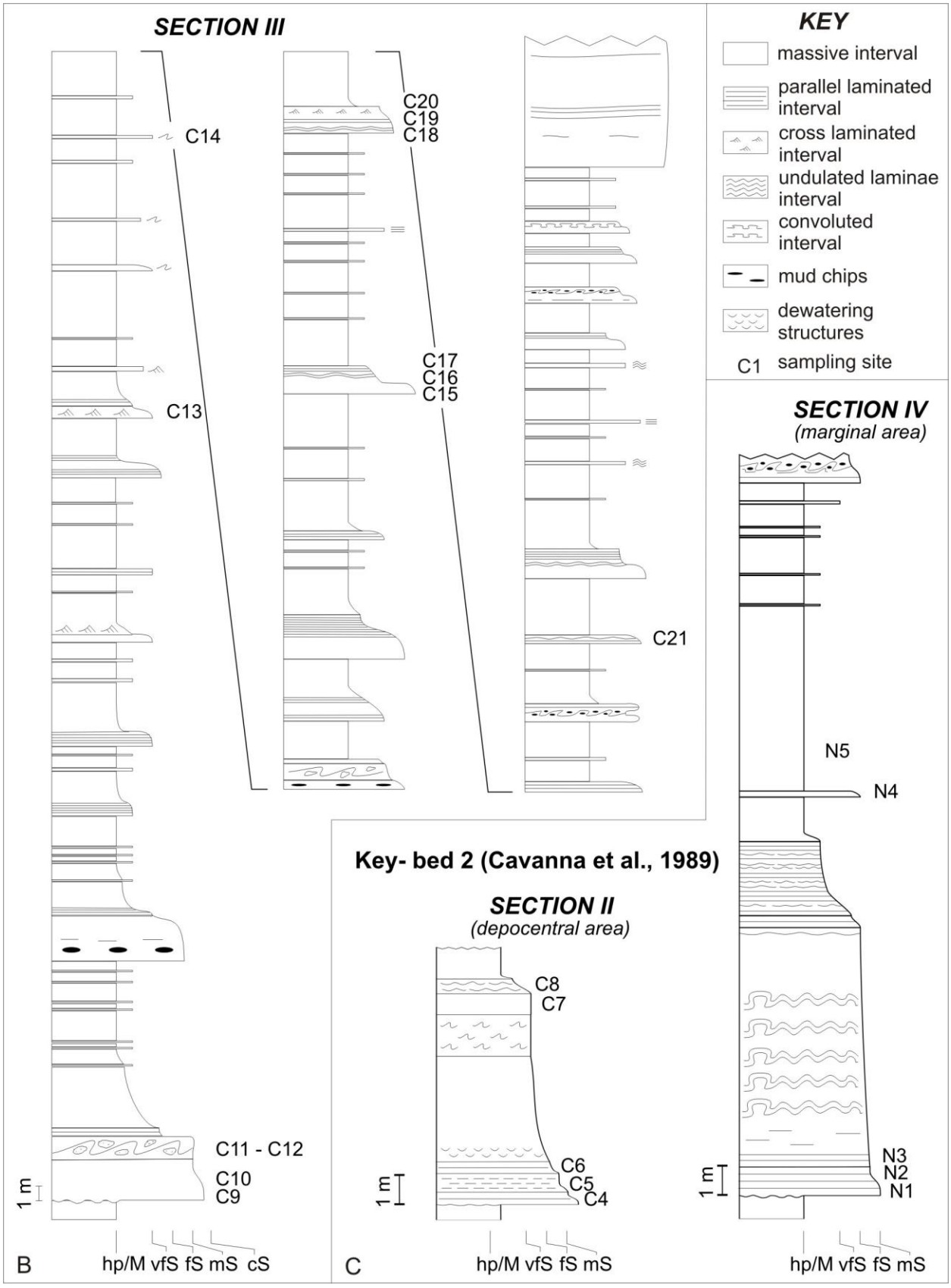

Fig. 4.4 – Stratigraphic logs of the studied sections with the location of the sampled sites. Sections I, II, III and IV are located in Fig. 4.1C

Magnetic fabric and flow dynamics

Equal-area stereographic projections of the samples' susceptibility axes are plotted in Figure 4.7 and 4.8 after correction for bedding tilt, whereas the susceptibility values, averaged at the site level, are reported in Table 4.2. A well-preserved anisotropy of magnetic susceptibility is observed in many sites (Tab. 4.2) and is due to the presence of paramagnetic and/or ferromagnetic (*s.l.*) grains. The mineralogic content of samples was studied throughout paleomagnetic analyses, thin sections observations and the image analysis. By means of IRM (Fig. 4.5A and C) and ThIRM curves (Fig. 4.5B and D), the ferromagnetic content was defined.

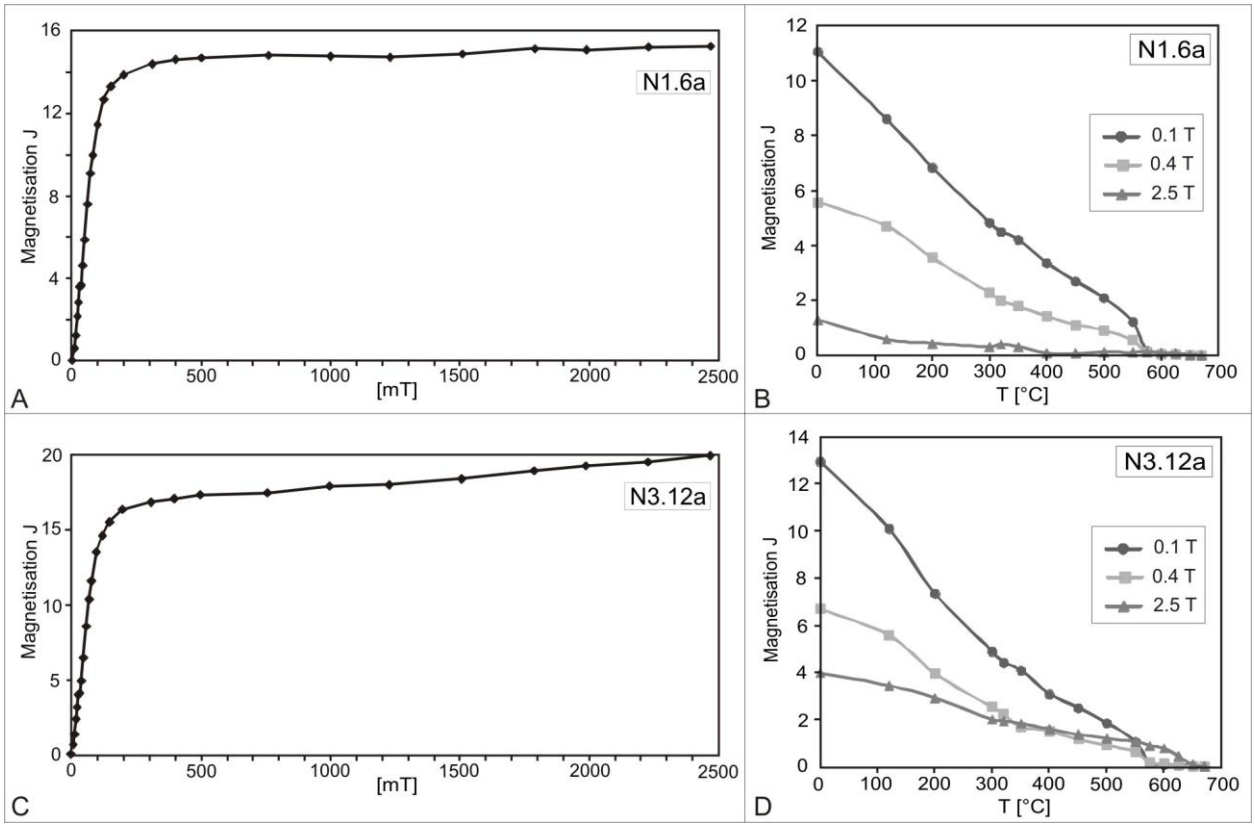

Fig. 4.5 – Isothermal remanent magnetization (IRM) acquisition curves (A and C) and thermal demagnetization of a 3-component IRM (B and D) of samples N1.6a and N3.12a

The analyses reveal the presence of a dominant low coercivity phase with maximum unblocking temperature of ~570 °C interpreted as magnetite coexisting with an intermediate coercivity phase with unblocking temperature of ~320 °C interpreted as a sulfide phase. A phase with an unblocking temperature of ~150 °C can be interpreted as presence of goethite. Hematite with high coercivity and maximum unblocking temperature of ~680 °C is occasionally present in sample N3.12a from site N3). Magmatic lithics, quartz, feldspars, and phyllosilicates

(muscovite) have been recognized (Fig. 4.6) in thin sections. The image analysis was conducted in massive sandstones (site C3; section I in Fig. 4.2C and in Fig. 4.3) in order to isolate the minerals responsible of AMS signal. The original photo (Fig. 4.6A and B) was elaborated (Fig. 4.6C) in order to obtain the best division between grains. Grains with an anisotropic shape were selected and divided in three different classes of orientation (dipping up-current, sub-horizontal and dipping down-current; Fig. 4.6D). According to our analysis, paramagnetic phyllosilicates and magmatic lithics, likely containing magnetite, dominate the current-induced AMS signals.

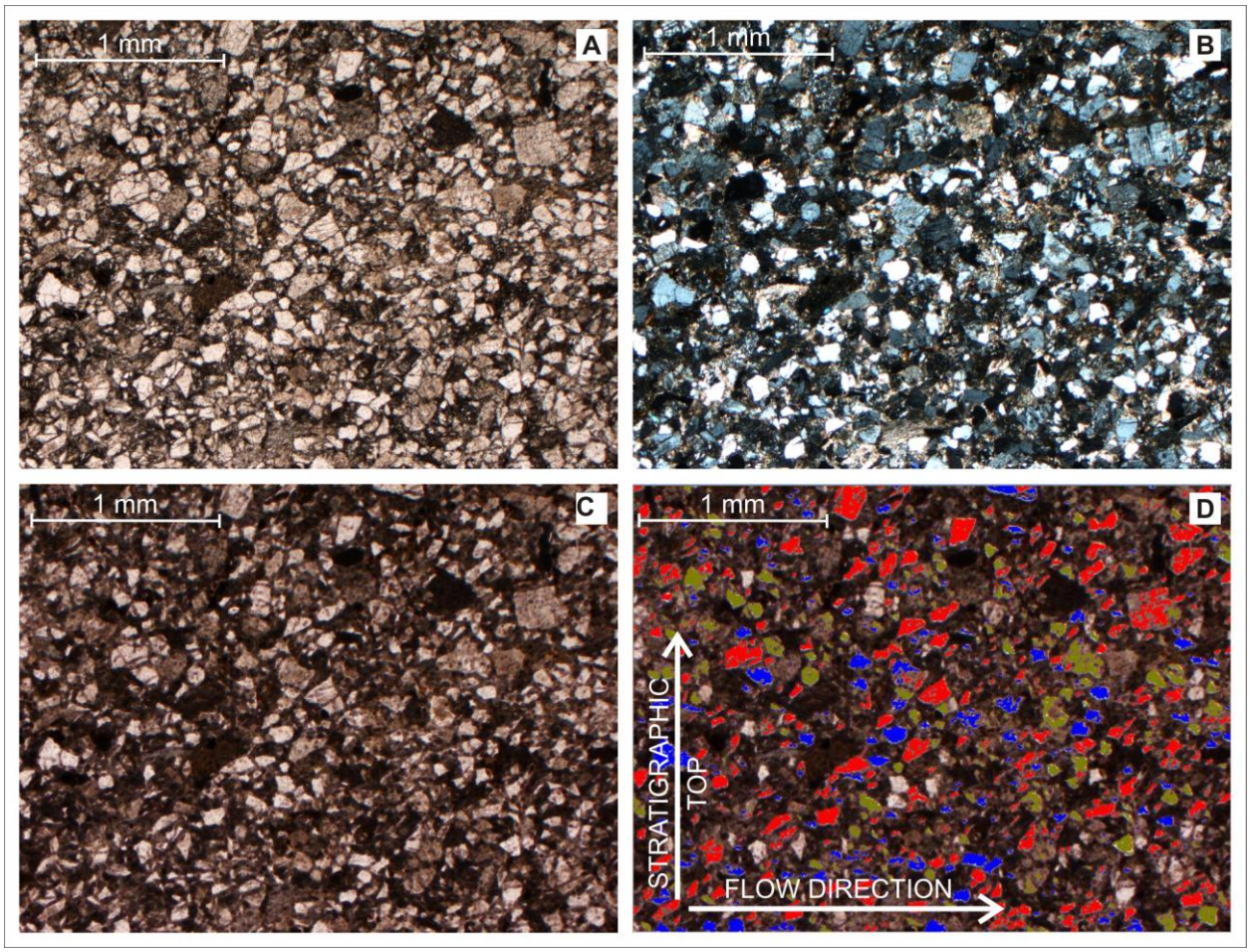

Fig. 4.6 – Thin section of sample C3: (A) original photo with one nicol; (B) original photo with two nicols; (C) photo elaborated with philters to better distinguish grains' edges; (D) photo elaborated throughout image analysis techniques (red are grains imbricated up-current, blue are grains subhorizontal, green are grains imbricated down-current)

The AMS stereoplots obtained in the studied succession were associated to the different depositional intervals in which they were collected (Fig. 4.7). Looking at these AMS plots, the strata can be divided in two different groups: 1) strata showing a well-preserved anisotropic fabric with clustered k_{max}, k_{int} and k_{min} axes and 2) strata showing stereoplots in which the

different axes are dispersed. Notably, purely foliated fabrics with k_{max} and k_{int} axes scattered in the depositional plane have been observed in a single site. With interest we observed that these two groups are, in some way, related to turbidite bed thickness. Figure 4.8 clearly shows that depositional intervals sampled in strata thicker than 1.20 m (Fig. 4.8A) are characterized by a stereoplot in which the different axes are dispersed, instead plots obtained for strata thinner than 1.20 m (Fig. 4.8B) present a clustering of the three axes, with the k_{min} (circles) perpendicular to the bedding plane and the k_{max} aligned parallel to the paleoflow direction (the whole dataset in Fig. 4.8 is normalized to a mean paleocurrent coming from 240°E in order to compare all the sites sampled).

In the following paragraphs, the description of the observed magnetic fabrics has been organized considering separately sandstone beds thicker and thinner than 1.20 m.

Magnetic fabric - Beds > 1.20 m

A very thick bed, composed of coarse- to very fine-grained sandstone with an erosional base (key-bed 2 of Cavanna et al., 1989), was sampled in two different parts of the basin, corresponding to the depocentral and marginal area (Fig. 4.7D) of the basin. The steroplots show a high dispersion of magnetic susceptibility axes in the depositional intervals (parallel-laminated sandstones) sampled at the base of bed in the depocentral area (C4, C5 and C6; Fig. 4.7D). This behavior suggests a broad range of grain long-axis orientations that may be caused by high apparent viscosity due to high near-bed sediment concentrations combined with frequent clast collisions during rapid settling from suspension. This dispersion slightly reduces upward in the bed (C7; Fig. 4.7D):the minimum axes began to cluster in the pole area and there is a distinct flow-aligned magnetic fabric with the k_{max} parallel to the paleocurrent measured at the base of the bed and directed toward the NE. Cross-laminated sandstones sampled at the top of the bed (C8; Fig. 4.7D) represent the final flow stages, in which flow density and velocity are sufficiently low for bedform development; these samples show a relatively large offset from a flow-aligned fabric. This behavior can be explained considering two alternative possibilities: (i) the current ripples in Tc-divisions dominantly have linguoid crest-lines accompanied by highly variable flow directions at the sediment surface and (ii) the impact of basin topography on flow behavior that produce complex interaction between the dense basal part of the flow and the passage of internal waves present in the less dense part of the flow (Felletti; 2002).

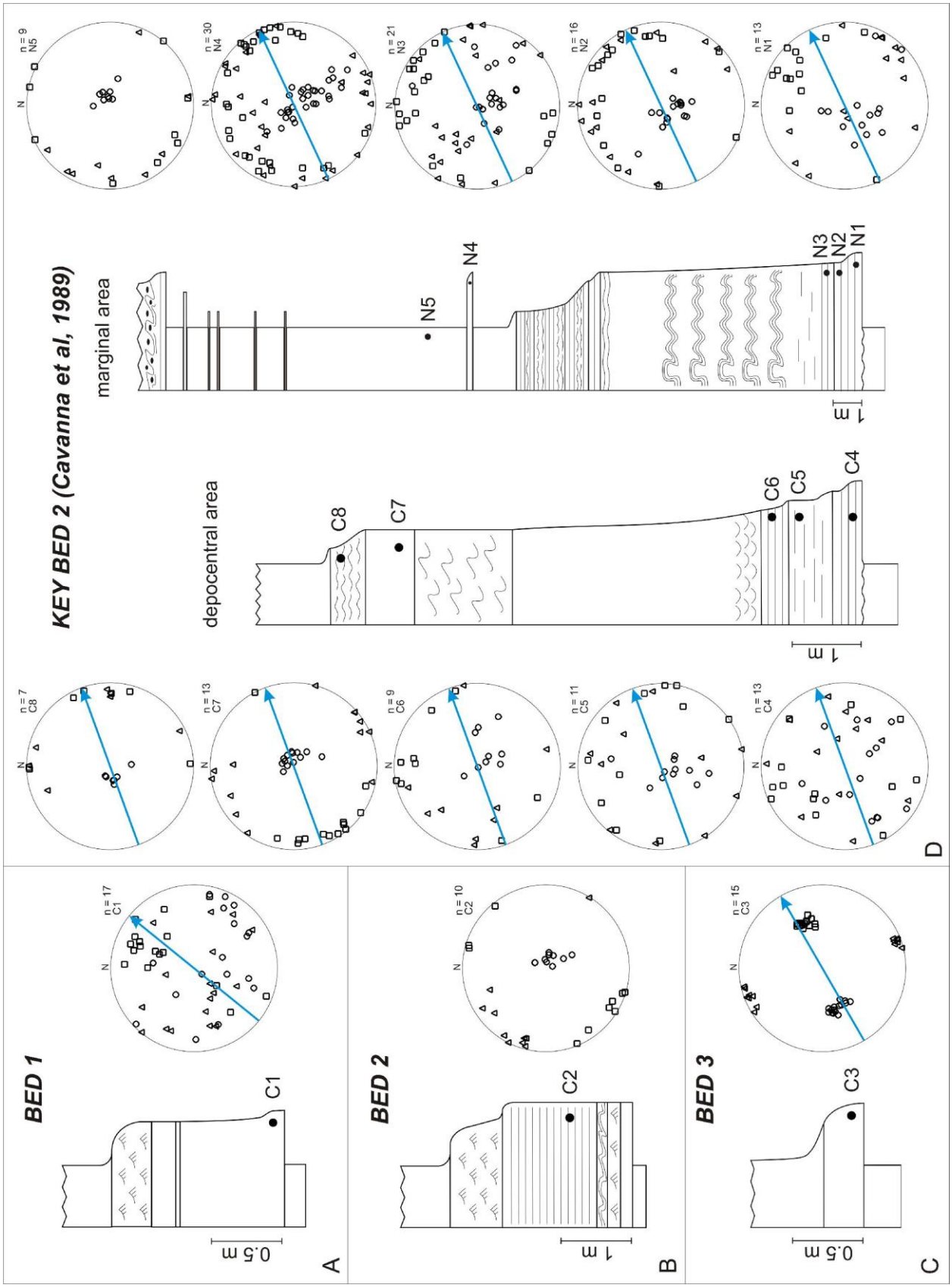
BED 1
n = 17
C1
C1
0.5 m
A
BED 2
n = 10
C2
C2
1 m
B
BED 3
n = 15
C3
C3
0.5 m
C
D
n = 7
C8
n = 13
C7
n = 9
C6
n = 11
C5
n = 13
C4
KEY BED 2 (Cavanna et al, 1989)
marginal area
depocentral area
C8
C7
C6
C5
C4
N5
N4
N3
N2
N1
1 m
n = 9
N5
n = 30
N4
n = 21
N3
n = 16
N2
n = 13
N1

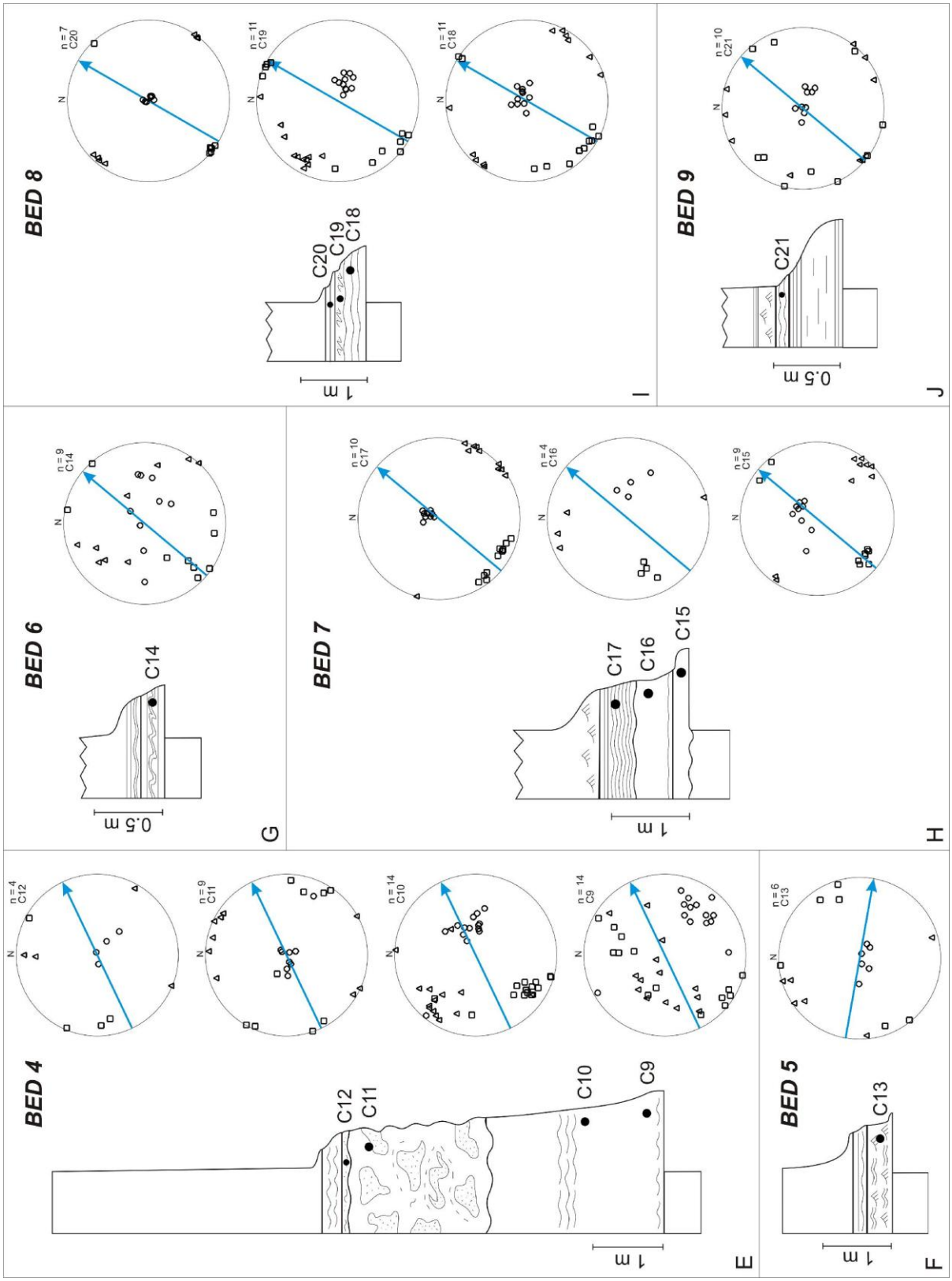

Fig. 4.7 – Stratigraphic logs of the single sampled beds and the associated AMS stereoplots with indication compared to the paleoflow directions from flute-casts (blue arrow). The axes of magnetic susceptibility (k_{max} = squares, k_{int} = triangles, k_{min} = circles) are plotted in tilt-corrected coordinates [N = geographic north; sites = number of sites; n = number of samples; blue arrow = paleoflow direction from flute-casts at the base of the sampled bed]

Table 4.2 – AMS parameters of the sites shown in Figure 4.7 [n: number of samples per site; K_{mean} = mean susceptibility; k_{max} = maximum susceptibility; k_{int} = intermediate susceptibility; k_{min} = minimum susceptibility; L = magnetic lineation; F = magnetic foliation; σ = standard deviation]

	n	K_{mean} ± σ [*10E-6 SI]	k_{max} ± σ [*10E-6 SI]	k_{int} ± σ [*10E-6 SI]	k_{min} ± σ [*10E-6 SI]	L ± σ	F ± σ
C1	17	77.39 ± 4.93	77.66 ± 4.98	77.35 ± 4.91	77.17 ± 4.90	1.0040 ± 0.0030	1.0023 ± 0.0012
C2	10	712.87 ± 39.28	748.66 ± 45.76	736.23 ± 41.71	653.72 ± 31.04	1.0167 ± 0.0063	1.1258 ± 0.0162
C3	15	147.57 ± 11.36	150.58 ± 11.77	147.63 ± 11.43	144.51 ± 10.87	1.0199 ± 0.0035	1.0215 ± 0.0032
C4	13	50.12 ± 12.74	50.93 ± 12.71	50.37 ± 12.84	49.07 ± 12.70	1.0126 ± 0.0091	1.0277 ± 0.0223
C5	11	31.16 ± 2.16	31.75 ± 2.24	31.23 ± 2.22	30.50 ± 2.08	1.0168 ± 0.0099	1.0240 ± 0.0123
C6	9	36.75 ± 0.88	37.27 ± 0.84	36.85 ± 0.87	36.14 ± 0.99	1.0114 ± 0.0043	1.0199 ± 0.0134
C7	13	79.25 ± 6.73	80.16 ± 6.93	79.61 ± 6.79	77.98 ± 6.48	1.0069 ± 0.0025	1.0206 ± 0.0058
C8	7	142.14 ± 7.80	143.90 ± 7.84	143.11 ± 7.71	139.42 ± 7.89	1.0054± 0.0028	1.0267 ± 0.0064
C9	14	94.59 ± 9.11	95.66 ± 9.75	94.77 ± 9.32	93.35 ± 8.47	1.0091 ± 0.0080	1.0148 ± 0.0202
C10	14	160.31 ± 26.69	162.76 ± 27.17	160.47 ± 26.45	157.68 ± 26.46	1.0142 ± 0.0062	1.0181 ± 0.0083
C11	9	275.06 ± 18.49	281.95 ± 18.88	279.21 ± 18.48	264.01 ± 18.16	1.0098 ± 0.0036	1.0577 ± 0.0062
C12	4	166.13 ± 23.51	169.47 ± 24.35	168.30 ± 54.59	160.61 ± 21.60	1.0072 ± 0.0024	1.0467 ± 0.0123
C13	6	178.53 ± 16.95	180.88 ± 17.31	180.17 ± 17.42	174.56 ± 16.14	1.0040 ± 0.0013	1.0318 ± 0.0064
C14	9	147.58 ± 32.88	148.92 ± 32.27	147.97 ± 33.12	145.84 ± 32.26	1.0065 ± 0.0026	1.0141 ± 0.0055
C15	9	659.13 ± 25.07	676.68 ± 29.69	657.41 ± 24.89	643.32 ± 21.94	1.0291 ± 0.0089	1.0218 ± 0.0120
C16	4	921.80 ± 43.08	942.79 ± 40.72	920.71 ± 43.42	901.92 ± 45.06	1.0241 ± 0.0044	1.0209 ± 0.0044
C17	10	396.65 ± 43.70	410.04 ± 46.09	404.12 ± 45.16	375.79 ± 39.89	1.0146 ± 0.0028	1.0748 ± 0.0097
C18	11	81.11 ± 4.35	81.86 ± 4.33	81.46 ± 4.32	80.02 ± 4.42	1.0050 ± 0.0022	1.0180 ± 0.0035
C19	11	83.60 ± 4.20	84.31 ± 4.26	83.84 ± 4.30	82.63 ± 4.03	1.0056 ± 0.0024	1.0145 ± 0.0047
C20	7	98.48 ± 3.02	99.94 ± 3.01	99.43 ± 3.03	96.06 ± 3.04	1.0051 ± 0.0009	1.0351 ± 0.0027
C21	10	490.21 ± 41.94	505.24 ± 43.43	498.68 ± 40.81	466.72 ± 42.19	1.0129 ± 0.0059	1.0693 ± 0.0206
N1	13	34.69 ± 1.99	35.30 ± 1.98	34.74 ± 2.06	34.05 ± 1.97	1.0164 ± 0.0091	1.0202 ± 0.0107
N2	16	44.62 ± 3.07	45.15 ± 3.21	44.75 ± 3.09	43.97 ± 2.93	1.0090 ± 0.0070	1.0176 ± 0.0080
N3	21	52.11 ± 3.62	52.66 ± 3.59	52.21 ± 3.69	51.45 ± 3.62	1.0089 ± 0.0066	1.0148 ± 0.0091
N4	30	118.49 ± 3.24	119.84 ± 3.40	119.02 ± 3.28	116.63 ± 3.11	1.0069 ± 0.0038	1.0205 ± 0.0081
N5	9	205.02 ± 6.97	209.68 ± 7.58	207.47 ± 6.96	197.92 ± 7.22	1.0106 ± 0.0085	1.0486 ± 0.0023

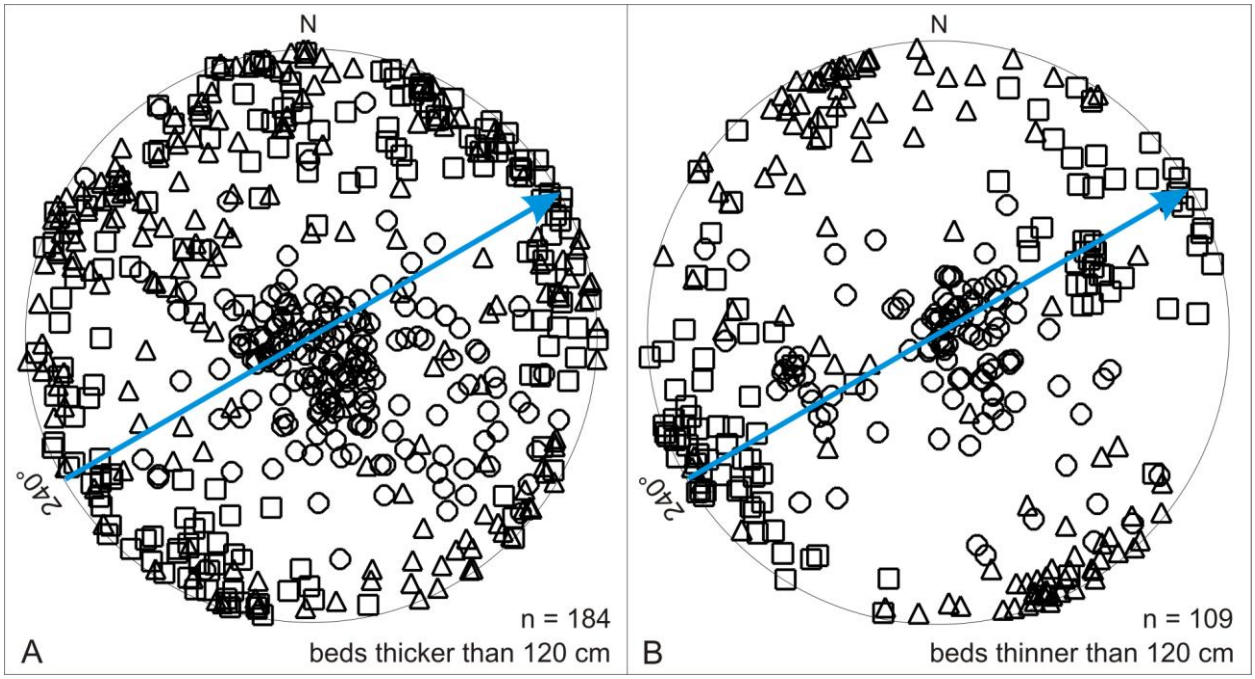

Fig. 4.8 – AMS steroplot of sites (A) thicker than 1.20 m and (B) thinner than 1.20 m [k_{max} = squares, k_{int} = triangles, k_{min} = circles; N = geographic north; n = number of samples; blue arrow = paleoflow direction from flute-casts at the base of the sampled bed]

Considering the same key-bed toward the northern basin margin the data dispersion reduces (Fig. 4.7D), if compared with the up-current depocentral area: the minimum axes are well-clustered in the pole area and there is a distinct magnetic fabric with the k_{max} parallel (N2 and N4 – Fig. 4.7D) or transversal (N1 and N3 - Fig. 4.7D) to the paleocurrent measured at the base of the bed and directed toward the NE. A small but relatively consistent offset of up to ~25–30° counterclockwise with respect to the mean paleoflow direction from flute casts has been observed in sites N1 and N3 (Fig. 4.7D). Imbrication angles of ~15° and dipping up-current (i.e., to the SW) have been observed at these sites. This feature suggests that these turbidites flowed from the NE to the SW, in opposite direction with respect to the flute cast-generating stage of turbidity currents.

Excluding systematic measurement errors, the cause of the observed offset and imbrication angles may be sought in differences of flow directions between the erosive, flute cast-generating stage of turbidity currents and the subsequent depositional stages during which planar stratifications are formed (assuming substantial flow alignment of k_{max} axes in these facies). Processes such as local changes in current direction due presence of the northern basin margin (i.e., deflection and/or reflection of turbidite current) may have contributed to the observed offset. The presence of a confining northern slope, 50° oblique to the main turbidite flow (Felletti, 2002) and at least 60 m high, caused turbidity currents a density stratification: the dense, basal part of the flow is partially blocked and deflected (N1, N2 and N3 – Fig. 4.7D), whereas the less dense muddy and silty fraction (N4 – Fig. 4.7D) surmounts the paleoslope and surges backwards as a series of reflections towards the center of the basin, where it is mainly deposited. This interpretation is supported by basal paleocurrent measurements (flute structures) that show an easterly deflection of flows approaching the northern slope (Felletti, 2002). The large dispersion of ripple orientations, principally southerly directed, may have resulted from the close proximity of the slope. The presence of a thick mudstone cap suggests that the obstacle (paleoslope) was sufficiently high to block the entire flow. The AMS stereoplot sampled within this thick mudstone cap (N5 – Fig. 4.7D) is characterized by a high dispersion of the k_{max} e and k_{int} on the horizontal plane and the k_{min} clustered vertically. This behavior suggests that the turbidite mudstone cap was deposited by slow settling of particles..

A similar behavior can be observed in Bed 4 (Fig. 4.7E), represented by a very thick bed, composed of coarse- to very fine-grained sandstone. The samples collected close to the base (C9) shows a very high dispersion of magnetic axes. This dispersion slightly reduces upward in the bed (C10 and C11): the minimum axes began to cluster and there is a distinct aligned magnetic

fabric with the k_{max} showing a relatively consistent offset of up to ~30–35° counterclockwise (C10) and clockwise (C11) with respect to the mean paleoflow direction from flute casts measured at the base of the bed and directed toward the NE. Imbrication angles of ~20° and dipping down-current (i.e., to the NNE) have been observed (C10), suggesting that these turbidites flowed from the SSW to the NNE (assuming substantial flow alignment of k_{max} axes in these facies), in a different direction with respect to the flute cast-generating stage of turbidity currents (from SW to NE). Processes such as local changes in current direction due presence of the northern basin margin (i.e., deflection of turbidite current) may have contributed to the observed offset. Cross-laminated sandstones sampled at the top of the bed (C12) represent the final flow stages; these samples show a relatively large offset from a flow-aligned fabric.

Samples from Bed 1 (sampled at the base of the massive basal division of medium- to very fine-grained sandstone; Fig. 4.7A) show a high dispersion of magnetic susceptibility axes in the depositional intervals bed in the depocentral area. As previously explained, this behavior suggests a broad range of grain long-axis orientations that may be caused by high apparent viscosity due to high near-bed sediment concentrations combined with frequent clast collisions during rapid settling from suspension.

Magnetic fabric - Beds < 1.20 m

A distinct magnetic fabric has been observed for strata thinner than 1.20 m (Bed 3, Bed 5, Bed 6, Bed 7, Bed 8, Bed 9; Fig. 4.7 C, F, G, H, I, J), with a good clusters of the minimum magnetic axis (k_{min}) disposed in the pole area and with the k_{max} parallel or oblique to the paleocurrent measured at the base of the bed. Samples collected in massive, parallel-laminated, undulated and convoluted sandstones are characterized by well clustered k_{max} axes with an overall mean direction parallel to the overall mean paleocurrent direction from flute-casts. These features suggest relatively low density suspensions with clasts transported by traction and rapidly deposited in flow-aligned fabrics. Imbrication angles of ~30° and dipping the NE (down-current with respect to the flute cast-generating stage of turbidity currents) have been observed at a site (C16, Bed 7 – Fig. 4.7H). A small but relatively consistent offset of up to ~20° clockwise with respect to the mean paleoflow direction from flute casts has been observed in cross-laminated sandstones sampled in Bed 5 (C13 - Fig 4.7F). This behavior can be explained considering that current ripples in Tc-divisions dominantly have linguoid crest-lines accompanied by highly variable flow directions at the sediment surface. The convoluted sandstones of sites C14 and C21

(Bed 6 and Bed 9) show a high dispersion of magnetic susceptibility axes, suggesting a broad range of grain long-axis orientations. This behavior can be explained considering post- or syndepositional soft-sediment deformation (e.g., liquefaction and/or fluidization processes).

Our observations indicate that the different magnetic fabrics observed in the studied Castagnola Turbidite System are in some measure related to changes in paleocurrent directions and intensity of turbidite currents. Furthermore, we observed a strong correlation between magnetic fabric and bed-thickness: beds thicker than ~1.20 m show a wide range of variability of magnetic fabrics with offset of up to ~35° with respect to the mean paleoflow direction from flute casts measured at the base of the bed, whereas beds thinner than ~1.20 m show principally a flow oriented magnetic fabric.

In order to better understand this interesting behavior, we decided to compute a statistical analysis of bed-thickness distribution. Some recent statistical studies on turbidite successions show that the distribution of bed thickness is related to both the geometry of the basin (i.e., degree of confinement, irregularities of bottom and marginal slopes) and the sediment input (volume, type and dynamics of flows). It has been shown that confined basins have characteristic processes that can modify significantly the bed thickness population. In the specific case of confined basins, deposition from sediment gravity flows is strongly controlled by the interactions among flow magnitude and/or duration, flow efficiency, size and morphology of the depocentres (Mutti, 1979; Malinverno,1997; Kneller,1995; Kneller and McCaffrey,1999; Mutti et al.,1999; Winker,1996; Prather et al.,1998; Talling, 2001; Carlson and Grotzinger, 2001; Sinclair and Tomasso, 2002; Sinclair and Cowie, 2003; Kneller and McCaffrey, 2004; Lomas and Joseph, 2004; Smith, 2004 among many others).

Bed-thickness distribution

Bed-thickness within turbidite systems is, in some ways, related to basin geometry and to the magnitude and duration of depositional events. Cumulative distribution of turbidite bed-thicknesses is often interpreted in terms of a power law (Rothman and Grotzinger, 1995; Beattie and Dade, 1996; Malinverno, 1997; Pirmez et al., 1997; Chen and Hiscott, 1999; Drummond, 1999; Awadallah et al., 2001; Sinclair and Cowie, 2003; Felletti and Bersezio 2010). Alternatively, these distributions have been described by a lognormal mixture model (Ricci

Lucchi, 1967; Hiscott and Middleton, 1979; Drummond and Wilkinson, 1996; Murray et al., 1996; Drummond, 1999; Talling, 2001; Sylvester, 2007). Changes in the power-law exponent can be related to the rheological properties of the gravity-driven flows and to the geometry of the basin (Malinverno, 1997, Felletti and Bersezio 2010).

Malinverno (1997) and Sinclair and Cowie (2003) focused their studies on the relation between bed thickness distributions and the geometrical features of the turbidite beds, showing how confinement can alter the bed thickness distribution at the basin center. If turbidite sandstone thickness is expressed by power laws and it is assumed that sandstone bed shape is well described by disc-like bodies with circular bases inside a mudstone matrix (mud framework), then a relationship between the power law exponents of bed thickness and exponents of the geometrical characteristics of the beds (bed volume, spatial distribution, thickness-bed length relationship) can be found. Malinverno (1997) showed that if there is independent geological evidence that the turbidites were deposited under confinement, the relationship can be simplified and the exponents of bed volume and thickness-bed length relationship can be calculated from the exponent of the segmented cumulative bed thickness distribution.

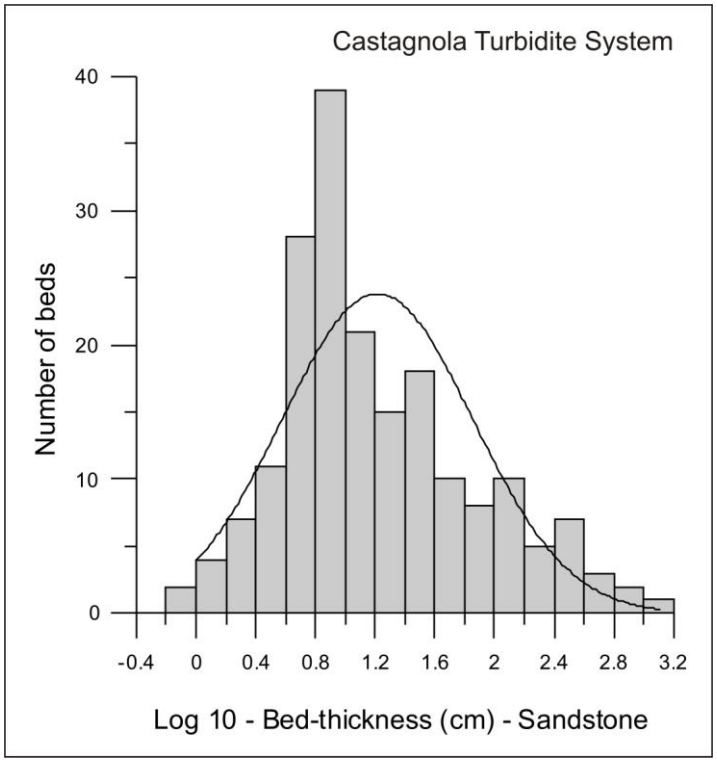

Fig. 4.9 – Frequency distribution of bed thickness of sandstone divisions

The succession of turbidite beds of the Castagnola Turbidite System invariably exhibits an inverse relationship of bed thickness against number of beds (i.e., there are many more thin beds than thick beds; Fig. 4.9). A notable feature is the common occurrence of isolated very thick-bedded sandstones; 5% of all beds are thicker than 1.20 m and 90% of beds are thinner than 0.80 m. The frequency distribution of the sandstone component of turbidite thickness computed in the depocentral locations (~200 beds) is positively skewed (Fig. 4.9). Plots in log-log space of number of beds thicker than *h*, vs. *h*, consist of segmented convex-upward curves with some linear trends (Fig. 4.10) suggesting, as a general rule, that the distribution is not straightforward. This behavior is particularly evident when the thickness distributions for the "sandy" and for the "muddy" divisions of the turbidites are plotted separately (Fig. 4.9).

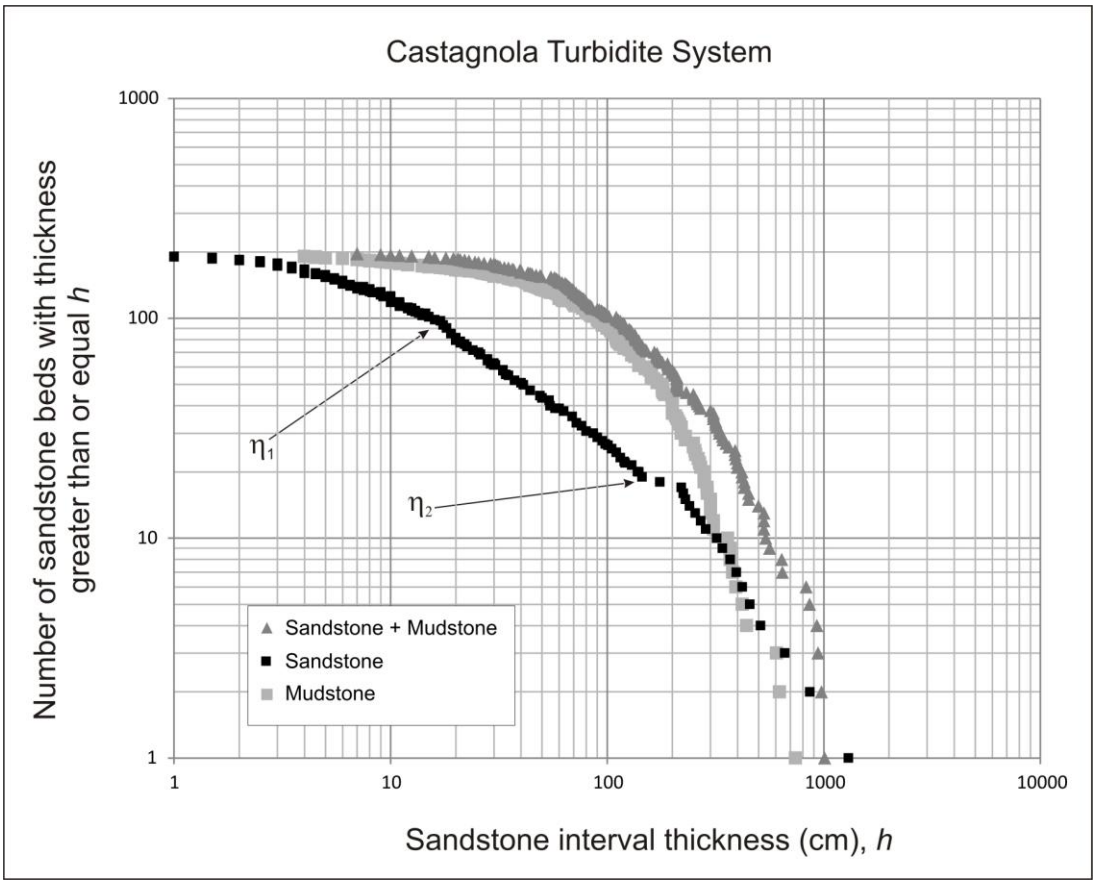

Fig. 4.10 – Log–log plot of the cumulative frequency of beds

Two deviations are observed from a straight line on the log-log plot, η1 and η2, that correspond respectively to bed ~0.15 m and 1.20-1.50 m thick (Fig. 4.10). We interpreted the step η1 as a consequence of down-current variations of flow rheology and corresponds to the separation between two different statistical populations. These two populations are associated with two

facies groups: (i) classical Tc-e/Td-e Bouma sequences (< η1; dilute turbulent flows) and (ii) classical graded Ta-e/Tb-e Bouma sequences with massive and plane-parallel laminated depositional divisions (> η1; concentrated flows with aggradational depositional features). The effect of down-current variations of flow rheology, from dilute and turbulent to more concentrated flows, is to increase the slope of the power law distribution by a factor > 2. A similar behavior has been observed in many ancient turbidite systems (Talling, 2001; Carlson and Grotzinger, 2001; Sinclair and Cowie, 2003; Felletti and Bersezio, 2010) and corresponds for the Castagnola turbidite system to the separation between two different statistical populations that show dissimilar bed thickness distributions, depending principally by the duration of deposition and rate of sedimentation.

The step η2 corresponds to a decrease of the slope of the distribution of a factor >2: it means that there are more thick beds than one would expect if the distribution would follow the same steep line as before. This deviation from a straight line (step η2) is ascribed to a thickness threshold that marks the minimum thickness of a specific group of beds (massive sandstone and thick sandstone-mudstone couplets) generated by flows that were able to cover the entire basin floor. In this case, the entering large volume and poorly efficient sand-laden gravity flows responsible for these beds were not free to spread laterally and, consequently, were forced to aggrade vertically producing a significant impact on the bed thickness populations, modifying significantly the original input signal. In Figure 4.10, the straight lines between η1 and η2 (dotted lines) should indicate the expected trend of the bed-thickness plots if there was no confinement, if extrapolated to bed thicknesses greater than η2.

In summary, flow confinement has a significant impact on the bed thickness population, causing thickening of the beds thicker than 1.20-1.50 m (η2). We believe that 1.20 m could represent a thickness threshold that marks the minimum thickness of a specific group of beds generated by flows that were able to cover the entire basin floor. The large-volume and poorly efficient sand-laden gravity flows responsible for these beds were fully contained within an area of enclosed bathymetry, that was too small to permit the development of flow transitions. As a result the depositional system was forced to aggrade vertically producing a significant impact on the bed thickness populations. Physical correlation of several key-beds throughout the basin confirms the presence of a thickness threshold that is exceeded, above a thickness gap, by those beds that occur basin-wide. In contrast, the turbidity flows that deposited the medium- to thin turbidites were sufficiently small relative to the basin width, to be able to develop down-current changes in

textures and facies. For these thinner beds, the main effect of basin confinement was to control the facies and stacking patterns in areas close to the marginal slopes.
These considerations are well supported by strong correlation between magnetic fabric and bed-thickness.

Conclusions

Sedimentological reconstructions and interpretations of the Castagnola turbidite system (Baruffini et al., 1994; Di Giulio and Galbiati, 1998; Mutti, 1992; Felletti, 2002) testify a sea-floor topography that generate a confined basin with the potential to trap all (or a part) of the incoming flows. In this paper we have evaluate the use of the AMS as a tool investigates the effects of basin confinement on changes of flow rheology.
It comes out that within this small and confined turbidite system, the correlation between magnetic fabric and depositional intervals (with an overall flow-aligned fabric) is not straightforward. By contrast, a strong correlation between magnetic fabric and bed-thickness distribution was observed. The ~1.20 m thickness represents the threshold that marks the minimum thickness of a specific group of beds generated by flows that were able to cover the entire basin floor and that had the potential to be deflected or reflected. Beds thicker than ~1.20 m show a wide range of variability of magnetic fabrics, whereas beds thinner than ~1.20 m show a much better developed flow-oriented magnetic fabric.
A statistical analysis of bed thickness distribution allowed us to better define this threshold, distinguishing two different scenarios: 1) large volume flows (ponded scenario) and 2) small volume flows (non-ponded scenario)

Large volume flows (ponded scenario)

Because of the geometry of the depositional area, large volume entering flows were not free to spread laterally and they interact with basin margins, consequently, were forced to aggrade vertically producing beds thicker than 1.20 m in which the interaction between flows is not able to orient grains. This hypothesis is confirmed by the scattered AMS axes in the investigated sedimentary facies at the base of beds thicker than 1.20 m. Nevertheless, the AMS stereoplots (Fig. 4.7D and E) become more clusterized upward in the beds, testifying change of flow rheology (which evolved from high-density to low-density turbidity currents). and, cosequentely,

the increasing capability of the flow to orient grains during its runout. The presence of a confining northern slope, 50° oblique to the main turbidite flow, caused turbidity currents to lose energy and deposit a large proportion of their sediment load near the base of the slope, where the nose of the current climbed the opposing counterslope. As suggested by Felletti (2002) the dense, basal part of the flow is partially blocked and deflected, whereas the less dense muddy and silty fraction surmounts the palaeoslope and surges backwards as a series of reflections towards the centre of the basin, where it is mainly deposited. This mechanism of flow decoupling has been proposed by Kneller and McCaffrey (1999) and shows several analogies with the process referred to as flow stripping (Piper and Normark, 1983). In this case, the height of the slope is assumed to be greater than the maximum run-up height of the flow. This interpretation is supported by our AMS data that show an easterly deflection (or a southerly reflection) of flows approaching the northern slope; and by the large dispersion of grain orientations measured at the base of the thick beds.

Small volume flows (non-ponded scenario)

Small volume entering flows, that had no interactions with basin margins, were able to orient grains, producing AMS stereoplots with a good clustering of axes in massive, parallel laminated, cross laminated and undulated depositional intervals (Fig. 4.7C, F, H, I). Convoluted depositional interval that are subjected to post-depositional processes that disrupt the original current-induced fabric (e.g., post-depositional dewatering) are characterized by scattered AMS stereoplots (Fig. 4.7G) confirming the sedimentary origin of the AMS fabric.

We conclude that within small confined turbidite system the AMS signal is primarily driven by bed thickness and then by sedimentary structures of the deposit.

From this study it appears that there is no unique relationship between grain fabric and sedimentary structure in deep-marine deposits. This outcome demands further validation, based on more comprehensive data sets than those available from the literature, because it challenges the common assumption that grain long-axis orientation is a direct measure of paleoflow direction, or at least dominantly so. Anyway, when integrated with data on sedimentology and basin morphology, AMS analysis can provide general guidance about interpretation of depositional settings, degree of confinement, changes of flow rheology and volume, improving and assisting the development of geological/sedimentological models of facies distribution.

References

Agico KLY-3 User's Guide (Ver. 2.2 Nov. 1998) Modular system for measuring magnetic susceptibility, anysotropy of magnetic susceptibility, and temperature variation of magnetic susceptibility. *AGICO Advanced Geoscience Instruments CO. Brno, Czech Republic.*

Allen, J.R.L. (1991) The Bouma division A and the possible duration of turbidity currents. *Journal of Sedimentary Petrology*, **61**, 2, 291-295.

Arnott, R.W.C. and Hand, B.M. (1989) Bedforms, primary structures and grain fabric in the presence of suspended sediment rain. *Journal of Sedimentary Petrology*, **59**, 1062-1069.

Awadallah, S.A.M., Hiscott, R.N., Bidgood, M., and Crowther, T. (2001) Turbidite facies and bed-thickness characteristics inferred from microresistivity images of Lower to Upper Pliocene rift-basin deposits, Woodlark Basin, offshore Papua New Guinea. In: Huchon, P., Taylor, B., Klaus, A,. (Eds), *Proc. ODP, Sci. Results*, **180**, 1-30

Baas, J.H. (1999) An empirical model for the development and equilibrium morphology of current ripples in fine sand. *Sedimentology*, **46**, 123–138

Ballance, P.F. (1964) Streaked-out mud ripples below Miocene turbidites, Puriri Formation, New Zealand. *Journal of Sedimentary Petrology*, **34**, 91–101

Baruffini, L., Cavalli, C., and Papani, L. (1994) Detailed stratal correlation and stacking patterns of the Gremiasco and lower Castagnola turbidite systems, Tertiary Piedmont Basin, northwestern Italy. In: 15th Annual Research Conference Submarine Fans and Turbidite Systems (Eds P. Weimer, A. H. Bouma and B. F. Perkins), *GCSSEPM Foundation*, 9-21

Beattie, P., and Dade, W.B. (1996) Is scaling in turbidite deposition consistent with forcing by earthquakes? *Journal of Sedimentary Research*, **66**, 909-915

Biella, G. C., Clari, P., De Franco, R., Gelati, R., Ghibaudo, G., Gnaccolini, M., Lanza, R., Polino, R., Ricci, B., and Rossi, P.M. (1992) Geometrie crostali al nodo Alpi/Appennino: conseguenze sull'evoluzione cinematica dei bacini neogenici. *Riassunti 76a Riunione estiva Società Geologica Italiana*, Firenze 1992, 192-195

Borradaile, G.J., Fralick, P.W., and Lagroix, F. (1999) Acquisition of anhysteretic remanence and tensor subtraction from AMS isolates true palaeocurrent grain alignments. In: Palaeomagnetism and Diagenesis in Sediments (Tarling, D.H. and Turner, P. Eds), *Geological Society, London, Special Publications*, **151**, 139-145

Bouma, A.H. (1962) Sedimentology of Some Flysch Deposits: a Graphic Approach to Facies Interpretation. *Elsevier*, Amsterdam. 168 pp

Bouma, A.H., and Pluenneke, J.L. (1975) Structural characteristics of debrites from the Philippine Sea. *Initial Reports of the Deep Sea Drilling Project*, **31**, 497–505

Carlson, J., and Grotzinger, J.P. (2001) Submarine fan environment inferred from turbidite thickness distributions. *Sedimentology*, **48**, 1331-1351

Cavanna, F., Di Giulio, A., Galbiati, B., Mosna, S., Perotti, C. R., and Pieri, M. (1989) Carta geologica dell'estremità orientale del Bacino Terziario Ligure-Piemontese. *Atti Tic. Sc. Terra*, **32**

Chen, C., and Hiscott, R.N. (1999) Statistical analysis of facies clustering in submarine-fan turbidite successions. *Journal of Sedimentary Research*, **69**, 505-517

Clark, J.D., and Stanbrook, D.A. (2001) Formation of large-scale shear structures during deposition from high-density turbidity currents, Grès d'Annot Formation, south-east France. In: McCaffrey, W.D., Kneller, B.C., Peakall, J. (Eds.), Particulate Gravity Currents. *International Association of Sedimentologists, Special Publication*, **31**, 219–232

Crowell, J.C. (1955) Directional-current structures from the Prealpine Flysch, Switzerland. *Bulletin of the Geological Society of America*, **66**, 1351–1384

Di Giulio, A., and Galbiati, B. (1993) Escursione nell'estremità orientale del Bacino Terziario Piemontese. Interazione tettonica-eustatismo nella sedimentazione di un bacino tardo-post orogenico. In: 3° Convegno del gruppo informale di sedimentologia del C.N.R. Dip. di Scienze della Terra, Università di Pavia, Salice Terme.

Di Giulio, A., and Galbiati, B. (1998) Turbidite record of the motions along a crustal-scale tectonic line: the motions of the Villarvernia-Varzi line during the Oligocene-Miocene (North-Western Italy). In: 15th International Sedimentological Congress, pp. 293-294. IAS - Universidad de Alicante, Alicante.

Drummond, C.N. (1999) Bed-thickness structure of multi-sourced ramp turbidites: Devonian Brailler formation, Central Appalachian Basin. *Journal of Sedimentary Research*, **69**, 115-121

Drummond, C.N., and Wilkinson, B.H. (1996) Stratal thickness frequencies and the prevalence of orderedness in stratigraphic sections. *The Journal of Geology*, **104**, 1-18

Ellwood, B.B. (1980) Induced and remanent magnetic properties of marine sediments as indicators of depositional processes. *Marine Geology*, **38**, 233-244

Felletti, F. (2002) Complex bedding geometries and facies associations of the turbiditic fill of a confined basin in a transpressive setting (Castagnola Fm., Tertiary Piedemont Basin, NW Italy). *Sedimentology*, **49**, 645-667

Felletti, F., and Bersezio, R. (2010) Quantification of the degree of confinement of a turbidite-filled basin: a statistical approach based on bed thickness distribution. *Marine and Petroleum Geology*, **27**, 515-532

A statistical approach based on bed thickness distribution

Gelati, R., and Falletti, P. (1996) The Piedmont Tertiary Basin. *Giornale di Geologia*, **58**, 1-2, 11-18

Ghibaudo, G. (1992) Subaqueous sediment gravity flow deposits: practical criteria for their field description and classification. *Sedimentology*, **39**, 423-454

Hamilton, N., and Rees, A.I. (1970) The use of magnetic fabric in paleocurrent estimation. In: Paleogeophysics (Runcorn, S.K. Ed.). *London, Academic Press*, 445-464

Harms, J.C. (1975) Depositional environments as interpreted from primary sedimentary structures and stratification sequences. *Society of Economic Paleontologists and Mineralogists*. 161 pp.

Haughton, P., Davis, C., McCaffrey, W., and Barker, S. (2009) Hybrid sediment gravity flow deposits – classification, origin and significance. *Marine and Petroleum Geology*., **26**, 1900–1918

Hiscott, R.N., and Middleton, G.V. (1979) Depositional mechanics of thick-bedded sandstones at the base of a submarine slope, Tourelle Formation (Lower Ordovician), Quebec, Canada, in: Larry, J., Pilkey, O.H., (Eds), Geology of Continental Slopes. *Society of Econonomic Paleontologists Mineralogists*, Spec. Publ., **27**, 307-326

Hiscott, R.N., and Middleton, G.V. (1980) Fabric of coarse deep-water sandstones, Tourelle Formation, Quebec, Cananda. *Journal of Sedimentary Petrology*, **50**, 703-722

Hiscott, R.N., Hall, F.R., and Pirmez, C. (1997) Turbidity-current overspill from the Amazon channel: texture of the silt/sand load, paleoflow from anisotropy of magnetic susceptibility and implications for flow processes. *Proceedings of the Ocean Drilling Program*, Scientific Results, **155**, 53-78

Hurst, A., Verstralen, I., Cronin, B., and Hartley, A. (1999) Sand-rich fairways in deep-water clastic reservoir: genetic unit, capturing uncertainty, and a new approach to reservoir modeling. *AAPG Bulletin*, **83**, 1096–1118

Kneller, B.C. (1995) Beyond the turbidite paradigm: physical models for deposition and their implications for reservoir prediction, in: Hartley, A.J, Prosser, D.J., (Eds.), Characterization of deep clastic systems. *Geol. Soc. Spec. Publ.*, **94**, 31- 49

Kneller, B.C., and McCaffrey, W. (1999) Depositional effects of flow non-uniformity and stratification within turbidity currents approaching a bounding slope. Deflection, reflection and facies variation. *Journal of Sedimentary Research*, **69**, 980-991

Kneller, B.C., and McCaffrey, W. (2004) Scale effects of non-uniformity on deposition from turbidity currents with reference to the Grès d'Annot of se France, in: Lomas, S.A., Joseph, P., (Eds.), Deep-water sedimentation in the Alpine basin of SE France: new perspectives on the Grès d'Annot and related systems. *The Geololgical Society of London*, Spec. Publ., **221**, 301-310

Kneller, C., and Branney, M.J. (1995) Sustained high-density turbidity currents and the deposition of thick massive sands. *Sedimentology*, **42**, 4, 607-616

Laubscher, H.P., Biella, G.C., Cassinis, R., Gelati, R., Lozej, A., Scarascia, S., and Tabacco, I. (1992) The collisional knot in Liguria. *Geol Rundsch*, **81**, 275–289

Lomas, S.A., and Joseph, P. (2004) Confined turbidite systems, in: Lomas, S.A., Joseph, P., (Eds.), Confined turbidite systems. *The Geololgical Society of London*, Spec. Publ., **222**, 1-7

Lowe, D.R. (1982) Sediment gravity flows II: Depositional models with special reference to the deposits of high-density turbidity currents. *Journal of Sedimentary Petrology*, **52**, 279-298

Lowrie, W. (1990) Identification of ferromagnetic minerals in a rock by coercivity and unblocking temperature properties. *Geophysical Research Letters*, **17**, 2, 159-162

Lowrie, W., and Hirt, A.M. (1987) Anisotropy of magnetic susceptibility in the Scaglia Rossa pelagic limestone. *Earth and Planetary Science Letters*, **82**, 349-356

Malinverno, A. (1997) On the power law size distribution of turbidite beds. *Basin Research*, **9**, 263-274.

McBride, E.F. (1962) Flysch and associated beds of the Martinsburg Formation (Ordovician), Central Appalachians. *Journal of Sedimentary Petrology*, **32**, 39–91

Middleton, G.V., and Hampton, M.A. (1973) Sediment gravity flows: mechanics of flow and deposition. In: Middleton, G.V., Bouma, A.H. (Eds.), Turbidites and Deep-Water Sedimentation, S.E.P.M. Pacific Section, *Short Course, Anaheim*, 1–38

Middleton, G.V., and Hampton, M.A. (1976) Subaqeous sediment transport and deposition by sediment gravity flows. In: Stanley, D.J., Swift, D.J.P. (Eds.), Marine Sediment Transport and Environmental Management. John Wiley, New York, 197–218

Murray, C.J., Lowe, D.R., Graham, S.A., Martinez, P.A., Zeng, J., Carroll, A., Cox, R., Hendrix, M., Heubeck, C., Miller, D., Moxon, I.W., Sobel, E., Wendebourg, J., and Williams, T., (1996) Statistical analysis of bed-thickness patterns in a turbidite section from the Great Valley Sequence, Cache Creek California. *Journal of Sedimentary Petrology*, **66**, 900-908

Mutti, E. (1979) Turbidites et cones sous-marins profonds. In: Homewood P. (Ed.), Sedimentation detritique (fluvial, littoral et marin). *Institut de Géologie, Univerité de Fribourg (Suisse)*, 353-459

Mutti, E. (1992) Turbidite sandstones. *ENI – Università di Parma*, 275 pp.

Mutti, E., Tinterri, R., Remacha, E., Mavilla, N., Angella, S., and Fava, L., (1999) An introduction to the analysis of ancient turbidite basins from an outcrop perspective. *AAPG Continuing Education Course Note Series*, **39**, 86 pp.

Mutti E, Ricci Lucchi F, and Roveri M (2002) Revisiting Turbidites of the Marnoso-arenacea Formation and their Basin-Margin Equivalents: Problems with Classic Models. Excursion Guidebook. Workshop organized by Dipartimento di Scienze della Terra (Universita` di Parma) and Eni- Divisione Agip, 64th EAGE Conference and Exhibition, Florence, Italy, May 27–30, 120 pp.

Parés, J.M., Hassold, N.J.C., Rea, D.K., and van der Pluijm, B.A. (2007) Paleocurrent directions from paleomagnetic reorientation of magnetic fabrics in deep-sea sediments at the Antarctic Peninsula Pacific margin (ODP Sites 1095, 1101). *Marine Geology*, **242**, 261–269

Parkash, B., and Middleton, G.V. (1970) Downcurrent textural changes in Ordovician turbidite greywackes. *Sedimentology*, **14**, 259–293

Piper, D.J., and Normark, W.R. (1983) Turbidite depositional patterns and flow characteristics, Navy submarine fan, California borderland. *Sedimentology*, **30**, 681–694

Pirmez, C., Hiscott, R.N., and Kronen, J.D.Jr (1997) Sandy turbidite successions at the base of channel levee systems of the Amazon Fan revealed by FMS logs and cores: unravelling the facies architecture of large submarine fans. *Proc. ODP Scientific Results*, **155**, 7–33

Prather, B.E., Booth, J.R, Steffens, G. S., and Craig, P.A. (1998) Classification, lithologic calibration, and stratigraphic succession of seismic facies of intraslope basins, deep-water Gulf of Mexico. *AAPG Bulletin*, **82**, 701-728

Rasband, W. S. (2008) ImageJ. US National Institutes of Health, Bethesda, Maryland,USA. http://rsb.info.nih.gov/ij/index.html

Rees, A.I. (1983) Experiments on the production of transverse grain alignment in a sheared dispersion. *Sedimentology*, **30**, 437–448

Rees, A.I., Von Rad, U., and Shepard, F.P. (1968) Magnetic fabric of sediments from the La Jolla submarine canyon and fan, California. *Marine Geology*, **6**, 145–178

Ricci Lucchi, F. (1967) Recherches stratonomiques et sedimentologiques sur le flysch Miocene de la Romagna. *Giornale di Geologia*, **35**, 163-192

Rothman, D.H., and Grotzinger, J.P. (1995) Scaling properties of gravity-driven sediments. *Nonlinear Processes in Geophysics*, **2**, 178–185

Sagnotti, L., and Meloni, A. (1993) Pleistocene rotations and strain in southern Italy: the example of the Sant'Arcangelo Basin. *Annali di Geofisica*, **XXXVI**, 2, 83-95

Scott, K.M. (1967). Intra-bed palaeocurrent variations in a Silurian flysch sequence, Kirkcudbrightshire, Southern Uplands of Scotland. *Scottish Journal of Geology* , **3**, 268–281

Sestini,G., and Pranzini, G. (1965) Correlation of sedimentary fabric and sole marks as current indicators in turbidites. *Journal of Sedimentary Petrology*, **35**, 100–108

Shor, A.N., Kent, D.V., and Flood, R.D. (1984) Contourite or turbidite? Magnetic fabric of fine-grained Quaternary sediments, Nova Scotia continental rise. In: Fine-Grained Sediments; Deep- Water Processes and Facies (Stow, D.A.V. and Piper, D.J.W. Eds.). *Geological Society of London, Special Publication*, **15**, 257-273

Sinclair, H. D., and Tomasso, M. (2002) Depositional evolution of confined turbidite basins. *Journal of Sedimentary Research*, **72**, 451-456

Sinclair, H.D., and Cowie, P.A. (2003) Basin-Floor Topography and the Scaling of Turbidites. *The Journal of Geology*, **111**, 277-299

Smith, R. (2004) Turbidite system influenced by structurally induced topography in the multi-sourced Welsch Basin, in: Lomas, S.A., Joseph, P., (Eds.), Confined turbidite systems. *Geological Society of London, Special Publication*, **222**, 209-228

Stanley, D.J. (1963) Vertical petrographic variability on Annot Sandstone turbidites: some preliminary observations and generalisations. *Journal of Sedimentary Petrology*, **33**, 783–788

Stocchi, S., Cavalli, C., and Baruffini, L. (1992) I depositi torbiditici di Guaso (Pirenei centro meridionali), Gremiasco e Castagnola (settore orientale del BTP): geometria e correlazioni di dettaglio. *Atti Ticinensi di Scienze della Terra*, **35**, 154-177

Sylvester, Z. (2007) Turbidite bed thickness distributions: methods and pitfalls of analysis and modelling. *Sedimentology*, **54**, 847-870

Taira, A. (1989) Magnetic fabric and depositional processes. In: Sedimentary facies in the Active Plate Margin (Taira, A. and Masuda, F. Eds). *Tokyo, Terra Scientific Publishing*, 44-77

Taira, A., and Scholle, P.A. (1979) Deposition of resedimented sandstone beds in the Pico Formation, Ventura Basin, California, as interpreted from magnetic fabric measurements. *Bulletin Geological Society of America*, **90**, 952-962

Talling, P.J. (2001) On the frequency distribution of turbidite thickness. *Sedimentology*, **48**, 1297-1331

Tarling, D.H., and Hrouda, F. (1993) The Magnetic Anisotropy of Rocks. Chapman & Hall, London.

Von Rad, U. (1970) Comparison between "magnetic" and sedimentary fabric in graded and cross-laminated sand layers, southern California. *Geologische Rundschau*, **60**, 331–354

Walker, R.G. (1967) Upper Flow Regime Bed Forms in Turbidites of the Hatch Formation, Devonian of New York State. *Journal of Sedimentary Research*, **37**, 1052-1058

Walker, R.G. (1984) Shelf and shallow marine sands. In: Facies Models 2nd edition (Walker, R.G. Ed.). *Geoscience Canada, Reprint Series*, **1**, 141-170

Winker, C. D. (1996) High resolution seismic stratigraphy of a late Pleistocene submarine fan ponded by salt-withdrawal mini-basins on the Gulf of Mexico Continental slope. *Proc. 1996 Offshore Technology Conference, paper OTC 8024 (May 6 9, 1996, Houston, Texas)*, 619 628

Yagishita, K., Ashi, J., Ninomiya, S., and Taira, A. (2004) Two types of plane beds under upper-flow-regime in flume experiments: evidence from grain fabric. *Sedimentary Geology*, **163**, 229–236

Chapter 5

Textural analyses: the relationship between crystallographic preferred orientation and AMS

The applicability of the AMS as a tool to define paleocurrent directions, discriminate different mechanisms of deep-water deposition and flow dynamics was discussed in the previous chapters. The next important step is to investigate the relationship between the crystallographic preferred orientation and the AMS signal. In order to do this, some textural analyses have been carried out.

The starting point was the knowledge that the magnetic susceptibility intensities of the samples analyzed in the Marnoso Arenacea and in the Castagnola Formations were relatively low (1*10E-4). This suggests a prevalent contribution of paramagnetic minerals. The texture and the crystallographic preferred orientation have been analyzed throughout image analysis, neutron diffraction, and X-ray tomography. The data obtained from these techniques were compared to the AMS dataset.

The selected site – CP2 (see Fig. 1.2) – consists of massive sandstones of the Marnoso Arenacea Formation and is characterized by an AMS stereoplot showing good clustering of the three axes (Fig. 5.1). The grain size is homogenous, with a good sorting of grains that are from subangular to subrounded. Thin section analysis revealed that the minerals contained in the sample are quartz, muscovite, feldspars, volcanic and carbonatic lithics, and fragments of fossils (planctonic foraminifera).

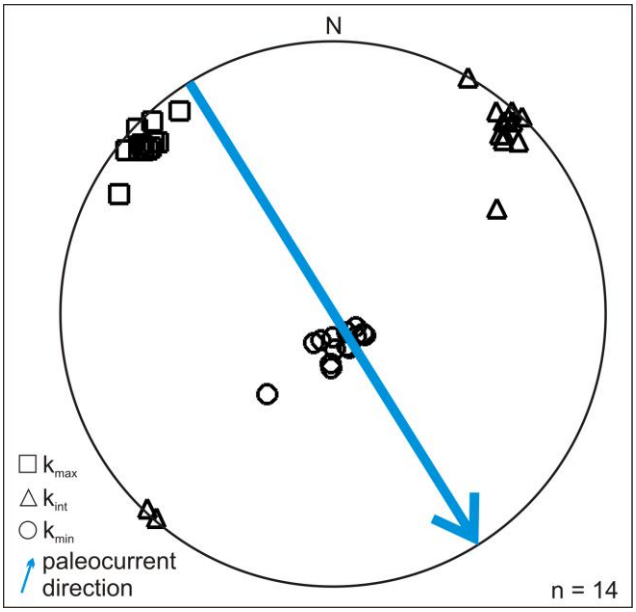

Fig. 5.1 – AMS stereoplot of sample CP2 with the representation of the three susceptibility axes: the major axes (squares), the intermediate axes (triangles) and the minor axes (circles). The paleoflow direction measured throughout flute marks at the base of the bed is represented with the blue arrow.

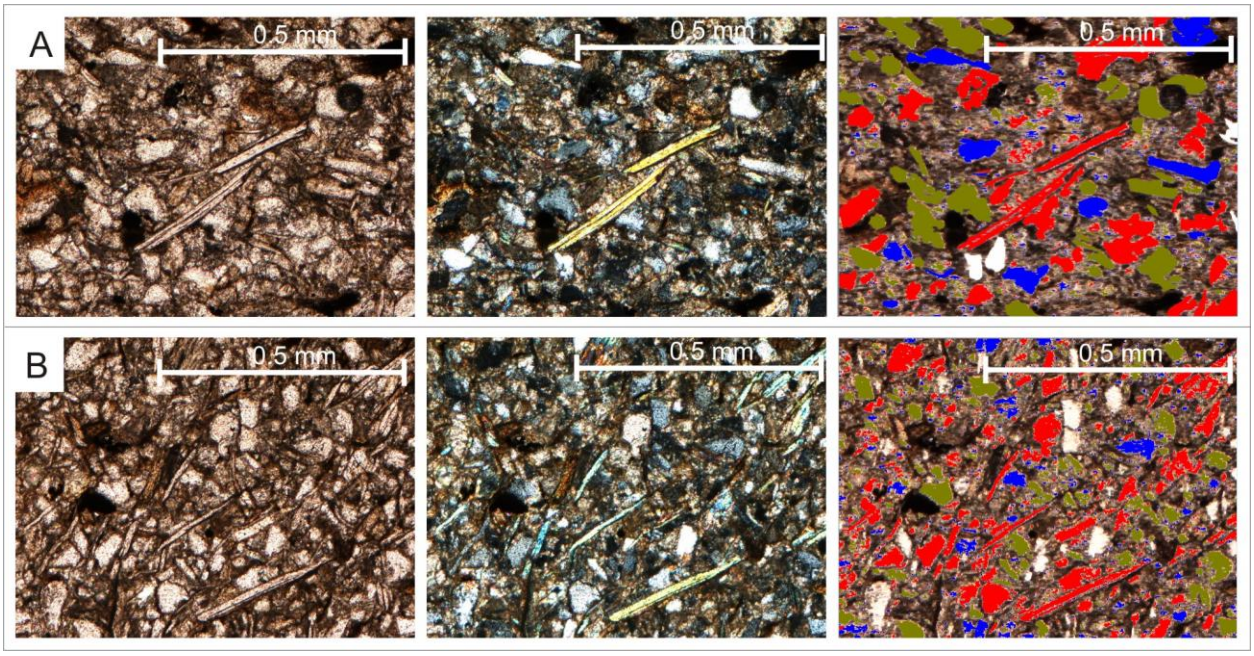

Fig. 5.2 – Photos of thin sections with and without crossed nicols and image analysis elaboration. A) Section cut parallel to the flow direction; B) section cut perpendicular to the flow direction.

Image analysis (Fig. 5.2)

Thin sections have been cut parallel (Fig. 5.2A) and perpendicular (Fig. 5.2B) to the flow direction. A photo was taken for each section (Fig. 5.2), and it was elaborated using the ImageJ software (Rasband, 2008). Morphological filters have been applied in order to make the edges of

the single grains better defined. Minerals of white color at parallel nicols (muscovite, quartz, feldspar) have been chosen for analysis. In particular, the orientation of the major axis of these grains with respect to the horizontal plane has been measured. Three classes of orientation have been defined: green and red objects represent grains characterized by an imbrication, and blue objects represent subhorizontal grains (Fig. 5.2). Muscovite grains appeared particularly well oriented in both sections; in particular, their long axis appear to be sub-parallel to the flow direction and also clearly imbricated.

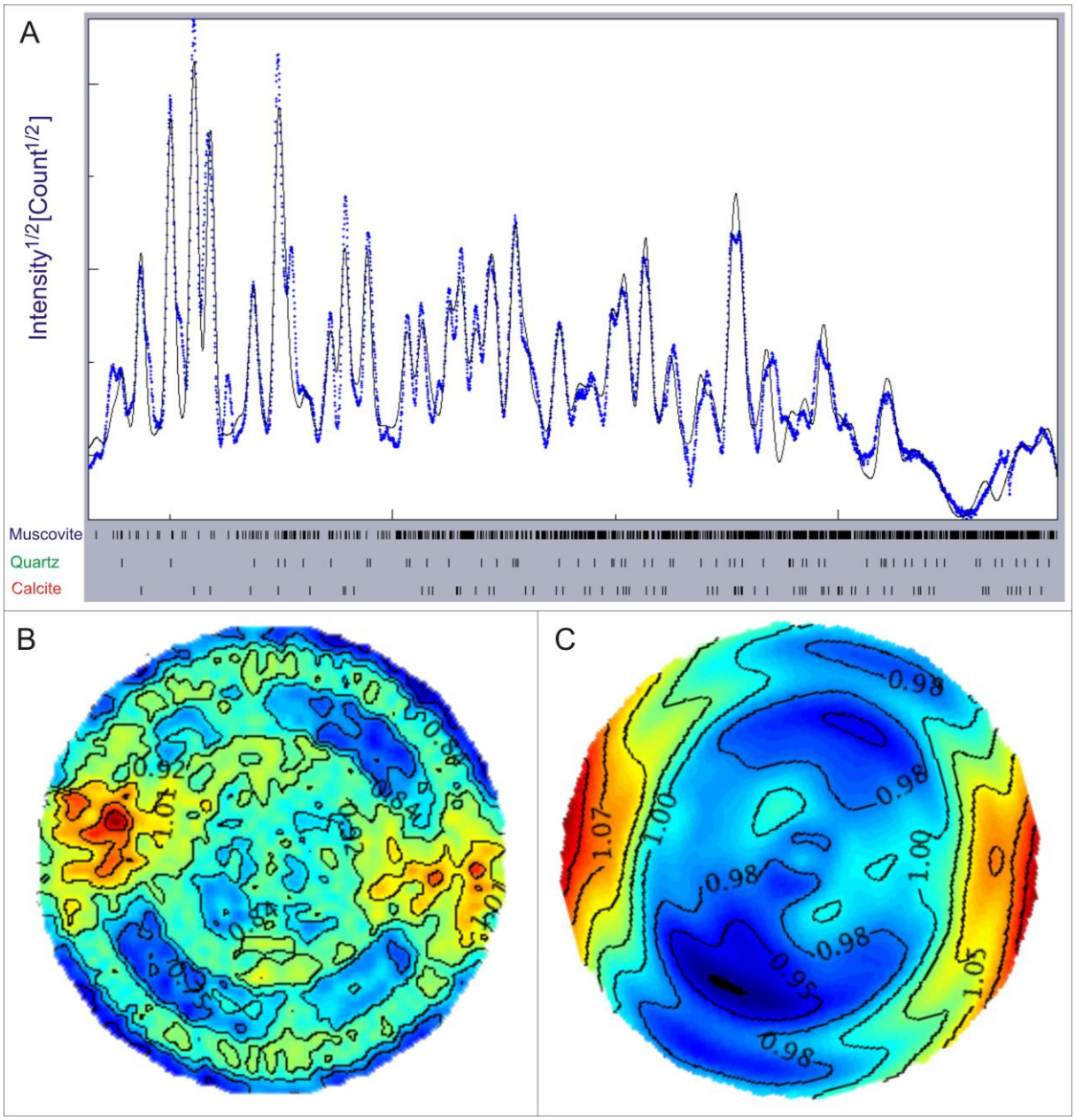

Fig. 5.3 – A) diffraction spectrum showing the mineral content of the rock sample; B) experimental pole figure of the normals to crystallographic plane {h00} of muscovite; C) reconstructed pole figure of the normals to crystallographic plane {h00} of muscovite.

Neutron diffraction (Fig. 5.3)

The neutron diffraction permits to obtain three-dimensional crystallographic information. Looking at the spectrum in Figure 5.3A, in which the blue line corresponds to the experimental spectrum and the black line to the theoretical spectrum, it is possible to affirm that the main minerals contained in the CP2 rock sample are muscovite, quartz and calcite. Crystal preferential orientations can be visualized through polar figures. Considering that quartz and calcite are diamagnetic minerals (they contribute with a negative value to AMS signal), the polar figures of paramagnetic muscovite was chosen. In order to reach the aim of this work, that is to compare neutron diffraction data with AMS and image analysis data, the crystallographic plane {h00} was selected because it is the one that contain the muscovite maximum axis. Polar figures in Fig. 5.3B and 5.3C are representative of the normal to this plane and they show a clear orientation of the maximum axis of muscovite. Figure 5.3B represents the experimental polar figure, whereas Figure 5.3C is the reconstructed polar figure, obtained by an elaboration of all the data referred to the sample analyses, and not only to the defined plane chosen (in this case the plane {h00}). The reconstructed polar figure is coherent with the experimental one, confirming the validity of the analysis. It is possible to say that the muscovite in the sediment is imbricated with an angle between 20° and 40° respect to the bedding plane, dipping up-current as expected. These imbrication angles agree with the published values of up to 30°–40° in massive turbiditic sandstone (Ta-divisions - Bouma, 1962; Hiscott and Middleton, 1980).

X-ray tomography (Fig. 5.4)

A three-dimension image of the volume of rock investigated is show in Fig. 5.4A. It is obtained by the overlapping of 434 X-ray-generated slices that represent separate projections around the object itself (Jerram and Higgins, 2007). In the figure the different phases can be visualized because of their different gray values (Fig. 5.4B, D, F) and they can be elaborated to highlight these differences (Fig. 5.4A, C, E, G). It was possible to separate minerals with an anisotropic shape (red objects), matrix (light blue color) and minerals that, compared with image analyses on thin sections, can be interpreted as quartz and feldspars (black objects). As an example, a single crystal has been taken into account (red object in the yellow square/circle in Fig. 5.4A), and its different shapes in three orthogonal planes have been observed: plane xz in Fig. 5.4B and 5.4C, plane xy in Fig. 5.4D and 5.4E, and plane yz in Fig. 5.4F and 5.4G. We interpret these red objects as the muscovite minerals that contribute to the AMS signal.

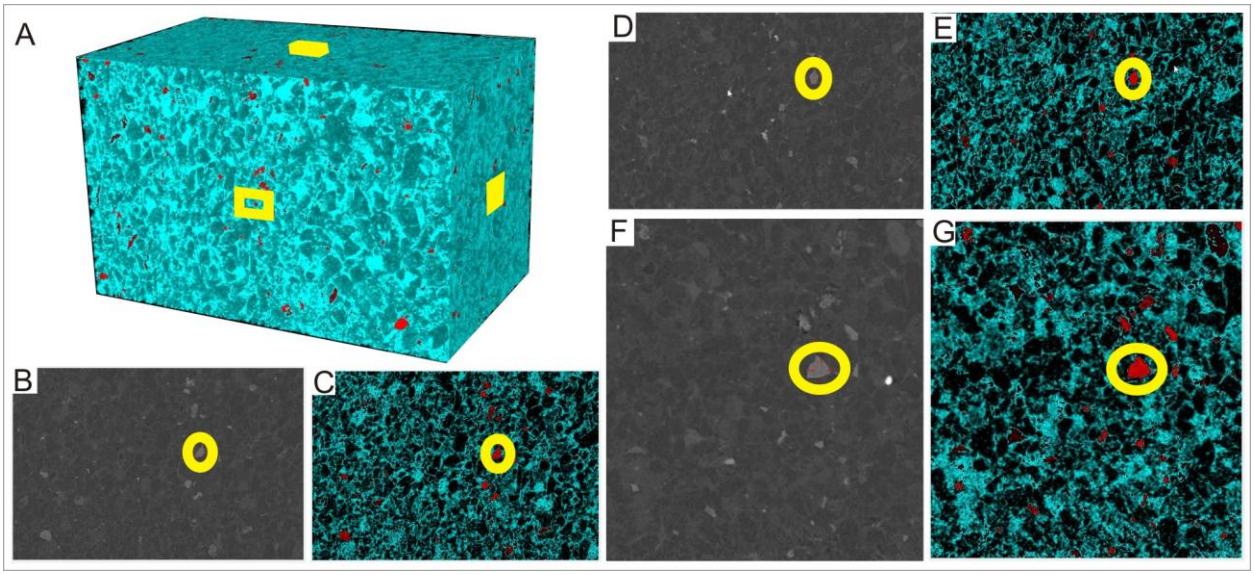

Fig. 5.4 – Virtual 3D reconstruction of the density of the rock analysed with X-ray tomography. (A) image of the volume of the rock obtained throughout the overlapping of 434 slices; the observed mineral (the red object in the yellow square) has been studied in three different planes: (B, C) plane xz; (D, E) plane xy; (F, G) plane yz.

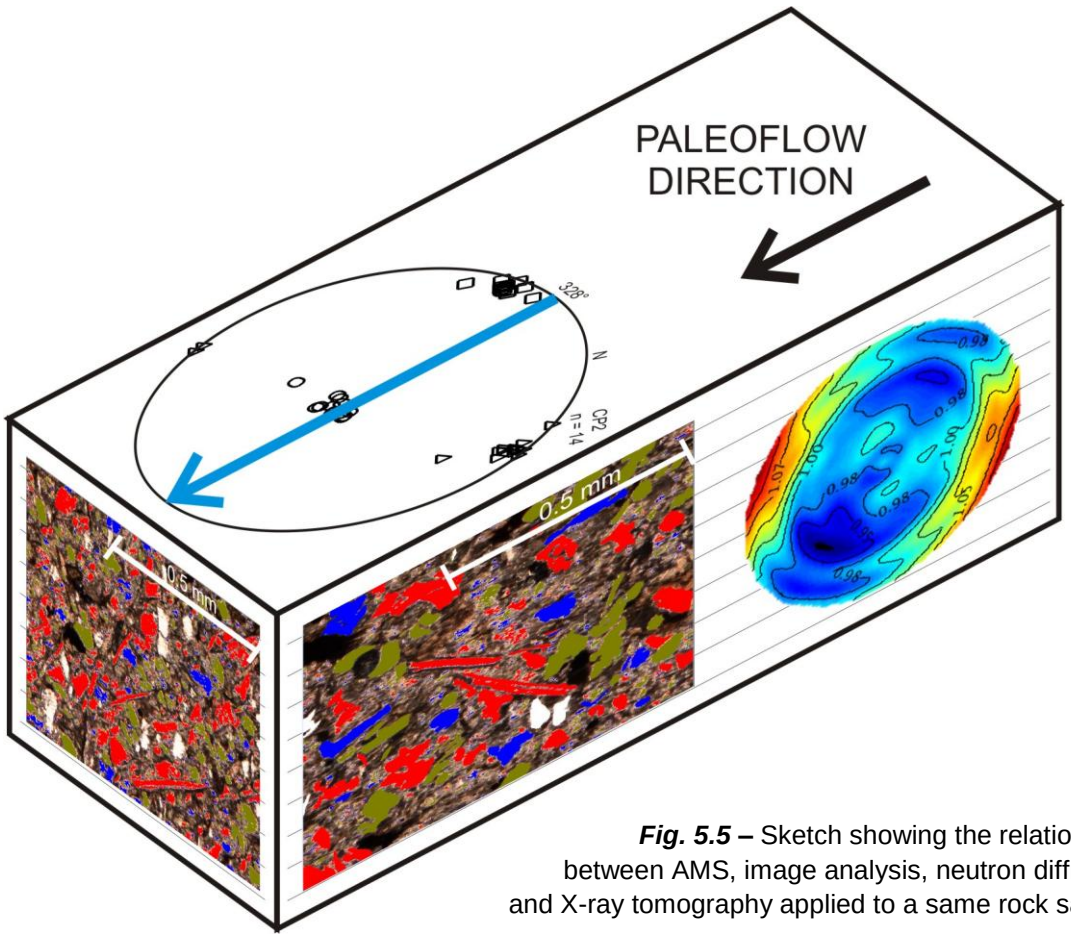

Fig. 5.5 – Sketch showing the relationships between AMS, image analysis, neutron diffraction and X-ray tomography applied to a same rock sample.

The analyses carried out (AMS, image analysis, neutron diffraction and X-ray tomography), give information that are referred to different planes. Figure 5.5 was assembled in order to compare all these data sets. It can be affirmed that the data are all coherent. The AMS ellipsoids in the investigated facies are consistently oriented subparallel to the flow direction estimated by sedimentological indicators (paleoflow arrow in Fig. 5.5). In the AMS stereoplot, a slight imbrication of the fabric can also be observed; the same imbrication can be observed in thin sections as well as in the polar figure of the neutron diffraction analysis. Moreover, neutron diffraction and image analysis indicate that paramagnetic muscovite control the observed, current-induced AMS fabric. Finally, the tomography validates the textural observations giving a three-dimensional representation of the investigated rock volume.

References

Bouma, A.H. (1962) Sedimentology of Some Flysch Deposits: a Graphic Approach to Facies Interpretation. *Elsevier*, Amsterdam. 168 pp

Hiscott, R.N., and Middleton, G.V. (1980) Fabric of coarse deep-water sandstones, Tourelle Formation, Quebec, Cananda. *Journal of Sedimentary Petrology*, **50**, 703-722

Jerram, D.A., and Higgins, M.D. (2007) 3D Analysis of Rock Textures: Quantifying Igneous Microstructures. *Elements*, **3**, 4, 239-245.

Rasband, W. S. (2008) ImageJ. US National Institutes of Health, Bethesda, Maryland, USA. http://rsb.info.nih.gov/ij/index.html

Chapter 6

Conclusions

This study demonstrates that the AMS is a very useful fabric analysis technique to quantify flow directions in turbiditic sandstones, discriminate different mechanisms of deep-water mudstone deposition, and investigate the effects of basin confinement on turbidity flow dynamics. It has been successfully applied to a wide range of depositional intervals selected by means of detailed sedimentological analyses, and cross-validated by direct estimates of flow directions from sedimentological indicators (*ripple marks, flute marks,* etc.). Particular advantages of the AMS technique are the significantly faster measurement time compared to standard petrographic fabric analysis and its capability to characterize the orientation of the entire population of (magnetic) grains in three dimensions, whereas standard image analysis on orthogonal thin sections is intrinsically limited to two-dimensional estimates of grains' orientations.

Turbiditic units outcropping in the northern Apennines ere deeply investigated for AMS, paleomagnetic, and sedimentologic analyses. Sampling was focused on the Marnoso Arenacea Formation (Miocene, northern Apennines) and on the Castagnola Formation (Oligo-Miocene, Tertiary Piedmont Basin) for a total of 853 samples. Both formations are characterized by measurable AMS signals carried essentially by paramagnetic grains (muscovite) and also ferromagnetic grains (magnetite) possibly contained within magmatic and/or metamorphic lithics. In the Marnoso Arenaca Formation, a robust correlation between magnetic fabric and paleocurrent directions obtained from sedimentological indicators (e.g., *flute casts*) was found in massive, parallel-laminated, and cross-laminated sandstones (Paper #1 – Chapter 2). These depositional intervals show well-clustered AMS data (see Fig. 2.5A, B, C, D, E, F) with an overall flow-aligned fabric. Imbrication angles of ~10-20° dipping up-current have been observed at a few sites. Instead, highly dispersed AMS fabrics are apparently common in convoluted and undulated sandstones as well as in debrites, suggesting depositional processes

that partially prevented grains' orientation (e.g., en masse freezing) or post-depositional processes that disrupted the original current-induced fabric (e.g., post-depositional dewatering) (see Fig. 2.5G, H, I, J). Small, but relatively consistent offset of up to ~15–20° counterclockwise, was observed in the Marnoso Arenacea Formation and tentatively explained as due to small variations of flow directions between the erosive, flute cast-generating stage of turbidity currents and the subsequent deposition of massive, planar, and cross stratifications. Speculatively, these variations of flow directions could have been triggered by flow interactions with the basin margins.

Regarding the very fine-grained sediments (hemipelagites) interbedded with the turbidity sands, AMS fabrics typical of deposition in standing water was observed in the hemipelagites of the Castagnola Formation (Fig. 4.6D). Here, the k_{min} axes resulted perpendicular to the bedding plane, whereas the k_{max} and the k_{int} resulted dispersed on the bedding plane. Instead, in the fine-grained sediments of the Marnoso Arenacea Fm. (White Marlstone beds - WM beds; Paper #2 – Chapter 3), previously interpreted as hemipelagites (Mutti and Ricci Lucchi, 1972, 1975; Mutti, 1977, 1979; Mutti and Johns, 1979; Talling et al., 2007), an AMS fabric interpreted as current-induced was observed. The stereoplots of this facies (see Fig. 2.5K – Fig. 3.4 and Fig. 3.5) are characterized by k_{max} axes are clustered within the depositional plane and broadly parallel to the average flow direction measured by flute casts at the base of turbidite beds. This fabric is interpreted as mainly sedimentary in origin, even though a partial tectonic contribution cannot be excluded, and it seems to suggest that weak velocity flows oriented the maximum susceptibility axes of paramagnetic grains (muscovite) and possibly also ferromagnetic grains (magnetite) parallel to the mean current direction in the final stages of transport. Two alternative depositional mechanisms have been taken into account to explain the WM beds: turbidity currents or bottom contour currents. The hypothesis of muddy contourites was favored based on sedimentological arguments, but in any case the effects of pirating by contour currents of fine-grained material originally supplied by turbidity currents, as demonstrated in similar depositional systems elsewhere (Rebesco et al., 1996, 1997; Pudsey, 2000; Escutia et al., 2000; Knutz et. al., 2002), was not excluded (see Chapter 3).

The study on the Castagnola Formation (Paper #3 – Chapter 4) was carried out to evaluate the use of the AMS as a tool investigates the effects of basin confinement on turbidity flow dynamics, i.e., changes in paleocurrent intensity and direction (e.g. flow ponding, reflection and/or deflection) related to basin geometry. This study revealed that within this small, confined turbidite system, the correlation between magnetic fabric and depositional intervals is not

straightforward. By contrast, we observed a strong correlation between magnetic fabric and bed-thickness distribution summarized as follows:

(a) beds thicker than ~1.20 m show high magnetic fabric variability with offsets of up to ~35° between maximum susceptibility axes and mean paleoflow direction from flute casts;

(b) beds thinner than ~1.20 m show better developed magnetic fabrics with maximum susceptibility axes oriented consistently along or close to the mean paleoflow direction from flute casts.

We believe that ~1.20 m represents a thickness threshold separating large flows that covered the entire basin floor and that interacted with the basin's margins from flows of small volume that did not cover the entire basin floor and therefore did not interact with the basin's margins. Entering flows of large volume were not free to spread laterally and, consequently, were forced to aggrade vertically, producing beds thicker than 1.20 m characterized by scattered AMS fabrics reflecting the complex flow rebounds at the basin's margins; in such beds, the AMS axes tends to become better grouped going upward, testifying for a reduction in flow volume and an enhanced capability of the flow to orient grains. Instead, entering flows of small volume, as they did not interact with the basin's margins, were more capable to orient grains, as shown by the well-defined AMS stereoplots (Fig. 4.7). We conclude that the AMS signal in confined basins is primarily controlled by bed thickness (and only secondarily by sedimentary structures), and that confined settings where turbidites can be considered fully ponded have a dramatic effect on associated bed thickness distributions.

Future developments

In order to deepen our understanding on the relationships between grains' orientations and magnetic minerals that contribute to the AMS signal, textural analyses, neutron diffraction and tomography have been carried out on a selected sample of massive sandstones from the Marnoso Arenacea Formation (Chapter 5). The results obtained on such sample (CP2) indicate that paramagnetic muscovite controls the observed, current-induced AMS fabric. These results need to be validated by additional experiments on other depositional intervals. Data on parallel laminated intervals in fine- and medium-grained sandstones were collected and will be elaborated in the mnear future.

The existence of a correlation between provenance direction of turbiditic flows (as indicated by *flute casts*) and AMS data suggests testing the AMS method on drill cores, where flow marks (i.e., flute casts) are either absent or non-observable. For this reason, a drill core taken in the modern Moroccan Turbidity System (Frenz et al., 2008) of the Agadir Basin, and stored at the National Oceanography Centre of Southampton (NOCS) was sampled in order to discriminate the provenance of the sampled turbidites that are known to have three main source areas: (1) from the northwest African margin, (2) from the volcanic Canary and Madeiran Islands, and (3) from a pelagic-draped seamount source west of the Madeira Abyssal Plain (de Lange et al. 1987; Jarvis and Higgs 1987; Weaver and Rothwell 1987). Nearly 200 cubic specimens will be cut from a 6 m u-channel core, and measured with a Kappabridge KLY-3. Since the cores were not oriented during drilling, they will need to be re-oriented so that the AMS-determined sediment transport direction could be referred to the geographic north. This will be achieved by the paleomagnetic method, using the present-day magnetic viscous overprint that is expected to characterize the natural remanent magnetization (NRM) of these sediments.

References

de Lange, G.J., Jarvis, I., and Kuijpers, A. (1987) Geochemical characteristics and provenance of late Quaternary sediments from the Madeira Abyssal Plain, N Atlantic. In: Weaver PPE, Thomson J (eds) Geology and geochemistry of Abyssal Plains. *Blackwell, Oxford*, 147–165.

Escutia, C., Eittreim, S.L., Cooper, A.K., and Nelson, C.H. (2000) Morphology and acoustic character of the Antarctic Wilkes Land turbidite systems: ice-sheets-sourced versus river-sourced fans. *Journal of Sedimentary Research*, **70**, 1, 84–93.

Frenz, M., Wynn, R.B., Georgiopoulou, A., Bender, V.B., Hough, G., Masson, D.G., Talling, P.J., and Cronin, B.T. (2008) Provenance and pathways of late Quaternary turbidites in the deep-water Agadir Basin, northwest African margin. *International Journal of Earth Sciences*, **98**, 4, 721-733; *DOI 10.1007/s00531-008-0313-4*.

Jarvis, I., and Higgs, N. (1987) Trace-element mobility during early diagenesis in distal turbidites: late Quaternary of the Madeira Abyssal Plain, N. Atlantic. In: Weaver PPE, Thomson J (eds) Geology and geochemistry of Abyssal Plains. *Blackwell, Oxford*, 179–213.

Knutz, P.C., Jones, E.J.W., Austin, W.E.N., and van Weering, T.C.E. (2002) Glacimarine slope sedimentation, contourite drifts and bottom current pathways on the Barra Fan, UK North Atlantic margin. *Marine Geology*, **188**, 129–146.

Mutti, E. (1977) Distinctive thin-bedded turbidite facies and related depositional environments in the Eocene Hecho Group (South-Central Pyrenees, Spain). *Sedimentology*, **24**, 107–131.

Mutti, E. (1979) Turbidites et cones sous-marins profonds. In Homewood P (ed.) Sédimentation Détritique (Fluviatile, Littorale et Marine), *Université de Fribourg, Institut de Géologie*, 353–419.

Mutti, E., Johns, D.R. (1979) The role of sedimentary by-passing in the genesis of basin plain and fan fringe turbidites in the Hecho Group System (South-Central Pyrenees). *Società Geologica Italiana, Memorie*, **18**, 15–22.

Mutti, E., and Ricchi Lucchi, F. (1972) Le torbiditi dell'Apennino settentrionale: introduzione all'analisi di facies. *Società Geologica Italiana, Memorie*, **11**, 161–199.

Mutti, E., and Ricchi Lucchi, F. (1975) Field Trip A-11: Turbidite facies and facies associations. In Mutti E, Parea GC, Ricci Lucchi F, Sagri M, Zanzucchi G, Ghibaudo G, Iaccarino I (Eds) Examples of Turbidite Facies Associations from Selected Formations of Northern Apennines: *International Association of Sedimentologists*, 9th International Congress, Nice, France, 21–36.

Pudsey, C.J. (2000) Sedimentation on the continental rise west of the Antarctic Peninsula over the last three glacial cycles. *Marine Geology*, **167**, 313–338.

Rebesco, M., Larter, R.D., Barker, P.F., Camerlenghi, A., and Vanneste, L.E. (1997) The history of sedimentation on the continental rise west of the Antarctic Peninsula. In: The American Geophysical Union (Ed.), Geology and Seismic Stratigraphy of the Antarctic Margin: Part 2. *Antarctic Research Series*, **71**, 29–49.

Rebesco, M., Larter, R.D., Camerlenghi, A., and Barker, P.F. (1996) Giant sediment drifts on the continental rise west of the Antarctic Peninsula. *Geo-Marine Letters*, **16**, 65–75.

Talling, P.J., Amy, L.A., Wynn, R.B., Blackbourn, G., and Gibson, O. (2007) Evolution of Turbidity Currents Deduced from Extensive Thin Turbidites: Marnoso Arenacea Formation (Miocene), Italian Apennines. *Journal of Sedimentary Research*, **77**, 3, 172-196.

Weaver, P.P.E., and Rothwell, R.G. (1987) Sedimentation on the Madeira Abyssal Plain over the last 300,000 years. In: Weaver PPE, Thomson J (eds) Geology and geochemistry of Abyssal Plains. *Blackwell, Oxford*, 71–86.